UNIVERSITY OF SOUTHERN QUEENSLAND

THE APPLICATION OF THE REAL-TIME MULTIVARIATE MADDEN-JULIAN OSCILLATION INDEX TO INTRASEASONAL RAINFALL FORECASTING IN THE MID-LATITUDES.

A Dissertation submitted by
Alexis May Donald, MSc (Forensic Science)
For the award of
Master of Science (Climatology)
2004

Abstract

The Madden-Julian Oscillation is a tropical atmospheric phenomenon detected as anomalies in zonal winds, convection and cloudiness. This perturbation has a definitive timescale of about thirty to sixty days, allowing its signal to be extracted from background data. The Madden-Julian Oscillation originates over the western Indian Ocean and generates a convective region which moves east along the equatorial region. This perturbation is thought to contribute to the timing and intensity of the eastern hemisphere monsoons, the El Niño/ Southern Oscillation and tropical storms and cyclones.

The current understanding of the Madden-Julian Oscillation is that it restricts the bulk of its' influence to the tropics, however some evidence suggested that the impact is more extensive. Analysis of about 30 years of data showed significant modulation of rainfall by the equatorial passage of the MJO. The real-time multivariate Madden-Julian Oscillation Index was used to estimate the location and amplitude of the Madden-Julian Oscillation, and forms the basis of the basic rainfall prediction tool developed.

The method developed here clearly linked the low latitude passage of the Madden-Julian Oscillation with suppressed and enhanced rainfall events in the Australasian region and beyond. A rudimentary forecasting capability at the intraseasonal time scale has been developed suitable for assisting Australian agricultural sector.

A subsequent and independent analysis of global mean sea level pressure anomalies provided evidence of teleconnections between the Madden-Julian Oscillation and

higher latitude atmospheric entities. These anomalies confirm the existence of teleconnections capable of producing the rainfall pattern outputs.

The MJO is strongly influenced by the season. However the seasonally dependant analysis of rainfall with respect to the Madden Julian Oscillation conducted was inconclusive, suggesting aspects of the MJO influence still require clarification. Considering the importance of rainfall variability to the Australian agricultural sector the forecasting tool developed, although basic, is significant.

CERTIFICATION OF DISSERTATION

I certify that the ideas, experimental work, results, analyses, software and conclusions reported in this dissertation are entirely my own effort, except where otherwise acknowledged. I also certify that the work is original and has not been previously submitted for any other award.

_____ _____

Signature of Candidate Date

ENDORSEMENT

_____ _____

_____ _____

Signature of Supervisor/s Date

Acknowledgements

I would like to acknowledge the invaluable assistance, both academic and personal, of the following people:
Joachim Ribbe, Matthew Wheeler, Roger Stone, Holger Meinke, Brendan Power, Peter deVoil, Graham Harris, Kerry Bell, Sarah, Grant Daggard and last, but not least, my family; Mum, Briony, Bruce and Yvonne.

I also acknowledge the institutions Bureau of Meteorology Research Centre, Australian Bureau of Meteorology (Melbourne), World Meteorological Organization (Geneva) and National Centre for Environmental Protection for providing data that are invaluable to research such as this, and the financial support of Queensland Department of Primary Industries and Fisheries via Grain Research and Development Corporation and Cotton Research and Development Corporation grants DAQ469 and DAQ104C.

Table of Contents

Table of Contents i
Table of Figures 3
Chapter 1 Introduction 6
1.1 The Problem 6
1.2 Background - The MJO 7
1.3 Objectives of this dissertation. 9
Chapter 2 The Madden-Julian Oscillation 10
2.1 Introduction 10
2.2 Defining the MJO 10
2.2 The Structure and Dynamics of the MJO 12
2.3 Spatial and temporal distribution of the MJO 21
2.4 Propagation of the MJO 22
2.5 Detection of the MJO 25
2.6 The MJO and ENSO 26
2.7 The MJO and the Asian and Austral Monsoons 29
2.8 MJO and Tropical Cyclone Activity 30
2.9 MJO Ocean Interactions 31
2.10 Extra-tropical MJO signals 33
2.11 Discussion 35
Chapter 3 Modelling and Predicting the MJO 37
3.1 Introduction 37
3.2 Modelling the MJO 37
3.3 The MJO in Climate Models 39
3.4 Forecasting the MJO 42
3.4 Discussion 47
Chapter 4 The relationship of the MJO and Rainfall in beyond the Tropics 49
4.1 Introduction 49
4.2 Data 51
4.2.1 Rainfall 51
4.2.2 MJO 52
4.2.3 Mean Sea Level Pressure 52
4.3 Methodology 52
4.3.1 MJO/rainfall 52
4.3.2 Mean sea level pressure 54
4.3.2 Rainfall lagging MJO 55
4.3.3 Strong MJO Signals 55
4.3.4 Phase Locking 56
4.4 Results 56
4.4.1 MJO and rainfall results 57
4.4.1.1 PHASE 1: 57
4.4.1.2 PHASE 2: 62
4.4.1.3 PHASE 3: 66
4.4.1.4 PHASE 4: 70
4.4.1.5 PHASE 5: 74
4.4.1.6 PHASE 6 77
4.4.1.7 PHASE 7 80
4.4.1.8 PHASE 8 83

4.4.2 Rainfall lagging MJO 86
4.4.3 Strong MJO Signals 87
4.4.4 Phase locking: 89
4.5 Discussion 93
4.5.1 MJO rainfall and MSLP 93
4.5.2 Lag 97
4.5.3 Strong signals 97
4.5.4 Locking the phases 98
Chapter 5 MJO and Seasonal Rainfall for Australia 99
5.1 Introduction 99
5.2 Data 105
5.3 Methodology 105
5.3.1 Four Seasons 105
5.3.2 Wet Season/ Dry Season 105
5.4 Results 106
5.4.1 Four Seasons 106
5.4.1.1 Spring 106
5.4.1.2Summer 108
5.4.1.3 Autumn 110
5.4.1.4 Winter 112
5.4.2 Wet Season/Dry Season 114
5.5 Discussion 118
Chapter 6 Conclusions 120
References 123
APPENDICES 133
Appendix 1 The hq dataset daily rainfall raw data sample 133
Appendix 2 The BoM dataset rainfall stations and daily rainfall raw data sample 134
Appendix 3 The WMO dataset daily rainfall raw data sample 136
Appendix 4 The MJO dataset daily rainfall raw data sample 137
Appendix 5 The MSLP dataset daily rainfall raw data sample 138

Table of Figures

1.1	Australian rainfall variability for the planting window of summer crops (September to November).	7
2.1	The eastward propagation of the MJO (40 day oscillation).	13
2.2	The Structure of the MJO (cross section).	18
2.3	Schematic of Cloud Clusters	20
3.1	OLR and 850hPa wind anomalies	45
3.2	RMM Index phase space diagram	46
4.1.a	Significant sites (p=.05) for K-S distribution of the hq rainfall datasets for MJO Phase 1	60
4.1.b	Significant sites (p=.05) for K-S distribution of the BoM rainfall datasets for MJO Phase 1	60
4.1.c	Significant sites (p=.05) for K-S distribution of the WMO rainfall dataset for MJO Phase 1	61
4.1.d	Phase 1 MSLP anomalies.	61
4.2.a	Significant sites (p=.05) for K-S distribution of the hq rainfall datasets for MJO Phase 2	64
4.2.b	Significant sites (p=.05) for K-S distribution of the BoM rainfall datasets for MJO Phase 2	64
4.2.c	Significant sites (p=.05) for K-S distribution of the WMO rainfall dataset for MJO Phase 2	65
4.2.d	Phase 2 MSLP anomalies.	65
4.3.a	Significant sites (p=.05) for K-S distribution of the hq rainfall datasets for MJO Phase 3	68
4.3.b	Significant sites (p=.05) for K-S distribution of the BoM rainfall datasets for MJO Phase 3	68
4.3.c	Significant sites (p=.05) for K-S distribution of the WMO rainfall dataset for MJO Phase 3	69
4.3.d	Phase 3 MSLP anomalies.	69
4.4.a	Significant sites (p=.05) for K-S distribution of the hq rainfall datasets for MJO Phase 4	71
4.4.b	Significant sites (p=.05) for K-S distribution of the BoM rainfall datasets for MJO Phase 4	72
4.4.c	Significant sites (p=.05) for K-S distribution of the WMO rainfall dataset for MJO Phase 4	72

4.4d	Phase 4 MSLP anomalies.	73
4.5.a	Significant sites (p=.05) for K-S distribution of the hq rainfall datasets for MJO Phase 5	75
4.5.b	Significant sites (p=.05) for K-S distribution of the BoM rainfall datasets for MJO Phase 5	75
4.5.c	Significant sites (p=.05) for K-S distribution of the WMO rainfall dataset for MJO Phase 5	76
4.5.d	Phase 5 MSLP anomalies.	76
4.6.a	Significant sites (p=.05) for K-S distribution of the hq rainfall datasets for MJO Phase 6	78
4.6.b	Significant sites (p=.05) for K-S distribution of the BoM rainfall datasets for MJO Phase 6	78
4.6.c	Significant sites (p=.05) for K-S distribution of the WMO rainfall dataset for MJO Phase 6	79
4.6.d	Phase 6 MSLP anomalies.	79
4.7.a	Significant sites (p=.05) for K-S distribution of the hq rainfall datasets for MJO Phase 7	81
4.7.b	Significant sites (p=.05) for K-S distribution of the BoM rainfall datasets for MJO Phase 7	81
4.7.c	Significant sites (p=.05) for K-S distribution of the WMO rainfall dataset for MJO Phase 7	82
4.7.d	Phase 7 MSLP anomalies.	82
4.8.a	Significant sites (p=.05) for K-S distribution of the hq rainfall datasets for MJO Phase 8	83
4.8.b	Significant sites (p=.05) for K-S distribution of the BoM rainfall datasets for MJO Phase 8	84
4.8.c	Significant sites (p=.05) for K-S distribution of the WMO rainfall dataset for MJO Phase 8	84
4.8.d	Phase 8 MSLP anomalies.	85
4.9	K-W test of rainfall lagged (0-60 days) behind MJO by a count of significant sites	86
4.10.a	RMM Strong Signals (RMM1 >|1|, RMM2 >|1|) Phases 1-4	88
4.10.a	RMM Strong Signals (RMM1 >|1|, RMM2 >|1|) Phases 5-8	89
4.11.a	Significant sites (p=.05) for K-S distribution of the BoM rainfall dataset for RMM Phases 1 and 2	91

4.11.b	Significant sites (p=.05) for K-S distribution of the BoM rainfall dataset for RMM Phases 3 and 4	91
4.11.c	Significant sites (p=.05) for K-S distribution of the BoM rainfall dataset for RMM Phases 5 and 6	92
4.11.d	Significant sites (p=.05) for K-S distribution of the BoM rainfall dataset for RMM Phases 7 and 8	92
4.12	Satellite image of the Western Pacific Region, 18/06/04.	94
4.13	Australian Region Mean Sea Level Analysis, 18/06/04	95
5.1	Major seasonal rainfall zones of Australia	100
5.2.a	Spring weekly rainfall anomalies (mm) for each phase	101
5.2.b	Summer weekly rainfall anomalies (mm) for each phase	102
5.2.c	Autumn weekly rainfall anomalies (mm) for each phase	103
5.2.d	Winter weekly rainfall anomalies (mm) for each phase	104
5.3.a	Spring K-S distributions of RMM Phases 1-8 and BoM rainfall data	107
5.3.b	Summer K-S distributions of RMM Phases 1-8 and BoM rainfall data	109
5.3.c	Autumn K-S distributions of RMM Phases 1-8 and BoM rainfall data	111
5.3.d	Winter K-S distributions of RMM Phases 1-8 and BoM rainfall data	113
5.4.a	Wet Season K-S distributions of RMM Phases 1-8	116
5.4.b	Dry Season K-S distributions of RMM Phases 1-8	117

Chapter 1 Introduction

1.1 The Problem

"Of droughts and flooding rains" (My Country, Dorothea Mackellar)

Australia experiences some of the most variable climate conditions on the globe, and northern and eastern Australian rainfall is highly variable (Nicholls, 1987). Climate variability is a major factor in rural sector dynamics, and these fluctuations impact upon many socio-economic parameters. Considerable resources have been applied to the development and application of seasonal forecasting, in an attempt to reduce the risks and flow-on impact of drought. The value of such forecasting is well established.

Despite agricultural adaptations designed to buffer climate variability, and increased forecasting skill and uptake of climate information (Horsley and Buckley, 2004), a significant temporal gap in information exists between synoptic and seasonal forecasting. Many on-farm management decisions (ground preparation, planting, irrigation, fertilization, pest-control programs, harvesting) are made at an intra-seasonal time scale, and information about possible rainfall events, or lack of them, could be used to reduce risk. Planting under highly variable rainfall regimes is a risky business (Figure 1.1).

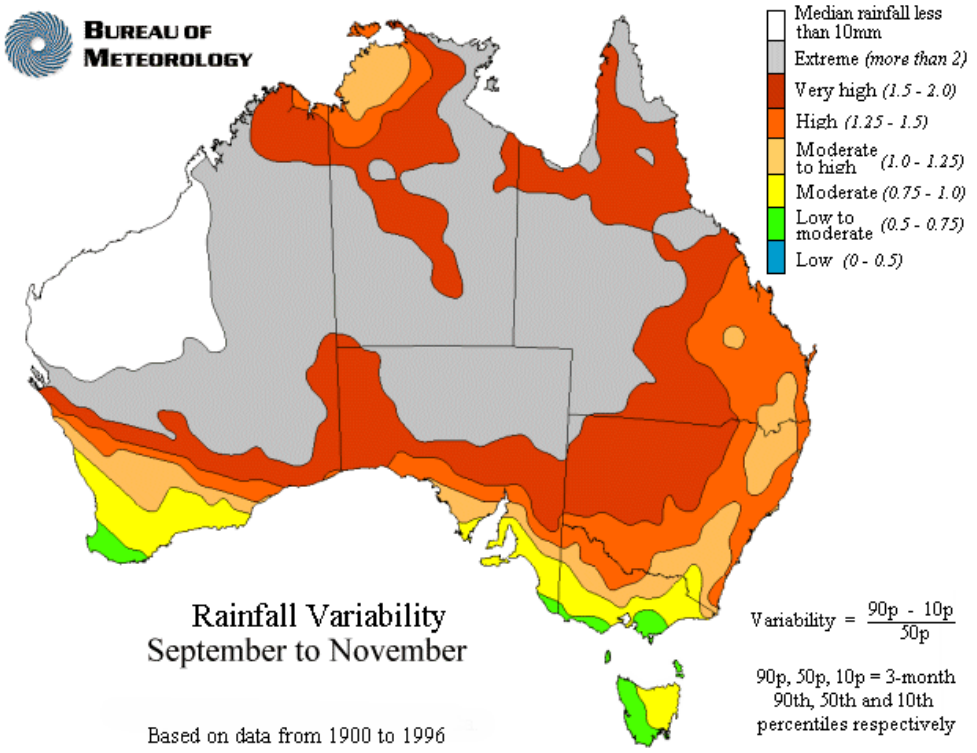

Figure 1.1 Australian rainfall variability for the planting window of summer crops (September to November) (Commonwealth of Australia Bureau of Meteorology).

For some time, anecdotal and limited scientific evidence had suggested the intra-seasonal Madden Julian Oscillation (MJO) contributes to the temporal and spatial variability of rainfall events in Australia. Yet, its significance or exact influence within Australia's weather systems is not fully understood. Broadscale restricted attempts have been made to quantify the MJO. Subjective rural sector indicators, and some limited analyses have suggested extra-tropical impacts. There is a need to remove the subjectivity, and define what, if any, is the correlation between the tropical passage of the MJO, and extra-tropical rainfall events.

1.2 Background - The MJO

The MJO is a large-scale atmospheric circulation anomaly that originates over the western Indian Ocean, and propagates eastward into the Pacific Ocean. Madden and

Julian (1971, 1972) initially identified the existence of the atmospheric oscillation while conducting spectral analysis of atmospheric pressure records at Canton Island (3 degrees S, 172 degrees W). The MJO is confined to the equatorial region between about 20 degrees N, and 20 degrees S. Its timescale is approximately 30 to 60 days, with a frequency of six to twelve events per year. In the Eastern Hemisphere the MJO is associated with convective anomalies and westerly wind bursts. While terms such as '40 day wave' are in common usage, throughout this dissertation the tropical, atmospheric, intraseasonal, oscillation with an interval between 22 and 70 days, will be referred to as the Madden Julian Oscillation (MJO).

The spatial distribution, periodicity, and some proposed propagation modes of the MJO are discussed. Theories regarding the interaction of the MJO and the El Niño Southern Oscillation (ENSO), the Austral and Asian monsoons, and the Indian and Pacific Oceans are outlined. The ability of global atmospheric general circulation models (AGCM) and global climate models (GCM) to represent the MJO is examined. Modelling of, and with, the MJO has been extensive, and the problems and resolution of some of the models are examined.

The role of the MJO in climate prediction is considered. The MJO produces climate variations that are coherent on a large scale. Therefore, predications of rainfall events can be made from these large scale patterns that are forced by observable fluctuations in synoptic measurements. Particular focus is upon the recent development of the Real-Time Multivariate MJO (RMM) Index (Wheeler and Hendon, 2004) that allows monitoring and prediction of MJO activity, by observation of OLR and zonal wind data. The RMM Index divides the convective element of the MJO into 8 phases.

1.3 Objectives of this dissertation.

The principal objective of this work was to test whether Australian rainfall could be predicted, using the RMM Index (Wheeler and Hendon, 2004) as a measure of the daily state of the MJO. A statistical distribution was constructed, and the ability to forecast regional areas of rainfall, given the RMM Index phase of the MJO was demonstrated. The distribution also revealed whether significant rainfall results were above (enhanced rainfall), or below (suppressed rainfall), the mean. The secondary objective was to develop a simple tool to forecast rain by monitoring the MJO, given forecasting based on the RMM Index were possible. This goal was met by the construction of maps that indicated Australian rainfall enhancement and suppression for every phase of the RMM Index.

Chapter 2 The Madden-Julian Oscillation

2.1 Introduction

Using the MJO to improve intra-seasonal rainfall forecasting requires an understanding of the nature of the MJO and the physical processes involved in its evolution and movement. This chapter examines the current understanding of the MJO, looks at its structure and dynamics, and the spatial and physical distribution of the MJO. The interaction of MJO with other climatic influences like the El Niño Southern Oscillation (ENSO), the Eastern Hemisphere monsoons, and the Indian and Pacific Oceans are reviewed.

2.2 Defining the MJO

The MJO was first identified and described by Madden and Julian (1971), when analysing data from Canton Island (3 degrees S, 172 degrees W) for near-surface zonal wind anomalies. The oscillation was noticed as a peak in station pressure, and in upper and lower level zonal winds. Additional spectral and cross-spectral analysis of rawinsonde data collected over periods of 5-10 years, at several tropical stations, confirmed the existence of definite, but diffuse, spectral peaks over a 40-50 day period (Madden and Julian, 1972). The observational evidence suggested that the surveyed oscillation was essentially the result of the eastward movement of large-scale circulation cells within the equatorial plane.

The MJO originates over the western tropical Indian Ocean basin (Madden and Julian, 1972), and is most easily detected in the tropics of the Eastern Hemisphere (von Storch and Xu 1990). The MJO signal is weaker, though detectable, throughout the Western Hemisphere tropics (Geerts and Wheeler, 1998). Although the MJO

signal is strongest in the Indian and western Pacific Oceans, where for example, it alters the intensity of the Austral and Asian monsoon systems, and interacts with ENSO, it affects the entire tropical troposphere (Elleman, 1997). It has been estimated that up to one half of tropical intra-seasonal variance in Outgoing Longwave Radiation (OLR) experienced in the western Pacific Ocean is attributable to the MJO (Kessler, 2001).

The signal of the MJO is composed of periodic fluctuations in station pressure, wind, air temperature, sea surface temperature (SST), cloudiness and rainfall (Geerts and Wheeler 1998). This global climate pattern can be described by an episodic modulation of tropical winds and precipitation that travels from Asia to the Americas, and having a characteristic repeat time (Maloney and Hartmann 2000). The period or repeat time varies from 22 to70 days, with a median of 45 days (Madden and Julian, 1994)

Madden and Julian (1994) describe the MJO as the most dominant intraseasonal climatic variation in the tropics. The MJO is discernible as an anomalously high and low OLR, associated with the eastward moving convective irregularities (Elleman, 1997). The MJO has a wavenumber of one to two (Madden and Julian, 1994) denoting that at any time there is at least one active phase of the MJO in the tropics, but never more than two. Therefore, there can be simultaneous evolving and decaying events.

Spatial coherence, eastward propagation at 5 to 10 metres per second, and a wide zonal band distinguish the MJO from other intraseasonal variations (Kessler 2001).

Hendon and Liebmann (1994) defined the MJO as a baroclinic structure, characterised by convection that is organised over a broad range of temporal and spatial scales.

In summary, the MJO can be identified as a large perturbation with a definitive intraseasonal timescale, travelling at approximately 5 metres per second in the equatorial zone, and originating over the Indian Ocean. Both convection and associated precipitation, and rainfall suppression are associated with the passage of an MJO. The passage of the MJO is confined to the equatorial zone.

2.2 The Structure and Dynamics of the MJO

Madden and Julian (1972) first suggested the association of the MJO with convection over an extensive area. They conjectured that a zonal circulation cell caused the fluctuations they had noted in station pressure, with convergence low in the troposphere (800 hectaPascal), and divergence in the upper troposphere (250 hectaPascal). They later found that surface level air pressure, zonal winds and air temperature at various levels were coherent (Madden and Julian 1994).

Madden and Julian (1972) described the behaviour of the oscillation (Figure 2.1) as follows: A time series from time A through H, commencing at time F and displaying a convective maximum at time A, when the MJO is most readily recognised. A negative pressure anomaly over east Africa/Indian Ocean occurs at time F, with increasing wide spread convection over the ocean. The pressure anomaly then travels east along with the circulation cell (G). By H the zonal circulation cell has reached Indonesia. At time A the oscillation has resolved into two symmetric circulation

cells, the western cell then shrinks. Convection starts to weaken at about the date line (B), weakening further as it travels east (C). When the signal reaches the Atlantic Ocean (D) there is upper tropospheric divergence, but no corresponding lower

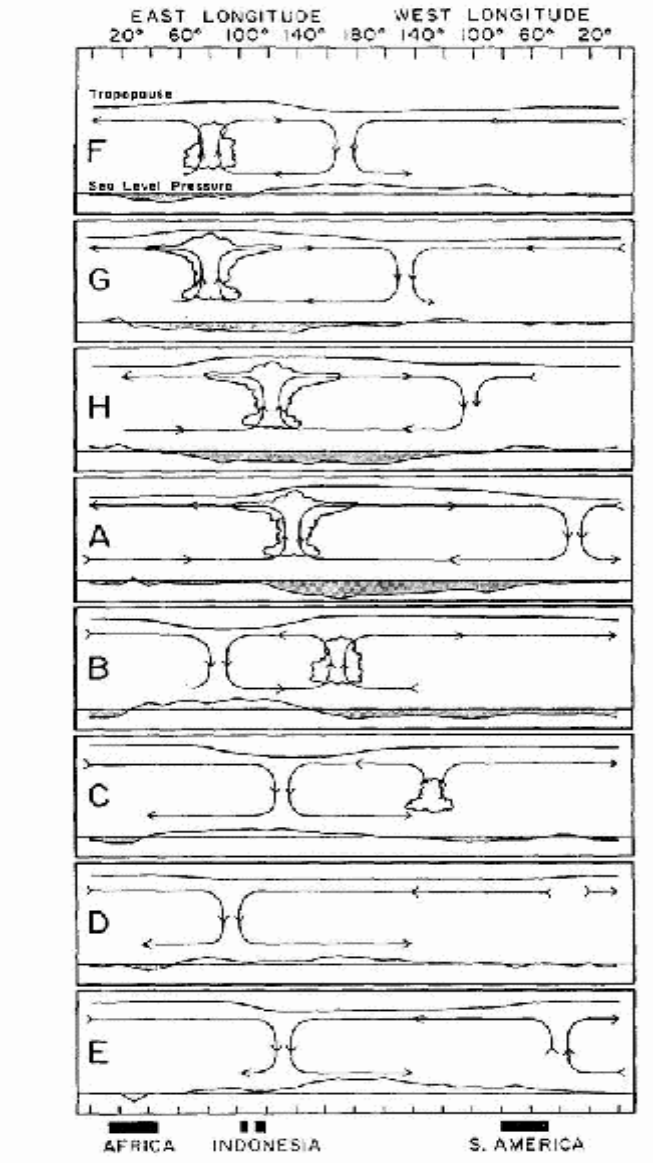

Figure 2.1 The eastward propagation of the MJO (40 day oscillation). Vertical scale is time A through H. At time F the MJO convective centre commences over the Indian Ocean and travels east as convective anomaly to around time C, when convection breaks down. The anomaly continues east in a drier form from time D. Horizontal scale is longitude, with the position of equatorial land-masses identified. The sea level pressure and tropopause height is identified, and the direction and relative height of convection. Cloudiness associated with the convection, and the relative extent of such cloud is represented from time F to C (From Madden and Julian, 1972)

tropospheric convergence. By time E the MJO is again two symmetric, zonal circulation cells. The temporal scale, as used by Madden and Julian (1972), includes A through H, with the MJO originating during time F, over the western Indian Ocean.

Madden and Julian (1971) thought the oscillation was similar in structure to atmospheric Kelvin waves. Since then, it has been shown that the MJO is associated with a Kelvin/ Rossby wave like structure (Gill, 1980; Yamagata and Hayashi, 1984). In the Eastern Hemisphere the wave travels an average 5 metres per second, between sea level and the top of the troposphere. Travel describes a longitudinal path between 30 degrees N and 30 degrees S, with a summer hemisphere preference.

In the Western Hemisphere, where the MJO is manifest as a Kelvin wave, it has an average velocity of around 10 metres per second, is a zonal wind feature, and has no associated convection (Elleman, 1997). Calm (zonal wind) conditions are often associated with suppression of the MJO signal to the east of convective systems. Westerly wind bursts often occurred to the west of active MJO convective systems, and a statistical mean westerly wind is to the west of (and follows) the active convection centre. Zhang (1998) noted that the influence of westerly wind bursts and calm conditions had significant effects on air-sea coupling.

Over Africa and South America the scale of the zonal circulation is smaller, convection is suppressed and velocity enhanced, compared with the MJO over the Indian and Pacific Oceans (Knutson and Weickmann, 1987). The drier Western Hemisphere MJO signal travels at velocities reaching 15 metres per second.

Matthews (no date provided) found that the mountain ranges of Central America and Africa, slow the Kelvin wave of this faster, drier phase MJO, returning it to the slower, convective phase.

The MJO is associated with masses of convective clouds, westerly wind bursts, and zonal wind perturbations in the upper and lower troposphere (Yanai and Chen 1998). The massed convective clouds are referred to as super cloud clusters (SCC), which originate over the Indian Ocean, then migrate east over the maritime continent and western equatorial Pacific (Nakazawa, 1988). Yanai, Chen and Tung, (2000) found that these SCC rapidly decayed over the cold eastern Pacific Ocean. A large convective energy source is required for SCC to form, and is provided by the (tropical) Indian Ocean (Madden and Julian, 1972). The Indian Ocean provides a source of convection as its (tropical) sea surface is heated, warm moist air rises, cooler air replaces the rising air, and in turn rises- ergo, convection .

Zou and Cho (2000) describe the MJO as a large scale eastward propagating SCC accompanied by mesoscale westward propagating smaller cloud clusters. Their research suggests that there might be a propagation envelope, in which the smaller clusters travel at group velocity. Most coherent in the Austral summer (December to May), MJO deep convection always coincides with extensive ascent, and SCC accompany a wide area of warm air (Yanai, Chen and Tung, 2000). They suggest that the kinetic energy required is maintained by potential energy, generated through convective heating.

An atmospheric Kelvin wave, with a period of up to 70 days, has a zonal width equal to the Pacific Basin (twice the width of the MJO), and travels at about 2-3 metres per second. Compared with the 5 metres per second velocity of the MJO, atmospheric Kelvin waves must be associated with the lower frequency components of the MJO. West of 180 degrees the phase speed of the MJO and the Kelvin wave, increase to around 10-15 metres per second, due to near resonant forcing of the MJO stress induced anomalies, (Hendon, Liebmann and Glick, 1998).

Zhang and Hendon (1997), found no standing oscillation component to the MJO, and argued that the propagating mode accounts for almost all convective variance. They proposed that the impression of a standing mode comes from modulation of the easterly propagating convective disturbance. Lau and Peng (1987) suggested that the selective amplification of Kelvin waves affects heat sourcing, propagating MJO to the east. This idea is supported by the findings of Goswani and Rameshan (2000), who also found that the selective excitation of Kelvin waves is responsible for a wide spectrum of tropical variability, including the MJO. In addition, Elleman (1997), states that tropical oscillations, including the MJO, have a common dynamic origin, but differing dynamic evolutions.

Hendon and Glick (1997) discovered that spatially coherent SST anomalies of approximately 0.3 degrees C develop in the Indian Ocean. They move eastward, in conjunction with an extended convection irregularity. The authors demonstrated that anomalous SST in the Indian Ocean is caused by surface insolation anomalies, associated with exceptionally large scale convection. They also showed that anomalous SST in the western Pacific Ocean are driven by anomalous latent heat

flux, and an increase in surface insolation. The difference in genesis was thought to be a reflection of structural changes in the MJO during its evolution.

Fink and Speth (1997) propose three forcing mechanisms for triggering the MJO. Firstly, a tropical SST rise, or secondly the phase of ENSO, or finally, atmospheric precipitable water participating in a feedback mechanism triggered the oscillation. Jones and Gautier (1998) stated that MJO was maintained by wave conditional instability of the second kind (CISK), and not by evaporation wind feedback, because surface latent heat flux anomalies were positive to the west of anomalous convection (and vice versa). However, Chao and Chen (2001) later found that wave CISK surface friction did not play an instability enhancing role in MJO.

The structural components of the MJO may be summarised as follows (Figure 2.2): In the Eastern Hemisphere, a stronger than normal trade wind inversion results in clear skies and an area of suppressed convection. Within the centre of suppressed convection, the clear skies (associated with stable air) allow maximum shortwave radiation to reach the ocean's surface, slightly raising the SST as the oscillation moves east.

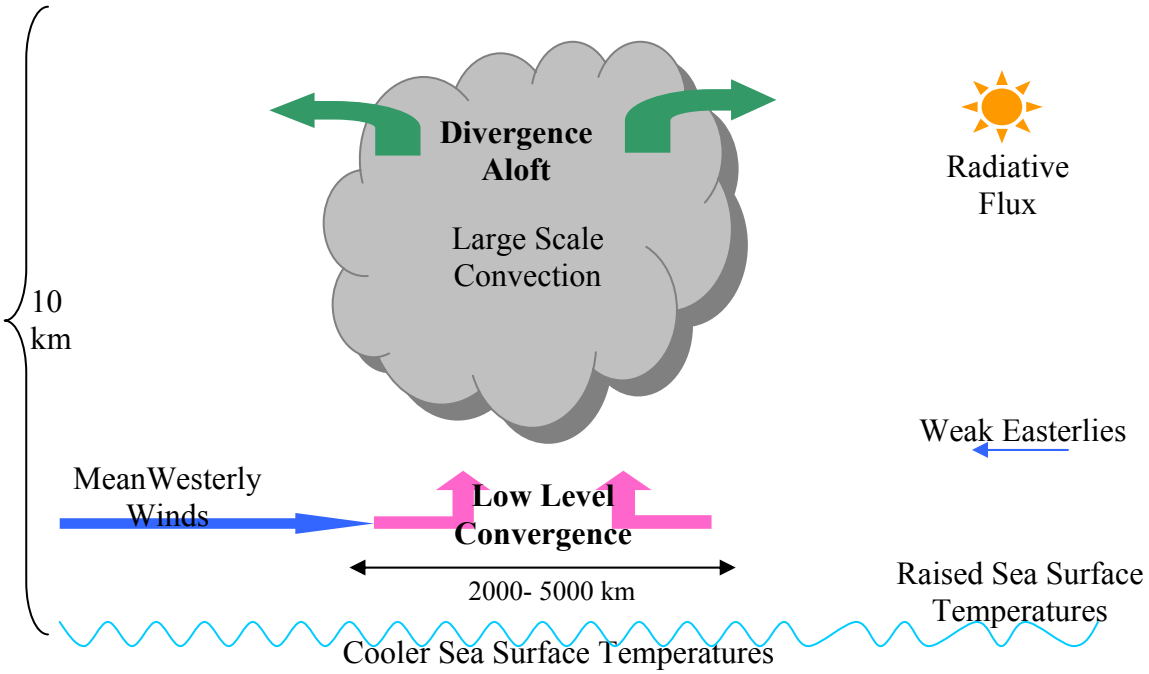

Figure 2.2 The Structure of the MJO (cross section). Large scale (2000-5000km x 500km x 10km) convective anomalies involved converging winds at sea level, and divergence at the top of the troposphere). To the east of (preceding) the MJO the surface of the ocean is anomalously warm, trailing (west of) the MJO are surface level bursts of westerly wind. The anomaly has a westward tilt when located over the Indian Ocean. (Adapted from Flatau et al 1997)

There are westerly wind bursts west of the convective region. Near the western edge of the area of suppressed convection, the trade winds weaken, triggering low-level tropospheric moisture convergence, leading to deep convection (Flatau et al, 1997). The vertical structure of the MJO changes as it propagates east. Myers and Waliser (2003) show that over the Indian Ocean there is a distinct westward tilt with height of the maximum moisture anomaly, while moist anomalies are almost vertical over the Pacific Ocean.

Seo and Kim (2003) summarise the propagation and initiation of the MJO thus: Kelvin and Rossby waves play a comparable role in zonal wind convergence. Moistening in the boundary layer occurs about 2 weeks before a new MJO develops, and is accompanied by Kelvin waves from the previous cycle and Rossby waves generated by reduced convection over the Indian Ocean. As the boundary layer is

already moist, convection is favoured. Therefore CISK is the primary propagation factor. This Kelvin/ Rossby interaction also explains suppression of convection to the west of the active convective core, as there is anomalous surface divergence.

The region of enhanced convection lies to the west of maximum moisture convergence. Zonal surface winds slow as they approach the central convergence. Nakazawa (1988) showed that the region of enhanced convection is characterised by SCC (Figure 2.3), which travel east at around 5 to 10 metres per second. The SCC are made up of cloud clusters that form in the east and break down at the western boundary of the SCC. The clusters are not long lived storm complexes, but a moving wave, that is, an oscillation. Milliff and Morzel (2003) were able to further demonstrate the westward moving cloud complexes amongst the eastward propagating MJO using statistical modelling techniques to analyse four times daily wind data.

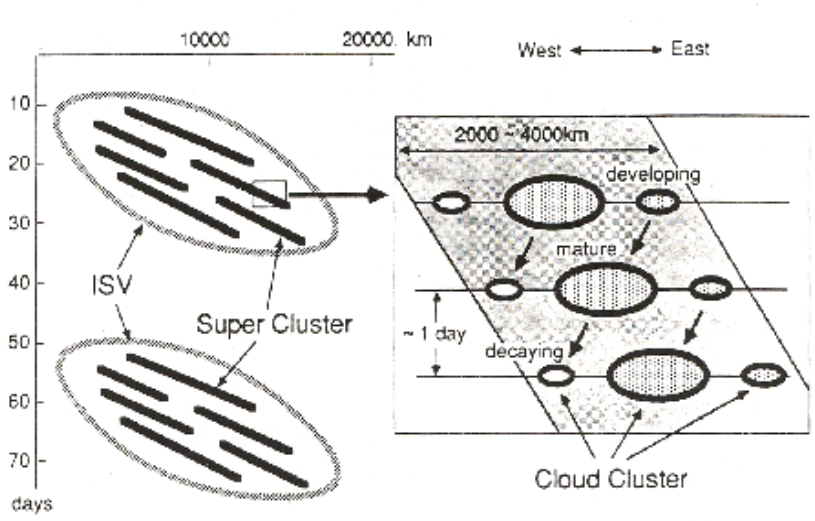

Figure 2.3 Schematic of Cloud Clusters. Vertical scale is time (days) while the horizontal scale shows zonal (east-west) scale (kilometres). Slanting heavy lines marked ISV represent Super Cloud Clusters (SCC). The fine structure within the SCC is illustrated at the left where smaller cloud clusters develop, move west and decay. (From Nakazawa, 1998).

In the Western Hemisphere surface air flows away from suppressed convection in both zonal directions towards regions of enhanced convection. In the upper troposphere, anomalous easterlies exit the western side of enhanced convection. In the lower troposphere, strong westerlies from the eastern side of enhanced convection flow into the area of suppressed convection (Madden and Julian 1994, Elleman 1997, Geerts and Wheeler 1998). Variations of 5-10 Dobson Units also appear in the MJO timescale in tropospheric ozone levels, significant against the mean background measure of 20 Dobson Units (Ziemke and Chandra, 2003). Not all of the elements outlined above can be located all of the time. The idealised MJO described above can only be detected when 30 to 60 day periods are extracted from the data. In reality the MJO varies in structure, amplitude and period.

Maloney and Hartmann (1998) report that frictional moisture convergence at the equator plays an important role in the MJO lifecycle. Regions of boundary layer convergence foster growth of positive water vapour anomalies east of convection, coinciding with 850 millibar easterly wind anomalies (consistent with Kelvin wave dynamics). Frictional convergence in front of convection helps slowly moisten the atmosphere to a state favourable for convection (this may set the time scale for initiation of convection in the Indian and west Pacific oceans after strong drying), and provides the mechanism for (slow) eastward propagation. Rapid drying, which occurs after convection passage with the onset of 850 hectaPascal westerly wind anomalies, may be the result of boundary layer divergence and subsidence or horizontal advection from the west/extra-tropics associated with Rossby wave circulation.

2.3 Spatial and temporal distribution of the MJO

The global scale of the MJO was first proposed by Madden and Julian (1972) and initial attempts to determine its size delineated an oscillation between 10 degrees N and 10 degrees S. (Madden and Julian, 1972). The MJO is now recognised from 20 degrees S to 20 degrees N and, while individual MJO events do travel farther into the mid-latitudes, the signal does not routinely penetrate these boundaries (Wheeler and Hendon, 2004).

The area of MJO activity may extend as wide as 60 degrees longitude, and reaches into the upper tropospheric boundary layer (250 millibars, 10000m), that is, the tropopause (Woolnough, Slingo and Hoskins, 2000). Mote et al (2000) used Empirical Orthogonal Functions (EOF) to clearly elucidate the MJO at 100hPa with coupled temperature and water vapour variations on the MJO timescale between about (tropical) 60 and 180degrees E. East of 180 degrees E Mote et al (2000) found the variations decoupled, and the water vapour variations appeared to speed up.

Geerts and Wheeler (1998) state that the maximum frequencies of occurrence for MJO convection lie between longitudes 60 and 80 degrees E, and 150 and 180 degrees E. Murakami (1980 i, 1980ii) found that during the Southern Hemisphere summer, there was a distinct tendency for OLR anomalies on 4-6 and 15-30 day timescales to propagate southward, illustrating the MJO's tendency to travel into the summer hemisphere.

The MJO is most prominent during the austral summer/autumn from November to March (Hendon, Zhang and Glick, 1999, Slingo et al, 1996). Maloney and Kiehl

(2002) confirm this, adding that the austral summer is when seasonal variability reaches a maximum over the equatorial Indian and western Pacific Oceans. Madden and Julian (1972) demonstrated, by processing data from as far back as the 1890's, that the MJO has existed throughout time, with a spatial duration comparable to the present observations.

The temporal distribution of the MJO was first described as 40 to 50 days (Madden and Julian 1971), however it was soon recognised that this temporal scale might be restrictive (Madden and Julian, 1972). Tropical stations show a slightly extended period of 30 to 60 days, but the phenomenon can extend from 22 to 79 days, with a median of 45 days (Madden and Julian, 1994). Lau and Peng (1987) proposed that this temporal scale is controlled by time taken for the MJO to circumnavigate the globe, its speed dependent on its vertical structure.

However, Maloney and Hartmann (1998) suggested that frictional moisture convergence in front of convection moistens the air, assists convection, thus promoting MJO onset, and determining time scale by re-initiation. It has also been suggested that the period is set by the build up and discharge of low-level moist static energy (Kemball–Cook and Weare, 2001).

2.4 Propagation of the MJO

The MJO shifts mass around the tropics by the easterly propagation of deep convective anomalies (Wang and Rui, 1989). Geerts and Wheeler (1998) outlined a process of surface air flowing away, in both zonal directions, from regions where there is suppressed convection, towards a region of enhanced convection. In the

upper troposphere anomalous easterly winds exit west of enhanced convection, and strong westerlies exit the eastern side of suppressed convection. Gyres are generated in the tropopause: cyclonic gyres trail suppressed convection and anticyclonic gyres trail enhanced convection.

The path of the MJO's centre of convection is affected by season, and Wang and Rui (1989) identified three main MJO propagation pathways: (1) eastward along the equator all the way to the mid Pacific Ocean, (2) eastward along the equator over Africa and the Indian Ocean and turning at the maritime continent NE (towards the NW Pacific Ocean) or SE (towards the SW Pacific Ocean), and (3) the main branch moves east to the date line with split centre/s moving northward over the Indian Ocean and/or western Pacific Ocean. Wang and Rui (1989) established that the path is season dependant because 78% of the MJO's taking the path (1) do so between December and May, path (2) dominates from November to April, and path (3) is favoured over the boreal summer (May to October).

In contrast, von Storch and Xu (1990) were only able to identify two migration pathways for the MJO: during the austral summer migration from the Indian Ocean, across northern Australia, into the South Pacific Convergence Zone (SPZC); or during the boreal summer, movement from the Indian Ocean, across southern Asia, and along the Inter-tropical Convergence Zone (ITCZ) to South America.

Matthews et al (1999) offered two reasons for propagation: a local mechanism operating over the Indian Ocean warm pool erodes to the west, and expands to the east via the equatorial Kelvin wave; a global convection feature initiates mean sea

level pressure (MSLP) anomalies which rapidly radiate eastward as dry equatorial Kelvin waves, slow at the Andes and over Africa, then reappear over the Indian Ocean basin in time to trigger the next MJO.

The average velocity of propagation increases from 5 metres per second in the Eastern Hemisphere to 10 metres per second in the Western Hemisphere (Geerts and Wheeler 1998). Hendon and Salby (1994) and Geerts and Wheeler (1998) attribute the acceleration to the changing structure of the MJO. To begin with the MJO responds as radiating Kelvin waves to a convective anomaly, then propagates faster in the Western Hemisphere as drier Rossby waves.

Matthews and Kiladis (1997) found that the position of the ITCZ is dependent upon an upper level westerly waveguide, and that this westerly waveguide is modulated on intraseasonal timescales by the MJO. When MJO convection is enhanced the westerly waveguide over the east Pacific Ocean is strengthened and there is an increase in high frequency (12days) convective activity. When convection is suppressed by the MJO in the west Pacific Ocean the westerly waveguide is weakened with reduction in high frequency convective activity.

Matthews et al (1996) performed a case study on a strong MJO event that occurred in 1988, and concluded that when an active MJO is over Indonesia, the anomaly progresses poleward and eastward along the SPCZ, possibly by a Rossby wave mechanism. Matthews and Kiladis (1999) found that high frequency waves propagating into the Indian Ocean may help initiate MJO. Near the dateline high frequency transients disturb the passage of the MJO and increase convective

variability of the MJO in the central Pacific Ocean during active phases of the MJO. Matthews (1993) described the easterly propagation of an MJO as most coherent during the southern summer and autumn, and disjointed in the Southern Hemisphere winter and spring.

2.5 Detection of the MJO

The cloudiness associated with MJO convection is the key to its detection using infrared satellite sensors. In fact, coherent convective cloud complexes have become markers for the MJO. The tops of convective clouds approach the tropopause, and are therefore very cold, and emit very little OLR. Variance of the OLR signal is measured, red noise rejected, and convective regions with the appropriate time scales extracted as MJO signals. The predictive skill with respect to the MJO from EOF of OLR data is about one week (Lo and Hendon, 2000).

The MJO incorporates super cloud clusters (SCC) (Figure 2.3) of about 1000 kilometres in width, made up of 100 kilometre cloud clusters with a lifetime of one to two days (Geerts and Wheeler, 1998).Therefore the MJO is easily discernible from satellite data and the presence of convection can be determined. Cloud masses are characteristic of the Indian and Australian monsoon onset (Madden and Julian 1994). There are 3 cloud types associated with tropical convection. Johnson et al (1999) report that cumulus, deep cumulonimbus and cumulus congestus all contribute to rainfall. All these clouds types, present in MJO convection, have the density and depth to distinguish them when using satellite data, allowing the MJO to be observed via satellite.

Wang and Rui (1989) found that clouds form west of the central equatorial Indian Ocean and west of equatorial Africa, and north of the equator during boreal summer, and from Australia to the date line and south of the equator during austral summer. Cloud activity favours the summer hemisphere and the general location of the ITCZ (Madden and Julian 1994). Observation of clouds in the tropical Eastern Hemisphere can be used to monitor the location and activity of the MJO.

Chen, Zhang and Houze (1998) observed that during convectively suppressed phases cloud systems are spatially small and with lifetimes of 3 hrs; they form, reach a maximum and die, preferentially in the afternoon when the ocean surface and adjacent atmosphere are the warmest. During convectively active phases with cold cloud coverage, spatially extensive areas of cloud tend to form in the afternoon and reach maximum aerial extent prior to dawn, and their decay extends into the next day. There is a tendency for the cloud tops to get progressively warmer. Preliminary results show boundary layer depth and mean virtual potential temperature have distinct afternoon maximums, indicating whether the phase is active or suppressed.

2.6 The MJO and ENSO

Perhaps the most recognised aspect of global climate, ENSO, interacts with the MJO (Madden and Julian 1994, Elleman 1997, Geerts and Wheeler 1998). Madden and Julian (1994) found that the MJO experienced a higher frequency oscillation (that is, the periods were generally shorter) during ENSO warm events. Gualdi, Navarra and Tinarelli (1999) demonstrated that while the MJO sustained an easterly shift over the date line during ENSO warm events, the overall level of MJO is not correlated with ENSO, except during exceptionally warm events when MJO is diminished.

During warm ENSO events MJO convection is able to propagate further eastward than typical, and westerly wind bursts trail further behind the MJO in ENSO years, compared with other (nuetral, La Ninã) years (Schrage,Vincent and Fink, 1999). Hendon, Zhang and Glick (1999) postulated that the level of MJO activity is weakly correlated with SST. Chen et al (2001) support this hypothesis and found the MJO/ENSO correlation coefficient has decadal scale variability and the strength of the relationship varies annually. In contrast, Slingo et al (1999) assert that the interannual MJO behaviour is not ENSO controlled.

This apparent conflict in ENSO/ MJO theory coupling is straddled by Kessler (2001), who speculated that while interannual changes in MJO are not ENSO related, relatively small zonal shifts of MJO produce proportionately large ocean effects. Two modes of MJO interannual variability were proposed by Kessler (2001):
(1) a zonally stationary variation of amplitude representing up to 20% of MJO variance (which is equal to 55% of the total tropical intraseasonal variance in OLR);
(2) an extension of the MJO envelope of approximately 20 degrees longitude during warm ENSO events.

There is an apparent problem when using MJO data to explore the teleconnection with ENSO. Measurements of the MJO activity prior to the mid 1970's are consistently lower, and only a weak, barely significant ENSO influence is apparent (Slingo et al, 1999). Further to these changes in the MJO, the Pacific Decadal Oscillation (PDO) was negative through the 1960's -70's (Mantua, 2000) which may account for the MJO appearing less pronounced. In addition to changes in the

manner of monitoring the MJO, the MJO itself may be modulated on a decadal timescale by the PDO.

Whether this difference is due to inaccuracies in data collection prior to satellite introduction, or reflects a real change in the MJO/ENSO teleconnection, is not yet determined. However, the ENSO/ MJO teleconnection has been described as follows: wind stresses cause SST cooling, flattening the SST gradient. This in turn spawns westerly wind anomalies and accelerated MJO growth, which then impacts upon, and promotes the strength of ENSO warm events (Kessler and Kleeman 2000, Zhang and Gottschalck 2002).

Zhang and Gottschalck (2002) also proposed that major warm events are preceded (from 6 to12 months) by very strong MJO Kelvin wave forcing. However, this link only holds true for data collected after 1980. They experienced similar problems to Slingo et al (1999) with data from1950 to 1979, and they could not establish an ENSO/ MJO connection. In contrast, the observed role of the MJO in the 1982/83 and 1997/98 ENSO warm events was clearly evident. Strong MJO activity seemed to trigger the actual onset of the warm phase (Weickmann 1991, Nakazawa 1998). For example, prior to the onset of El-Niño 1997 two episodes of large scale convection associated with the MJO reached the western Pacific Ocean, cooling the equatorial Pacific and generating Kelvin waves which displaced the western Pacific warm pool (Shinoda and Hendon, 2002). In turn, the activity of the MJO was diminished by the ENSO warm events it promoted in 1982/83 and 1997/98 (Hendon, Zhang and Glick, 1999).

2.7 The MJO and the Asian and Austral Monsoons

The MJO affects the intensity of, and the active and break periods in, the Asian and Australian monsoons (Yasunari 1979, Geerts and Wheeler 1998). The behaviour of the monsoons varies interannually due to the number of discrete MJO events, and their influence is most pronounced in the summer hemisphere (Kayano and Kousky, 1999, Lawrence and Webster, 2001). The early onset of the Indian monsoon in May 1995 was triggered by a strong MJO (Flatau et al, 1998). Knutson and Weickmann (1987) conjectured that the MJO influences the monsoon by retracting the East Asian Jet when the MJO is active in the Indian Ocean, allowing monsoonal convection. In 1980 Murkami Chen and Xie found that the onset and withdrawal of the Australian summer monsoon appeared to be determined by low frequency (24-91 days) oscillations, that is, the MJO.

Chen, Yen and Murakami (1988) suggested that the Indian Monsoon is initiated by water vapour interaction between the annual cycle and the MJO. The East Asian Monsoon is characterised by north south movement of water vapour fronts, which Chen, Yen and Murakami (1988) concluded results from eastward MJO propagation. The Australian summer monsoon exhibits the presence of a 30 to 50 day oscillation in rainfall variability, with wet spells around 40 days apart, which are related to the timing of the MJO (Suppiah, 1991, Hendon and Liebmann 1994, Geerts and Wheeler 1998). Linacre and Geerts (1998) indicate that rainfall records from Darwin reflect this cycle. When the MJO is active in the west central Pacific Ocean from May to October, it strengthens the typical winter westerly winds over southern Australia as it moves east (Knutson and Weickmann, 1987).

The MJO is important, but secondary to ENSO, in the onset of the monsoon in South China Sea (Wu and Wang 2000). Indian rainfall maxima also show fluctuations at intervals around 30 to 60 days when the monsoon is in its active phases (Madden and Julian 1994). Goswani and Mohan (2001) presented the idea that the active phase of the typical MJO intensifies the mean monsoonal flow. Drodowsky (1996) showed almost half of the monsoon events he studied had recurrence times between 30-60 days, suggesting that the MJO, although perhaps not dominant, is an important factor for timing within the Austral Monsoon season.

The MJO active phase displaces the ITCZ along with it, promoting convection, and strong monsoon years are associated with a higher probability of MJO active conditions (Goswani and Mohan 2001). Goswani and Xavier (2003) found that break periods were more predictable than active periods of the Indian Monsoon, and that the monsoon onset depends on modulation of large scale circulation by MJO activity. Goswani et al (2003) found that the wet and dry phases of the monsoon are dependent on space-time clustering of synoptic scale lows and depressions, and the clustering is modulated by the MJO.

2.8 MJO and Tropical Cyclone Activity

Eastern Hemisphere cyclones are associated with active MJO phases as proposed by Chappel and Bate (2000). The more active convective centres per season, the greater the cyclone activity. Hall, Matthews and Karoly (2001) discovered that the MJO is a strong modulator of cyclogenisis in the Australian region, with significantly more (fewer) cyclones when the MJO is active (inactive). They also found that the relationship between the MJO and cyclones became stronger in El Niño years.

Liebmann, Hendon and Glick (1994) document a relationship between cyclones of the western Pacific and the Indian Oceans. There is preferential cyclogenisis during the convective, active phase of an MJO, and cyclones cluster about the westward and poleward anomalies of the MJO. They found that all convective systems encourage cyclogenisis, so while the MJO is not unique in this it is important because it accounts for so much tropical variance. Maloney and Hartmann (2001) demonstrated that the westerly wind anomalies associated post-MJO-passage produce zonal variation in the westerly jet that concentrate eddy energy. Growing eddies create a favourable environment for the formation of tropical cyclones.

2.9 MJO Ocean Interactions

The MJO interacts with the ocean by modifying surface fluxes of momentum, heat and fresh water in the Indian and Pacific Oceans, where observed MJO signals are strongest (Zhang and Gottschalck 2002). Observational evidence of intraseasonal anomalies detected near the surface and in the upper layers of the ocean include temperature, salinity, mixed layer current and Kelvin waves (Jones and Gautier 1998, Zhang and Gottschalck 2002).

Feng et al (2000) stated that MJO zonal advection has a net warming and freshening tendency on the Pacific Ocean warm pool. Warming anomalies can reach 10 degrees Celcius in the western Pacific Ocean, and the MJO may be partially responsible. In the Bay of Bengal latent heat flux can vary by up to 20% (40 Watts per metre squared) under the influence of the MJO (Feng et al 2000). Maloney and Kiehl (2002) indicated that the MJO significantly modulates tropical eastern Pacific Ocean

SSTs during the Northern Hemisphere summer, typically by around 0.4 to 0.5 degrees Celcius, but by up to 2 degrees Celcius. They submit that the SST perturbations may be due to ocean dynamics and not surface heat fluxes, although Woolnough, Slingo and Hoskins (2000) found coherent relationships between surface fluxes and SST on intraseasonal time scales.

Zhang (2001) asserted that strong surface wind events associated with the MJO create a massive intraseasonal SST perturbation. Centred above the Equator, these anomalies have 0.5 degrees Celcius or larger amplitude, and extend approximately 2000 to 5000 kilometres longitudinally and 500 kilometres meridionally. These positive and negative perturbations show a tendency to move east and west and may be MJO forced oceanic Kelvin waves. The oceanic Kelvin waves modify the effect of equatorial upwelling, so that the mixed and surface layer temperatures may fluctuate.

Contrary to other interpretations of the MJO/ ocean interaction, the United Kingdom Universities Global Atmospheric Modelling Project (UKUGAMP) (no date provided) regarded the MJO as a coupled ocean atmosphere process. For this to be correct, they state that the MJO must impact on the ocean dynamics, and intraseasonal SST variation must organise convection. UKUGAMP found that convection associated with the MJO can generate SST anomalies, by modulation of shortwave and latent heat fluxes at the ocean's surface. This would result in a convection pattern with a positive SST anomaly before and to the east of convection, and negative anomaly to the west of and trailing convection. UKUGAMP's MJO model SST did organise convection with a structure similar to the observed MJO,

and the longer SSTs were inflated, the greater the magnitude of the precipitation anomaly. In contrast to other publications UKUGAMP proposed that the MJO is a coupled ocean atmosphere mechanism, with the periodicity determined by the strength of convection, surface fluxes and the heat capacity of the mixed layer.

2.10 Extra-tropical MJO signals

To complete the basic objective of this thesis it is necessary to investigate the impact of the MJO in the higher latitudes beyond the confines of the tropics. As the MJO is a tropical phenomenon much of the research with regards to impact has been with respect to tropical climate responses. Although research into the extra-tropical influence of the passage of an MJO is restricted, it exists, thus this section deals with other attempts to delineate the related atmospheric impacts of a large scale circulation anomaly in the tropics.

Chen and Marukami (1988) reported deep convective cloud over the western Pacific Ocean is modulated by the propagation of the 30-50 day mode (MJO). Chen, Yen and Murakami (1988) noted that the North Pacific Convergence zone shifts north-south, and water vapour fluxes merge over the South China Sea in response to the 30-50 day oscillation. Murakami, Chen and Xie (1980) noted that when there were strong OLR perturbations in the tropical Indian Ocean, there were corresponding southerly surges that originated over the cold mid-latitude Indian Ocean.

Development of convection along the South Pacific Convergence Zone (SPCZ) was linked with active MJO convection in the Indonesian region by Matthews et al (1996). They describe this as a response forced on the SPZC by the MJO via a

Rossby wave mechanism. Nogués-Paegle and Mo (1997) believed the meridonal seesaw of wet and dry conditions they observed over tropical and subtropical South America are related to the MJO.

Stone and McKeon (1993) looked at the relationship between the passage of the MJO through Darwin, and the probability of planting rains within 10 days and within the subsequent 30-50 day period. Their results, for Tamworth, Goondiwindi, Dalby Roma, Banana, Emerald and Charter's Towers, were inconclusive, and they suggested that a more accurate means of estimating the MJO was required for further research (Stone and McKeon, 1993). Hsu (2002) established that the western Pacific warm pool undergoes significant fluctuation on the intraseasonal timescale, and is strongly modified by the MJO. This modification is mostly in the Southern Hemisphere, and accounts for about 25% of the total modulation of the Pacific warm pool (Hsu 2002).

Bond and Vecchi (2003) relate the MJO to precipitation and flooding in Oregon and Washington. The impact differs between the Northern Hemisphere autumn (October, November, December) and Winter (January, February, March). Barlow et al (in review) found that during the Northern Hemisphere winter (November to April) the MJO modulates rainfall over southwest Asia (Afghanistan). They propose that when the MJO is inactive over the northwestern Indian Ocean, Afghanistan's winter rainfall is enhanced. The predominant reason appears to be modulation of the local jet resulting from MJO wind anomalies.

Goswani and Xavier (2003) and Goswani et al (2003) showed that modulation of the Indian monsoon was via a number of factors including: meridonal shear of the eastward component of winds; high cyclonic vorticity at low levels; and enhancement and/or weakening of zonal wind shear. The wind shear and low level vorticity were attributed to the MJO.

2.11 Discussion

The MJO is a large-scale tropical anomaly of the atmospheric circulation with a baroclinic structure. Convection, cloudiness, westerly wind bursts and zonal wind anomalies are all associated with the MJO. The periodicity of the MJO is about 30 to 60 days, and is generally confined to 20 degrees N and 20 degrees S of the Equator. The MJO propagates in a Kelvin wave-like manner at speeds of 5 metres per second and 10 metres per second in the Eastern and Western Hemispheres respectively.

MJO Kelvin waves are believed to trigger and intensify ENSO warm events. The on-set of the Indian and Australian monsoons can be initiated by MJO, and the activity of monsoons and cyclones is positively correlated with MJO activity. The MJO clearly influences Australian weather and climate but its exact role has not been defined. The use of real time indexes that identify and predict the MJO will assist in defining its influence. This could lead to the more accurate prediction of climate features, such as rainfall. There is some evidence that the MJO influences synoptic factors beyond the tropics.

At present, although there has been some examination of teleconnections between the MJO and rainfall at higher latitudes, analysis has been restricted by the ability to

accurately identify, forecast and/ or model the MJO. The following chapter discusses some of the attempts to represent the MJO, using models and statistical techniques. Given the temporal characteristics of the MJO, and the timing of many pastoral and agricultural tactical decisions, the ability to predict the timing and nature of MJO teleconnections will be important to the Australian rural sector.

Chapter 3 Modelling and Predicting the MJO

3.1 Introduction

Modelling climate systems assists with synoptic weather and climate forecasting. When models are capable of closely representing the observed behaviour of the MJO, it suggests the parameters used are accurate and reliable, and forecasting more dependable. A number of global scale climate models have been developed (see below), and some are being used to improve predictions of climate systems like ENSO. The MJO has been factored into some models, with implications for the prediction of MJOs, and other phenomena. To investigate any possible responses of rainfall to the MJO, a system able to approximate the state of the MJO is required.

3.2 Modelling the MJO

All climate modelling is limited by our knowledge of the physical processes, and our ability to accurately reproduce those physical features of climate via (computer) modelling. When models, or aspects within models, approach reality we can assume that the applied factors approach reality. Consistent problems with accurately modelling the MJO (or any other climatic feature) provide an insight into which physical aspects are being misrepresented.

Swinbank (1986) applied transformed (EOF) data to a general circulation model, and produced convective areas, and wind anomalies with a Kelvin wave like structure. The periodicity produced by this model was too long (90 days) or too short (20 days) to accurately represent the MJO. Using a CISK model, Miyahara (1987) produced a baroclinic fluctuation with a Kelvin/ Rossby wave-like pattern, but this decayed, and

the resultant pulse did not mimic the observed nature of the MJO. Stringer (1992) used Darwin MSLP to create an index for locating the MJO, and predicting rainfall for Darwin. He found that the events monitored were not coherent over a broad geographical area. Also, Stringer (1992) used data that was only updated weekly, creating accuracy problems in the last portion of any information produced.

A simple statistical model for the MJO was developed by Elleman (1997), which accurately predicted the propagation, spatial pattern and location of extreme anomalies, but failed to reproduce the magnitude of those anomalies, which were 5-10 days late. Elleman (1997) suggested that multiple regression techniques might best compliment dynamic forecast models. Lin, Neelin and Zeng (2000) introduced the rationale evaporation wind feedback (EWF) to explain maintenance of the MJO. Feedback from an interactive SST was thought to be an important factor in simulating intraseasonal variability in model perturbation experiments (Waliser, Lau and Kim 1998).

In contrast, Lin, Neelin and Zeng (2000) found that evaporation wind feedback does not account for oscillation sustenance in their model, and that mid-latitude excitation (storms), must assist feedback in maintenance of the signal. However, Mo (2001) asserted that while statistical models are good for real time monitoring of MJO, they are not able to capture the magnitude.

Raymond (2001) developed a model in which cloud radiation interactions make the tropical atmosphere susceptible to large scale radiative–convective overturning: disturbance dynamics are more balanced as low level flow vorticity, rather than

being divergence related. Hartmann and Maloney (2001) attempted to model the tropical cyclone responses to the eddy growth they had observed. Their stochastic barotropic model was able to capture some of the relationship between MJO associated zonal wind variation and the growth of eddies, but the modelled eddies were smaller scale and failed to travel west, as distinct from the observed eastward moving eddies.

Maloney (2002) found models are highly dependent on lower tropospheric moistening by surface convergence, eastward propagation of the MJO all the way to the coast of South America (which rarely occurs in reality), and fail to predict strong, low level Indian Ocean westerlies near to and west of convection. Using a non-hydrostatic global model that applies cloud-resolving convection parameterisation Grabewski (2003) produces coherent MJO structures. These simulations suggest that deep convection coupling, free tropospheric moisture and large scale flow are essential for coherence in MJO-like structures. There are complex stratiform precipitation and vertical heating profiles important to the maintenance of the MJO, however all the models lack a functional equivalent of stratiform precipitation (Lin et al 2003). Lin et al (2003) believe better understanding of the vertical structure of the active MJO phase will assist modelling.

3.3 The MJO in Climate Models

During the Atmospheric Model Intercomparison Project (AMIP) in the 1990s, over fifteen atmospheric Global Climate Models (GCM) were used to simulate tropical intraseasonal oscillation (Slingo et al, 1996). They used upper tropospheric potential and zonal wind data. Most of the models they reviewed did produce an eastward

propagating anomaly, but some models displayed unrealistic standing oscillations, or chaotic movements. The models that did have clear eastward movement, demonstrated typical periodicities that were reasonably close to those observed, but shorter.

Further, none of the AGCM's captured the dominance of the MJO over tropical fluctuations, and they all underestimated the strength of intraseasonal variability. Some of the models could reproduce the suppression of the MJO during the strong ENSO event of 1982/83, but Slingo et al (1996) concluded researchers needed more climate information to improve modelling.

Sperber et al (1997) stated that of those AMIP models they analysed, the Goddard Laboratory for Atmospheres (GLA) and United Kingdom Meteorological Office (UKMO) simulated the most realistic MJO. The GLA model produced a good prototype of convection over the western and central Pacific Ocean and into the South Pacific Convergence Zone (SPCZ), and was better at feigning the eastward propagation. Both models exhibited the baroclinic structure observed in the real MJO. They concluded that the models suggest wave-CISK is the eastward propagation mechanism rather than evaporative feedback.

Later, Wang et al (2001) re-investigated the AMIP runs, and found that some models reasonably reproduced the main aspects of the MJO. A Kelvin wave framework was used to synthesise the MJO into an 1800 day integration of the Hadley Centre Unified Model (Matthews et al 1999). These researchers produced a model MJO output that had realistically large spatial structure and propagation characteristics, but

deep convection was not as coherent, and the propagation was not smooth. The model provided no clues as to the origin of convective anomalies. The accuracy of this model suggested an underlying, but strongly modified, Kelvin wave mechanism within the MJO (Matthews et al 1999). The introduction of SST data did not improve model accuracy, as MJO variability results from the mean seasonal convection (Hendon, Zhang and Glick 1999).

Jones et al (2000) applied the National Centre Environmental prediction (NCEP) Medium Range Forecast (MRF) model, but found that it had difficulty maintaining the MJO, severely impacting its forecasting capabilities. Chao and Chen (2001) employed atmospheric GCM integrations, and found that they do not support the idea that surface friction plays an instability enhancing role in MJO. The effect of feedback mechanisms on simulated MJO was to generate a strong signal when there was turbulent surface flux, but the frequency generated was far too short: there were 16 to 28 MJO events a year compared with 6 to12 a year in reality (Colon, Lindesay and Suarez, 2002). They also found that simulated MJO is most sensitive to SST and moisture availability due to wind driven feedback.

Sperber et al (2001) assessed two atmosphere–ocean models (GOALS and SINTEX) and found both performed best over the Indian Ocean, with no ability to capture eastward propagation over the western Pacific Ocean. Using an ocean GCM and MJO observed conditions Watterson (2002) investigated MJO like activity in the Commonwealth Scientific and Industrial Research Organisation's GCM models. He found that while eastward propagation was modeled, these features only travelled at half the speed of the MJO. Using shallow mixed ocean layers, the models produced

propagation velocities closer to those observed. Waliser, Murtuguude and Lucas(2003) demonstrated that the MJO produces equatorial cooling, reduces the mixed layer depth in the Indian and (western) Pacific Oceans, produces warming about the Maritime Continent, and generates a current anomaly in the western Pacific and Indian Ocean.

None of the models were able to reproduce all the salient features of the MJO (periodicity, velocity, convection, zonal wind anomalies). The statistical techniques originally applied by Madden and Julian (1971) and later methods by others required time for data collection and subsequent manipulation. To produce MJO 'nowcasts', closer to synoptic style forecasting, required a method capable of locating the MJO in real time

3.4 Forecasting the MJO

As the timing and strength of each MJO event differs, many attempts have been made to forecast its onset and relative strength. To assess the impact of the MJO on Australian rainfall and develop a simple predictive tool it was imperative to have a system capable of monitoring the MJO, and predicting its eastward propagation rate. That is, the forecast must be capable of identifying when and where the MJO is, and will be, with some reasonable degree of accuracy. Information on the characteristics of the MJO at a time, might allow MJO predictions for some time period.

Waliser, Lau and Kim (1998) assessed the ability of a general circulation model to predict the MJO, and their results indicated that this model is useful to around 20-30 days for 200 hectaPascal velocity potential, and only 10-15 days for precipitation.

Hendon et al (2000) discovered that when model forecasts were initialised during active MJO periods, they failed to capture the eastward propagation, and systematically forecast weakening and/or retrograde movement. It was then found that EOF transformed data produced the best results in a model when the MJO was active at initiation (Lo and Hendon, 2000). Hendon (2000) conducted experiments that indicated that air-sea coupling does not alleviate MJO modelling problems

Lee et al (2001) attempted to include parameters, such as cloud radiation, into GCMs in order to improve their forecasting abilities, but found the introduction contaminated eastward propagation in their model. ECWMF use a 51-member ensemble to forecast the MJO (Vitart, 2003) and their model can predict the time evolution of the MJO well, however the model cannot propagate the MJO beyond the maritime continent, and suffers significant systematic SST and precipitation errors. Beyond about 10 days this model has little real skill.

The use of statistical analysis such as empirical orthogonal function (EOF) allows a spatially extensive, coherent signal to be extracted from unspecified variance (Kessler 2001). The use of EOF for multivariate analysis in climate research may be described as the derivation of dominant patterns of variability from a statistical field (von Storch and Zwiers, 1999). EOF coefficients are uncorrelated and independent for zero lag, and the bulk of variance is accounted for by the first few EOF's. Wheeler and Kiladis (1999) demonstrate that spectal peaks in OLR data, where estimated background spectrum are removed, provide proxy MJO information. Wheeler and Weickmann (2001) develop monitoring and prediction of tropical variability at the intraseasonal timescale using filtering of global data for the

measurement (eg OLR) of interest. Their method can monitor and predict (to about 15 days) the location of the MJO.

Wheeler and Hendon (2004) report an all season real-time multivariate MJO (RMM) index for monitoring and prediction in Australia. The index derives from three variants: OLR; and 800 and 250 hectaPascal winds. This index has a distinct advantage over other attempts to model MJO – it exists in real time. Extensive manipulation of data is unnecessary, so the index is practical for synoptic scale forecasting and fieldwork. Wheeler and Hendon's (2004) predictive system is based on an EOF analysis of MJO data. The MJO data consists of anomalous OLR spectra from satellite imagery, and the zonal wind at geopotential heights 800 and 250 hectaPascals (that is: the bottom and the top of the troposphere respectively). The all-season RMM Index fulfils the parameters delineated, and can forecast when and where the MJO is, and will be.

The RMM Index divides the eastward passage MJO from Africa to the central Pacific Ocean into Phases 1 to 8 inclusive. The MJO can be identified in one of the phases on a daily basis (the when and where). Each phase lasted from 4-10 days (Wheeler and Hendon, 2004) so that the MJO convective anomaly can be located and forecast. These RMM Index phase lengths are analogous with the 30 – 60 day MJO timescale.

Each phase can be associated with the Eastern Hemisphere location of the MJO's convective (convection can be identified from satellite data as a negative OLR anomaly) parcel (Figure 3.1): Phase 1 corresponds with negative OLR anomalies

over Africa and the western Indian Ocean; Phases 2 and 3 correspond with negative OLR anomalies over the Indian Ocean; Phases 4 and 5 correspond with negative OLR anomalies over the Maritime Continent; Phases 6 and 7 correspond with negative OLR anomalies over the Western Pacific Ocean; and Phases 8 and 1 correspond with negative OLR anomalies in the Western Hemisphere (mid Pacific Ocean) (Wheeler and Hendon, 2004).

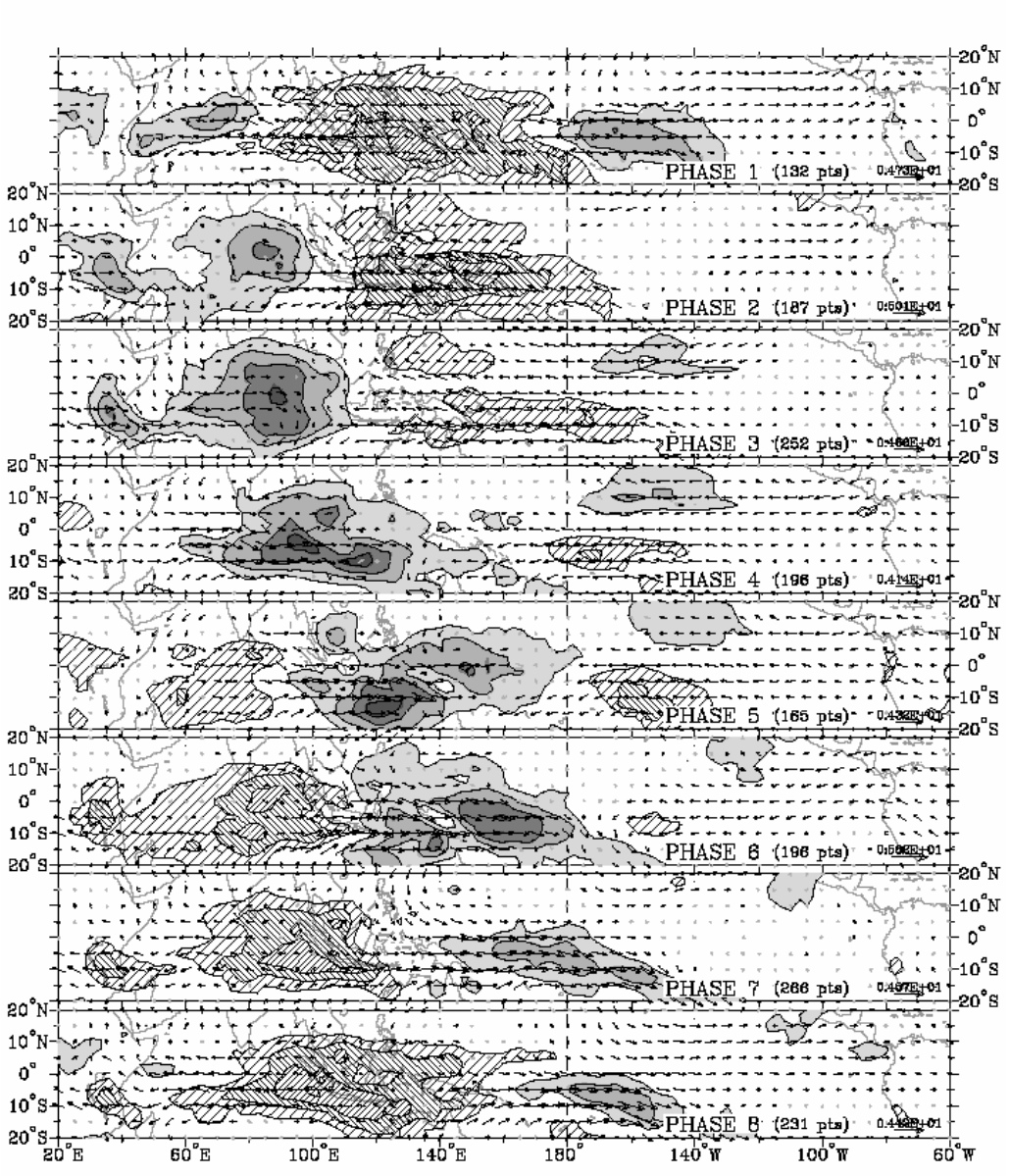

Figure 3.1 OLR and 850hPa wind anomalies. The strongest negative OLR anomalies (indicated by full shading, lined shading indicates positive OLR anomalies) correspond with the location of the eight RMM Index phases: Phase 1 -mid Pacific Ocean, Africa and the western Indian Ocean; Phases 2 and 3 negative OLR anomalies in the Indian Ocean; Phases 4 and 5- Maritime Continent; Phases 6 and 7 - Western Pacific Ocean (From Wheeler and Hendon, 2004, p39).

The RMM Index generates 2 independent numbers to describe the daily state of the MJO (Wheeler and Hendon, 2004). These results were used by Wheeler and Hendon, (2004) to produce phase-space diagrams (Figure 3.2), where the 8 phases of the MJO were defined. The 8 phases correlated with the geographical location of the negative outgoing longwave radiation (OLR) anomaly associated with convection in the active phase of the MJO (Figure 3.1).

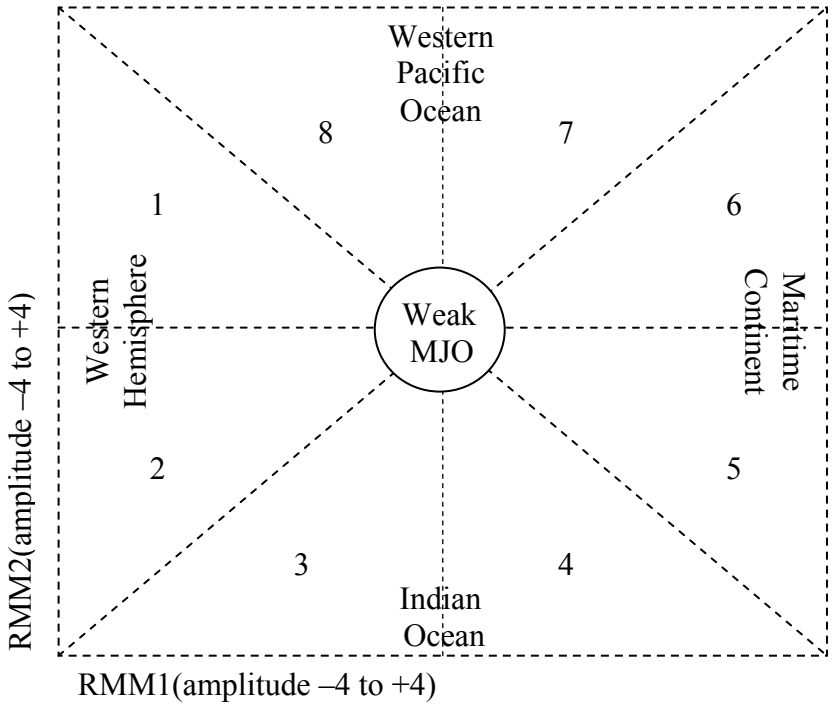

Figure 3.2: RMM Index phase space diagram (psd), including 8 equal angle phases (1-8), and the corresponding geographical location of the MJO active phase. The x axis is defined by RMM1, and the y axis defined by RMM2. RMM1 and RMM2, the two independent numbers describing the daily state of the MJO, are plotted against one against the other to produce a phase-space representation of the MJO. The weak MJO described at the centre of the phase space diagram refers to when both the RMM 1 and 2 have an absolute value of less than 1. The MJO can generally be observed to 'travel' counter clockwise about the centre. (Adapted from Wheeler and Hendon, 2004).

The RMM Index provides a (almost) real-time estimate of the status of the MJO, indicating both location and amplitude of the anomaly. Higher and lower frequency signals have been removed form the index during its construction (Wheeler and Hendon, 2004). The RMM Index phase of the MJO can be forecast out to 14 days. Forecasting the MJO using GCMs has not been successful, with the models unable to capture the eastward propagation that is a distinct MJO feature. Monitoring the MJO, and projecting its movement from its current location and past behaviour has proved viable, and is similar to traditional synoptic forecasting techniques. Using the RMM Index has a distinct advantage over using models to represent the state of the MJO.

One problem within the RMM Index occurs when the amplitude, or signal strength, of RMM1 and RMM2 is low. When the absolute value of the signals is less than one then the accuracy of the RMM Index is reduced (Wheeler and Hendon, 2004). The reduction in amplitude may occur because the convection and winds are not anomalous enough to generate a strong signal, or because other tropical features, such as the ITCZ, tropical cyclones, or convection, cause noise at the temporal scale of the MJO. When the signal strength falls below and absolute value of 1 for the first and second EOF, then no 14 day MJO forecast is produced.

3.4 Discussion

The MJO is a complex phenomenon, and is difficult to model statistically and dynamically, especially as some of the physical aspects are poorly understood. Models that take SST and shallow ocean layer depth mixing reproduce the MJO more accurately, indicating there is some MJO ocean interaction. Many models perform better over the Indian Ocean than elsewhere, suggesting that the models are

not reproducing some function of the Maritime Continental and Pacific Ocean regions accurately. Forecasting the MJO, especially in real time, has been challenging because analysis of data are required to extract the MJO signal. The RMM Index is a useful measure of the MJO because of its accuracy, almost real time reflection of the state of the MJO, and because it has some predictive capability.

Chapter 4 The relationship of the MJO and Rainfall beyond the Tropics

4.1 Introduction

Research into the MJO has been extensive (Waliser et al, 2004, Jones et al, 2004), and prediction capabilities have emerged, developed and are being refined, however most of the research has been focused on tropical regions. Despite the level of interest in the MJO, there is little empirical evidence defining possible mid- or high-latitude impacts. Some limited evidence suggested that the MJO might influence rainfall well beyond the tropics

Chen, Yen and Murikami (1988) noted the MJO caused an east-west shift in the convergent centre of water vapour over the Asian monsoon regions, that the North Pacific convergence Zone (NPCZ) undergoes north-south shifts, water vapour flux from the Indian monsoon westerlies move, and the Pacific anticyclone trade winds merge over the South China Sea. Chen and Murikami (1988) found that regional weather systems north of 20 degrees north and south respond to the eastward propagation of the MJO.

Barlow et al (in review) noted that southwest Asian precipitation is modified by the MJO, when it is located near that region. Stringer (1992) demonstrated an impact for Darwin, but could not demonstrate coherent events over a broad geographical area. The ability of the MJO to influence regional weather systems might be apparent in low *and* higher latitude Australian rainfall data.

This analysis provides an examination of the influence of the MJO on mid and high latitude Australian rainfall, via teleconnections. This work also includes an investigation of possible teleconnections and causal systems. It is argued that if the MJO were manipulating mid- and high- latitude weather and climate patterns, then an investigation of the teleconnections responsible for the expression of a tropical phenomenon in the higher latitudes should be conducted.

Australian and global daily rainfall data sets, ranging in quality and spatial coverage, were selected for this analysis. The different data sets produced consistent results, but indicated that while the larger data sets did not have the quality controls of the smaller ones, they might be utilized to produce a simple tool indicating regional areas of suppressed and enhanced rainfall, based on the RMM Index.

The RMM Index (Wheeler and Hendon, 2004) was selected to represent the MJO because it provides a timely, accurate and daily description of the state of the MJO. This index provided a means of removing the MJO signal from the background noise, so that statistical analysis could be applied. Initially Kruskal-Wallis tests were applied to a very limited subset (Queensland high quality stations) of the high quality data set, and results indicated that some RMM phases were influencing the timing of rainfall at several of the stations selected. These provisional results indicted that a full statistical analysis of the available data was viable.

The Kolmonogrov-Smirnov (K-S) test was applied, constructing the distribution of rainfall with respect to the eight phases of the RMM Index at a 95 % ($p = .05$) significance level. The objective was to provide generalized forecasts with respect to

regions, and not reproduce synoptic forecasting, so stricter statistical testing was not required (Stone, personal communication, 2004).

The investigation into the teleconnections and possible causal systems allowing the defined MJO-rainfall response was conducted using MSLP to represent the state of the atmosphere. Anomalies were defined for each RMM Phase, revealing the broad characteristics of the global atmosphere, for the tropical locations of MJO active convection. The temporal length of the data used was dependant on the length of the RMM Index, which was available from 1 June 1974 (satellite operation commenced). There is no RMM index data for the period 17 March 1978 to 31 December 1978 inclusive (satellite inoperable). This analysis used RMM Index data up to and including 30 April 2004. These dates define the temporal extent of all data processed for this analysis. The precipitation, RMM phase and MSLP data were all derived and sourced independently of one another.

4.2 Data

4.2.1 Rainfall

The high quality (hq) Australian daily rainfall records (Lavery, Kariko and Nicholls, 1992) were used (Appendix 1). From this point all testing with respect to this data set will be referred to as hq.

The Australian Bureau of Meteorology (BoM), (2003) maintains daily rainfall records (Appendix 2). From this point all testing with respect to this data set will be referred to as BoM.

A daily rainfall data set for the world was obtained through World Meteorological Organization (WMO) World Weather Watch Programme according to WMO

Resolution 40 (Cg-XII), from National Oceanic and Atmospheric Administration (NOAA) National Climatic Data Centre, USA (Appendix 3). From this point all testing with respect to this data set will be referred to as WMO.

4.2.2 MJO

The daily RMM Index (Appendix 4) phases of the MJO are available as text file for downloading from:

http://www.bom.gov.au/bmrc/clfor/cfstaff/matw/maproom/RMM/RMM1RMM2.74toRealtime.txt

4.2.3 Mean Sea Level Pressure

Daily MSLP data was obtained from the NCEP/NCAR- Reanalysis II (Kistler et al, 2000) dataset (Appendix 5) in 2.5 degrees latitude by 2.5 degrees longitude grids.

4.3 Methodology

4.3.1 MJO/rainfall

A statistical analysis was made of the possible correlation between Australian rainfall across the relevant latitudes (degrees south) and the low latitude passage of the MJO. Using the hq data set and the MJO, Kruskal-Wallis (K-W) testing was applied to determine if, at any of the rainfall data stations, some phase (or phases) was (were) significantly ($p = .01$) different from the other with respect to rainfall.

K-W testing compares cases where there are more than 2 sets of sample measurements. The assumption (null hypothesis) is that there is no significant difference between the samples (Fogiel, 1996).

Having determined that there were stations where rainfall was influenced by the MJO, further definition of the influence was sought by identifying the location of all the significant results. The statistical significance was relaxed from p=. 01 to p=.05 to provide the best spatially coherent results while maintaining a strong statistical relationship. Individual towns are not specifically identified by the results, and only spatially coherent regions of significant results identified.

The hq data set provided both spatially limited high quality results, for comparison with, and validation of, results from the lower quality but better spatial coverage of the BoM data set. The hq set has 180 and the BoM approximately 4237 rainfall stations Australia wide .The Kologmrov–Smirnov (K-S) statistic was applied to test the hypothesis that rainfall and the MJO were significantly related. The K-S distribution was applied to establish the 95% confidence interval (p= .05) for the cumulative distribution (rainfall). The K-S distribution tests the null hypothesis that the population distribution from which the data sample is drawn conforms to a hypothesized distribution (Fogiel, 1996). In this instance, the (K-S) statistic tested the hypothesis that any sample rainfall day came from the specified distribution (RMM Index phase). Significant results indicate rainfall for that phase at that location has a significantly different distribution to the rainfall at that data point for any other phase.

For each rainfall data recording station, a set of analogue days was created, with a corresponding set of analogues daily MJO phase. Missing rainfall values were simply ignored for the analysis, and the corresponding RMM Index values were also dropped from the analogues set. The K-S distribution was constructed. Significant

results were divided dependant upon whether they fell above or below the mean. That is, for those significant sites (p = .05) if the mean daily precipitation of analogue days was less than the mean daily precipitation from analogue days derived from all other phases then the rainfall was considered suppressed for that phase at that site. Otherwise, the rainfall was considered enhanced. Thus, regions of rainfall suppression (significant and below the mean) and enhanced rainfall (significant and above the mean) could be discerned.

4.3.2 MSLP

The results (see 4.4.1 below) for the K-S distribution of rainfall and MJO suggested the passage of the MJO across the tropics produces teleconnections that enhance or suppress the probability of rainfall across mid-latitude Australia. MSLP was identified as a relatively simple and accurate reflection of the synoptic state. The NCEP/NCAR reanalysis daily MSLP data was analysed with respect to RMM phase, to gain some insight into how the passage of the MJO might be impacting upon rainfall in the higher latitudes.

The MSLP anomaly was calculated for every phase at each grid point by determining the MSLP for that phase, and subtracting MSLP for all of the other phases, and then calculating the mean of that difference for every NCEP/ NCAR grid (2.5degrees x 2.5 degrees). Low (cyclone) and High (anti-cyclone) MSLP anomalies were revealed. The broad scale anomalies exposed by this method indicate a generalized synoptic picture for each phase. The anomalies revealed can be defined as the general or underlying synoptic picture for each phase. Each area of anomalous MSLP

tends to have a central area where the anomaly is strongest, or where the Low (L) or High (H) MSLP maxima tend to be located.

4.3.2 Rainfall lagging MJO

If the passage of the MJO were to more or less contemporaneously influence rainfall at higher latitude locations, then the correlations would decrease if the analogue sets of rainfall data were lagged behind the RMM phase data. The BoM data set was applied to perform this examination, as the other data sets were too spatially indistinct to generate a viable result. To examine lag, rainfall data was lagged behind (0 to 60 days) the MJO data for each BoM site. A sixty-day time frame accounts for the length of most MJO cycles. A K-W test was performed on the count of the significant sites ($\alpha = .05$). It was required to examine the lag at all the sites simultaneously, and a K-W test selected to perform this task. The K-W test determined how many sites remained significant for all the sites, as rainfall was lagged behind the phase (Figure 4.10). Therefore, at zero days every significant site across all the phases is summed.

4.3.3 Strong MJO Signals

When the first two EOF values (RMM1 and RMM2) are less than an absolute value of one, the MJO amplitude can be described as weak (Wheeler and Hendon, 2004). No 14 day MJO forecast can be produced when the amplitude is weak. The oscillations (anomalous movements from the mean state) are much smaller, as measured in the OLR and zonal wind data. The MJO may be regarded as having lower energy, and perhaps modifies the response determined for precipitation. To determine if the MJO signal strength could affect the forecasting tool developed here,

the BoM K-S distributions were reconstructed using only RMM 1 and 2 with a value greater than an absolute value of one. The same method of K-S testing as described in 4.3.1 (above) was then applied.

4.3.4 Phase Locking

The duration of an RMM phase can be as short as four days, giving very little lead time for agricultural forecasting. To 'expand' the lead time to extend forecasting each phase was 'locked', that is pairs of phases were treated together as supersets of the RMM phases. RMM Phases 1 and 2, 3 and 4, 5 and 6, and 7 and 8 were treated as four segments of an MJO cycle. The MJO divisions were reassigned, based on supersets of Wheeler and Hendon's (2004) 8 phases. The MJO is located in the same region (Eastern Indian Ocean, western Indian Ocean, Maritime Continent and western Pacific Ocean respectively) in the new RMM supersets.

4.4 Results

As the MJO propagated east from over the tropical Indian Ocean, corresponding broadscale changes in the precipitation pattern at higher latitudes occurred. Enhanced and suppressed precipitation areas for Australia responded to the passage of the MJO. Based on the RMM phase, distinct regions of enhanced and suppressed rainfall were established. Regions of enhanced rainfall tally with L pressure anomalies, or are coastal regions that would experience onshore flow as a result of the local MSLP anomaly. Where areas of suppressed rainfall were identified, corresponding regions of anomalous H pressure or expected off-shore flow are evident. These results were statistically independent from the phase/rainfall distribution results, yet demonstrated atmospheric characteristics that concurred with the rainfall patterns noted.

The MSLP/MJO results not only assisted interpretation of the rainfall results, but validated the MJO rainfall results. The large scale air flow that would result from such MSLP values, show a relationship with the broad scale precipitation suppression and enhancement patterns. Results were presented by RMM Index Phase 1-8. The various rainfall data sets were denoted as hq, BoM and WMO. All rainfall station sites tested were indicated on every map, and are coloured grey if no significant result was returned. Blue coloured rainfall station sites indicate a significant result above the mean, red coloured station sites indicate a significant results below the mean.

4.4.1 MJO and rainfall results

4.4.1.1 PHASE 1:

The hq / RMM Phase 1 K-S distribution (Figure 4.1.a.) shows the occurrence of enhanced rainfall along the south western coast of western Australia, and extending into the Avon River catchment. This rainfall response continues through the coastal South Australian Gulf catchments, coastal Victoria, and north-western Tasmania. Rainfall is suppressed when the RMM index is in Phase 1 across the northern and eastern Australian coasts.

The hq and BoM data set/ RMM Phase 1 K-S distribution concurs with the hq data set, with increased spatial coverage and density. Widespread rainfall suppression is noted through northern Australia, and the east coast. The eastern coast of Tasmania shows evidence of rainfall suppression during RMM Phase 1.Areas of enhanced

rainfall with respect to Phase 1 are located along the southwestern coat of Western Australia, the coastal South Australian Gulf catchments and northwestern Tasmania

An anomalous H pressure system dominates the Southern Hemisphere region from 40 E to 150 W, with the anomaly centred over eastern Australia when the MJO is in Phase 1. Corresponding precipitation distributions show suppressed rainfall across Australia's north and along the east coast, explained by the MSLP anomaly. The west and southern coasts have enhanced rainfall probabilities, a result of the onshore flow from westerlies to which this region would be subjected if a H pressure system were located near the east Australian coast.

During Phase 1, the RMM Index located the active centre for MJO convection over the western Indian Ocean basin (initiating) or the mid Pacific Ocean (breaking down) A corresponding L pressure anomaly was located over the northwestern Indian Ocean basin. The marked L pressure anomaly through the Middle East, the sub-continent and northern Asia is linked with enhanced rainfall across central India, and northern Asia. Enhanced rainfall patterns over central Africa and the United States, and rainfall suppression along the United States/Canadian seaboard are reflected by the RMM Phase 1 MSLP anomaly patterns.

An H anomaly spans the southern Eastern Hemisphere, extending into the Western Hemisphere over the Pacific Ocean. There is a corresponding, but very much smaller Northern Hemisphere H anomaly. The extreme of the austral anomaly is centred over eastern Australia. During Phase 1 suppressed rainfall is seen through northern Australia and along the eastern seaboard, and areas of enhanced rainfall along the

southern Western Australian coast and exposed coasts of South Australia, Victoria and Tasmania.

The anti-clockwise winds associated with the RMM Index Phase 1 H anomaly can offer some clarification of how the MJO influences the rainfall pattern. Moist onshore winds would be experienced along the southern coasts from the anticlockwise circulation of air about a H system. The suppressed regions of northern Australia would be associated with dry, offshore winds.

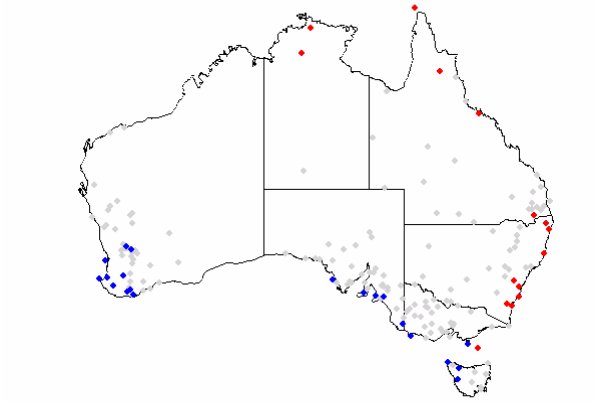

Figure 4.1.a Significant sites (p=.05) for K-S distribution of the hq rainfall datasets for MJO Phase 1 (Blue enhanced rainfall, Red suppressed rainfall, Grey site not significant).

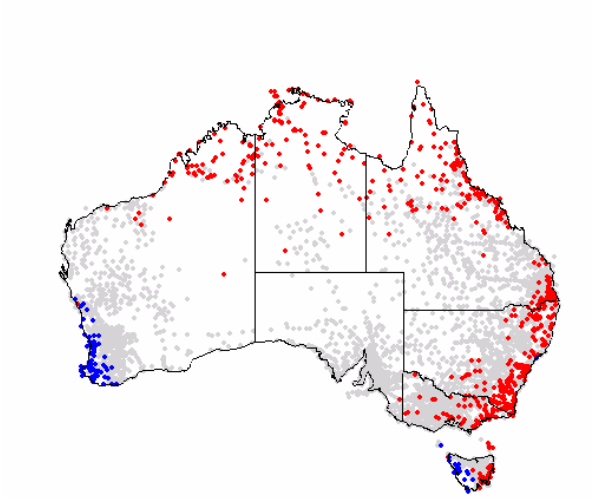

Figure 4.1.b Significant sites (p=.05) for K-S distribution of the BoM rainfall datasets for MJO Phase 1 (Blue enhanced rainfall, Red suppressed rainfall, Grey site not significant).

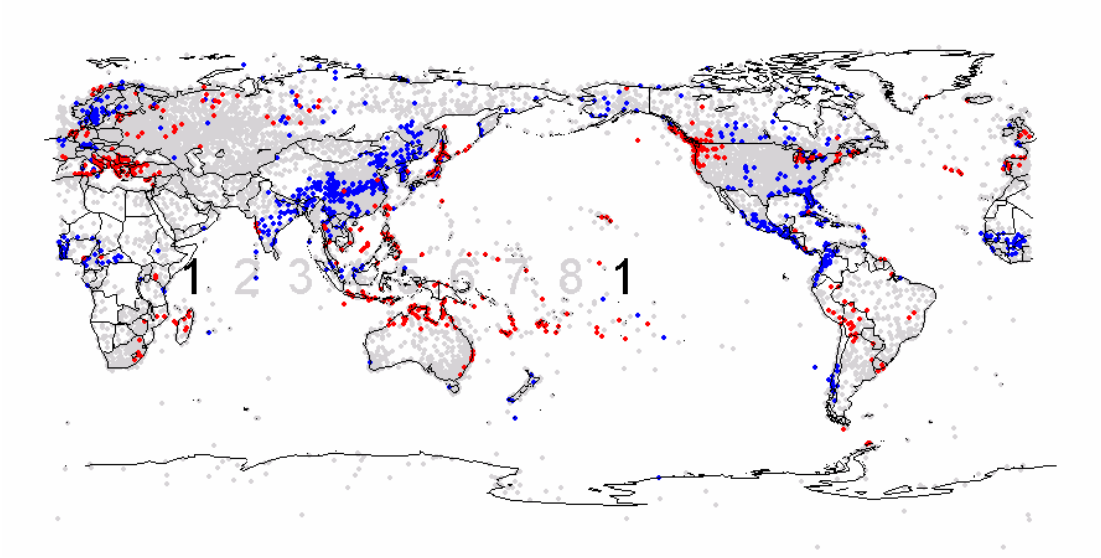

Figure 4.1.c Significant sites (p=.05) for K-S distribution of the WMO rainfall dataset for MJO Phase 1 (Blue enhanced rainfall, Red suppressed rainfall, Grey site not significant. Numbers represent the relative approximate location of active MJO convection for each phase, with relevant phase in bold).

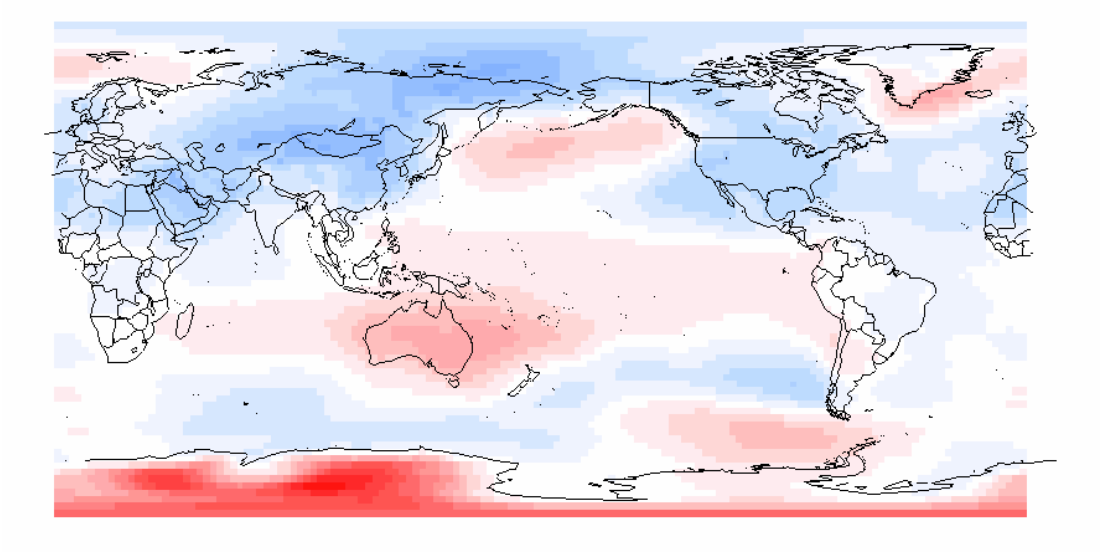

Key:

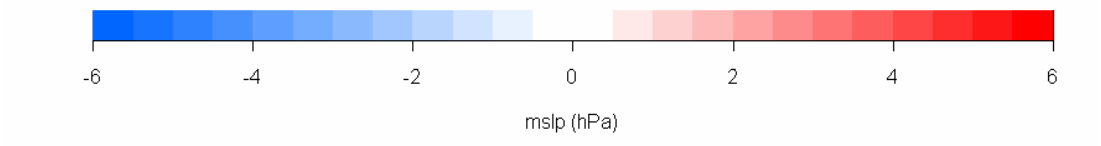

Figure 4.1.d Phase 1 MSLP anomalies. (Blue low pressure MSLP anomaly, Red high pressure MSLP anomaly).

4.4.1.2 PHASE 2:

During Phase 2 The hq data set (Figure 4.2.a) showed suppressed rainfall in the north, and along the middle and south-eastern coasts of Australia. The larger BoM (Figure 4.2.b) data set indicated extensive regions of suppressed rainfall with respect to RMM Index Phase 2 throughout the north of Australia, and along the east coast from central Queensland and south to the Portland Coast of Victoria.

The analysis of the BoM data set revealed extensive suppression across the north, through the Timor Sea and Gulf Division drainage basins, and across Cape York during Phase 2. The east coast of Australia from the Capricorn Coast to southern New South Wales also experiences a Phase 2 linked suppression of rainfall. No clearly defined regions of rainfall enhancement can be determined for Australia during Phase 2.

In the WMO (Figure 4.2.c) data set, suppression through northern Australia was discernable, and this suppressed pattern extends over, Tahiti and northern New Zealand. Rainfall appears enhanced for Phase 2 through much of northern and middle Asia, and southern India, as well as Central America and the east coast of the United States.

During Phase 2, as the MJO propagated east the MSLP anomaly moved in a similar fashion with the anomaly centred off the east coast of Australia. The rainfall patterns continue to be suppressed throughout the north and along the mid-east coast of Australia. These patterns of suppression and enhancement concur with the L and H MSLP anomalies. The L MSLP anomaly in the south eastern Indian Ocean has

moved from its Phase 1 position to adjacent the east coast of Australia and created the suppression patterns seen to the north and along the east coast as the anti-clockwise winds about the H MSLP anomaly promoted dry air conditions over these regions. Similarly, the enhanced rainfall on the east coast of the United States can be related to anti-clockwise circulation and onshore winds generated by a L MSLP anomaly located in that region. The enhanced rainfall across Asia is coupled with a L MSLP anomaly across the region.

The H pressure anomaly identified in Phase 1 has contracted, and the centre has moved east. The centre of the anomaly is centred over the southwestern Pacific Ocean. Similarly to Phase 1, during Phase 2 we see suppressed rainfall through northern Australia and along the eastern seaboard, but there are no areas of enhanced rainfall. The anti-clockwise winds associated with a H located east of the continent (such as the reported Phase 2 anomaly) would result in dry, offshore winds over much of Australia.

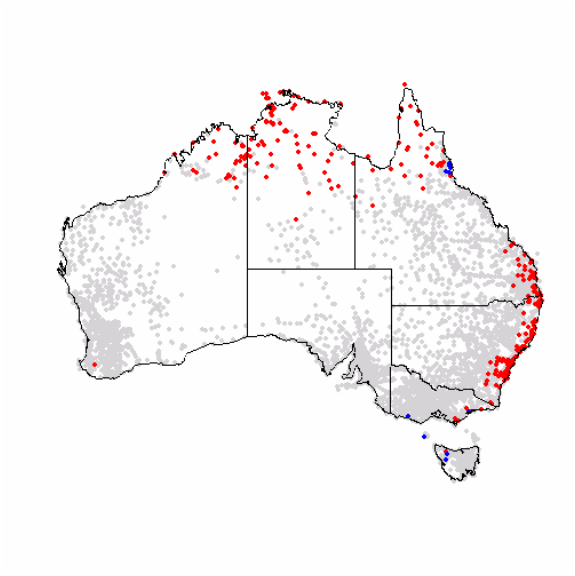

Figure 4.2.a Significant sites (p=.05) for K-S distribution of the hq rainfall datasets for MJO Phase 2 (Blue enhanced rainfall, Red suppressed rainfall, Grey site not significant).

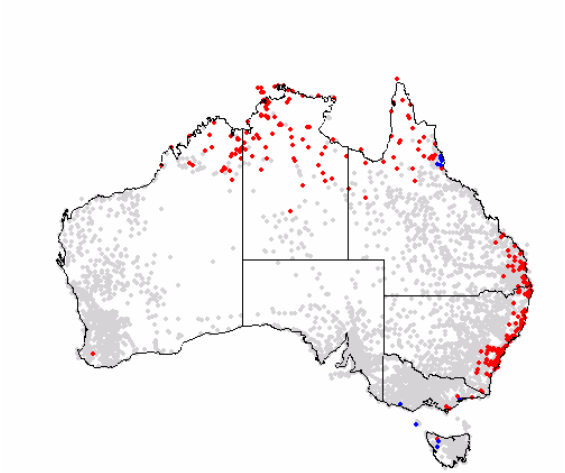

Figure 4.2.b Significant sites (p=.05) for K-S distribution of the BoM rainfall datasets for MJO Phase 2 (Blue enhanced rainfall, Red suppressed rainfall, Grey site not significant).

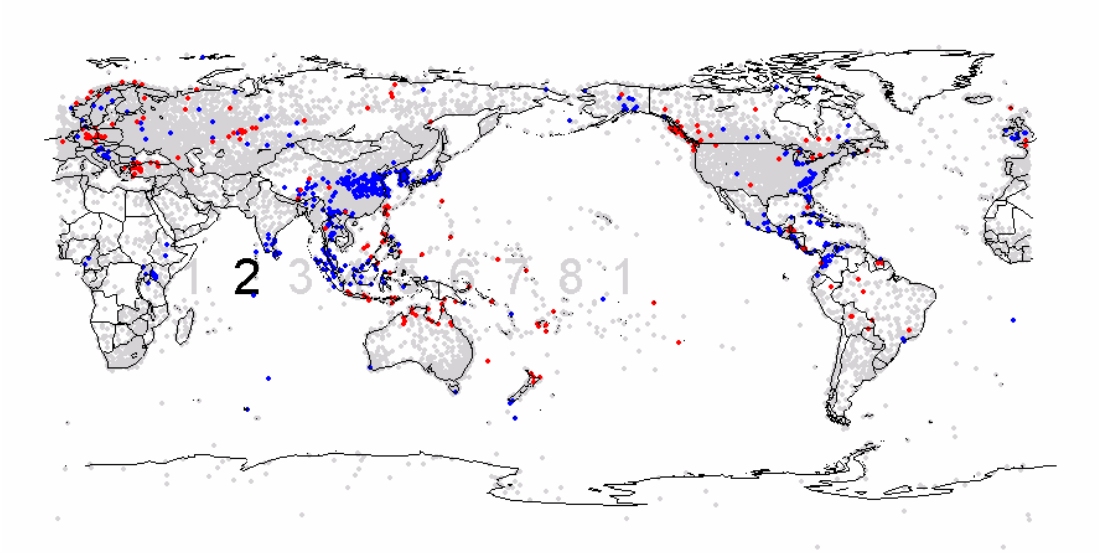

Figure 4.2.c Significant sites (p=.05) for K-S distribution of the WMO rainfall dataset for MJO Phase 2 (Blue enhanced rainfall, Red suppressed rainfall, Grey site not significant. Numbers represent the relative approximate location of active MJO convection for each phase, with relevant phase in bold).

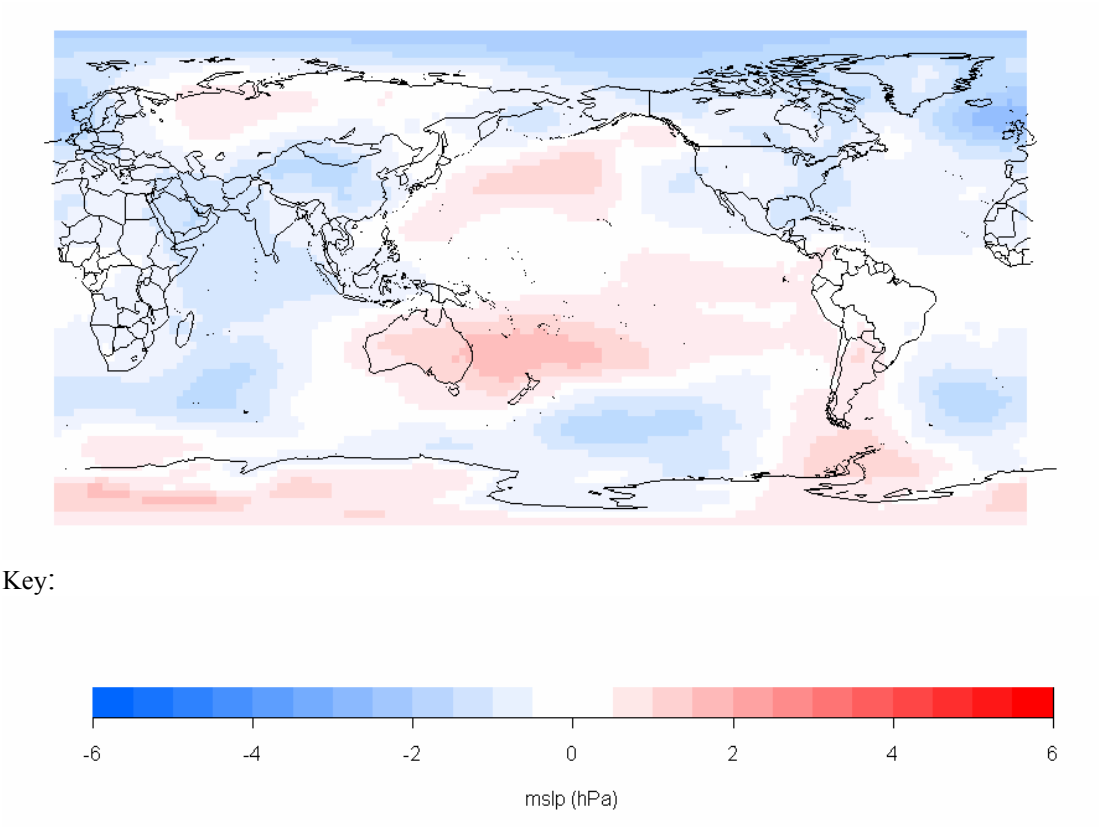

Key:

Figure 4.2.d Phase 2 MSLP anomalies. (Blue low pressure MSLP anomaly, Red high pressure MSLP anomaly).

4.4.1.3 PHASE 3:

Suppressed rainfall in the south west of Western Australia and along the coast from the Eyre Peninsula (South Australia) south to the Barwon River (Victoria) can be observed on the hq (Figure 4.3.a) output during Phase 3. The more spatially extensive BoM (Figure 4.3.b) data suggests that this suppression extends along the Western Australian coast, the southern South Australian coast from the Eyre Peninsula east, extending into Victoria, and the southern Highlands (New South Wales) and across much of Tasmania. Some enhancement of rainfall could be experienced along the east coast of Queensland, extending down the New South Wales coast.

The enhanced rainfall observed adjacent the Queensland coast, and suppression in South Australia Victoria, Tasmania and Western Australia can be discerned in the WMO (Figure 4.3.c) data set. Southern Asia and eastern China are still subject to enhanced rainfall conditions, while the beginnings of suppressed rainfall conditions can be identified in mid-China and Thailand. The eastern African nations and Madagascar, and the northwestern states of the United States of America (Washington, Oregon) are showing signs of enhanced rainfall conditions. By Phase 3 the active phase of the MJO has reached the western Indian Ocean between 80-100 degrees E.

The MSLP map (Figure 4.3.d) revealed that the high pressure anomaly has moved east and south, centred over the Tasman Sea. A L MSLP anomaly was located over the north west of Australia. For Australia, the westerlies from the H MSLP anomaly have generated coastal rain along the east coast, and the west and southern coast

experienced rainfall suppression. An L MSLP anomaly explained the enhanced rainfall noted in that region, while onshore winds resulting from the H MSLP anomaly over the United States of America helped to explain the coastal rainfall conditions observed there.

The H pressure anomaly identified in Phases 1 and 2 has further contracted in the Southern Hemisphere, and expanded in the Northern Hemisphere. The centre has remained over the southwestern Pacific Ocean, however the contraction of the H system means that a L has begun to encroach over western Australia. A wide, mildly anomalous L tongue protrudes east along the equator.

This arrangement of pressure systems would result in onshore, northeasterly winds along the Australian east coast, and the Phase 3 rainfall results (Figure 4.3.b and c) show corresponding coastal rain along the Queensland and northern New South Wales coasts. The southern coastal regions would experience dry winds under these pressure conditions, and this is reflected by the pattern of rainfall suppression we see in these areas for Phase 3.

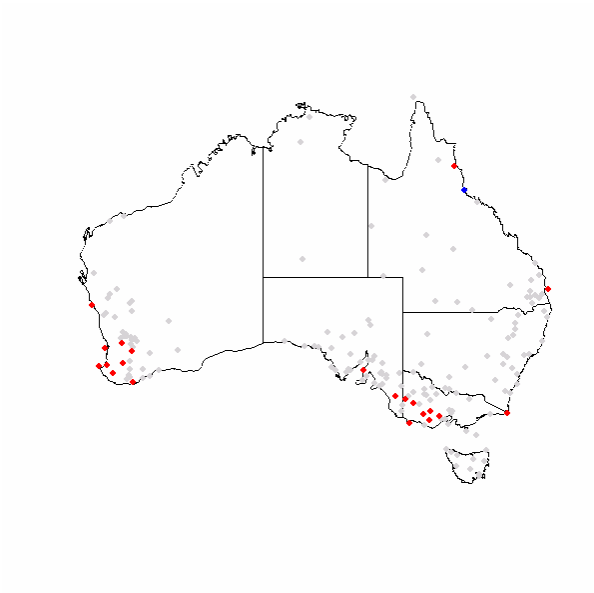

Figure 4.3.a Significant sites (p=.05) for K-S distribution of the hq rainfall dataset for MJO Phase 3 (Blue enhanced rainfall, Red suppressed rainfall, Grey site not significant).

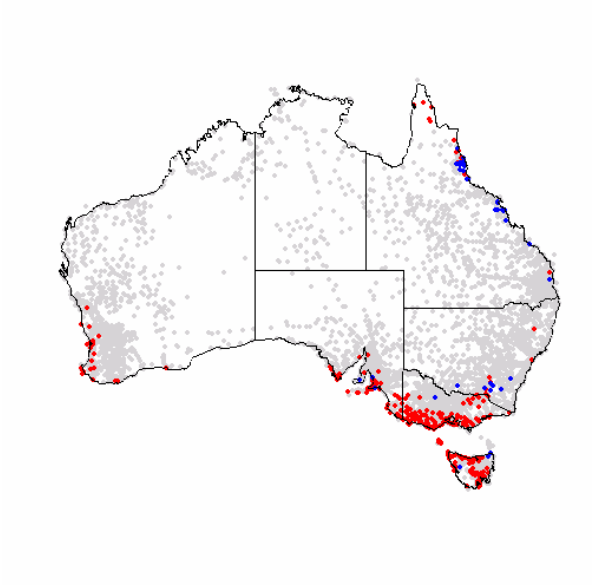

Figure 4.3.b Significant sites (p=.05) for K-S distribution of the BoM rainfall dataset for MJO Phase 3 (Blue enhanced rainfall, Red suppressed rainfall, Grey site not significant).

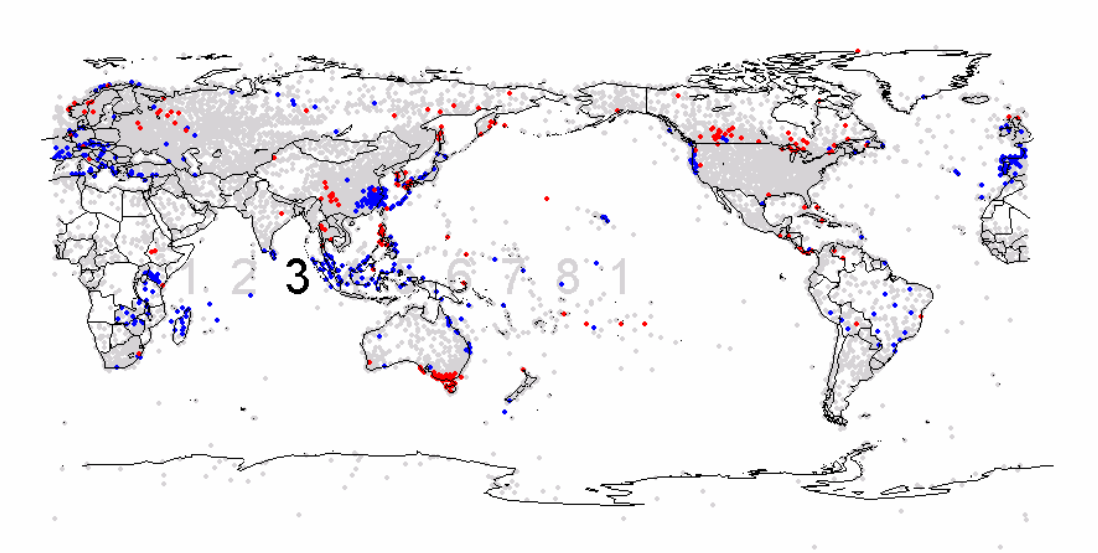

Figure 4.3.c Significant sites (p=.05) for K-S distribution of the WMO rainfall dataset for MJO Phase 3 (Blue enhanced rainfall, Red suppressed rainfall, Grey site not significant. Numbers represent the relative approximate location of active MJO convection for each phase, with relevant phase in bold).

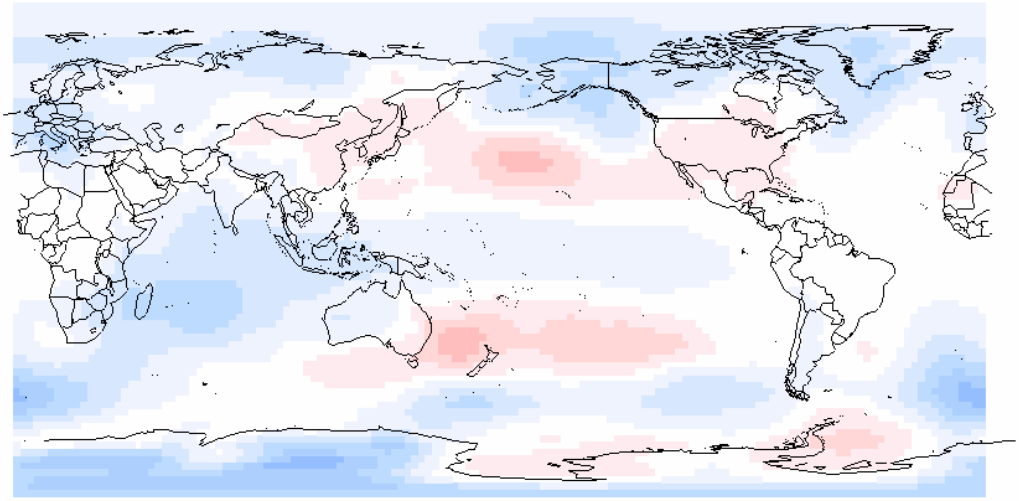

Key:

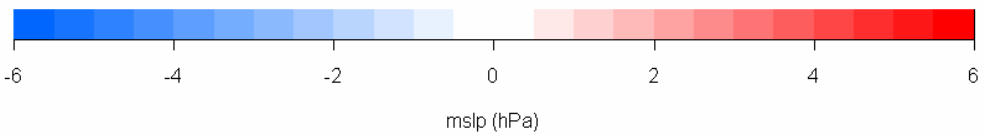

Figure 4.3.d Phase 3 MSLP anomalies. (Blue low pressure MSLP anomaly, Red high pressure MSLP anomaly).

4.4.1.4 PHASE 4:

During Phase 4 the hq (Figure 4.4.a) data set suggested rainfall enhancement along the east coast and extending inland along the Queensland /New South Wales border, and suppressed rainfall conditions in the south. However, the BoM (Figure 4.4.b) data set revealed more extensive regions of enhanced rainfall conditions. Phase 4 enhanced rainfall conditions may extend across the northeast of Australia, from Broome in the northwest to the southern highlands of New South Wales. Suppressed rainfall conditions were observed about coastal South Australia and Victoria, and across Tasmania, as seen for the hq data set.

During Phase 4 the WMO (Figure 4.4.c) data set indicates that as the active phase of the MJO is located over the eastern Maritime continent/Indonesian region, northern Australia experiences rainfall enhancement. All of coastal China, southeast Asia, and northern and eastern Australia reflect the rainfall enhancing effect of an active MJO system. New Zealand and northern and central America experience rainfall suppression.

The MSLP (Figure 4.4.d) anomalies revealed an L encroaching across Australia, moving west from the Indian Ocean, with corresponding enhanced rainfall. The H MSLP anomaly over the southwest Pacific Ocean helped explain the suppressed rainfall conditions noted for New Zealand and southeastern Australia. During Phases 3, 4, and 5, the MJO appeared to maintain a large tongue of L MSLP anomaly extended from southeast Asia, east along the tropics. The intensity of the H anomaly has diminished in the Southern Hemisphere, and intensified in the Northern

Hemisphere. In the Southern Hemisphere the H anomaly has moved east towards the southern central Pacific Ocean.

The large L anomaly continued to push east with a distinct L tongue along the tropics, which extended east well beyond the date line. The clockwise circulation that would be associated with such a L system would have bought moist onshore winds to much of northern and eastern Australia. An almost direct reflection of this was seen in the rainfall pattern (Figure 4.4.b) with broad spread precipitation enhancement throughout the Northern Territory (Figure 4.4.c), Queensland and New South Wales.

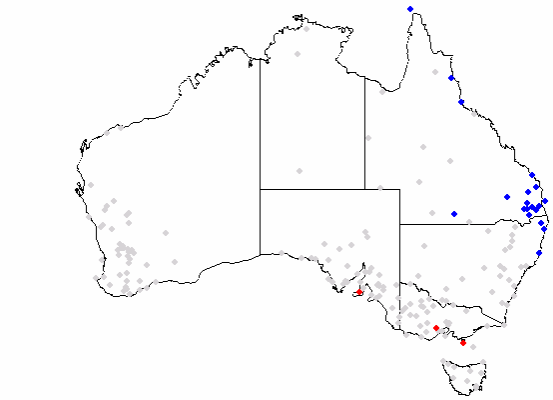

Figure 4.4.a Significant sites (p=.05) for K-S distribution of the hq rainfall dataset for MJO Phase 4 (Blue enhanced rainfall, Red suppressed rainfall, Grey site not significant).

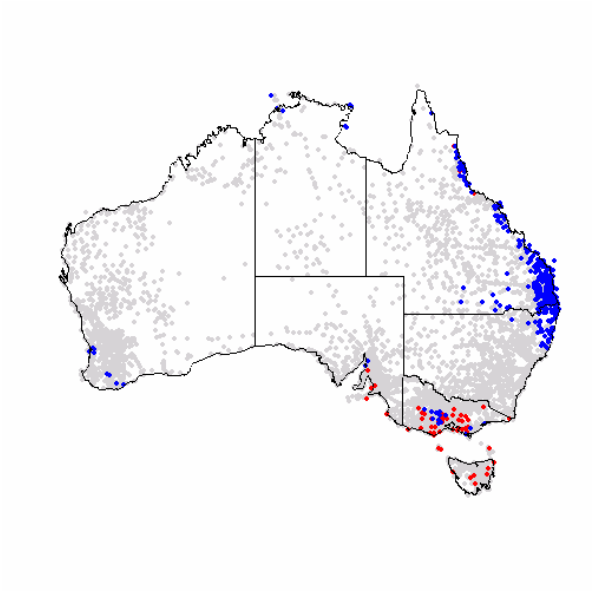

Figure 4.4.b Significant sites (p=.05) for K-S distribution of the BoM rainfall dataset for MJO Phase 4 (Blue enhanced rainfall, Red suppressed rainfall, Grey site not significant. Numbers represent the relative approximate location of active MJO convection for each phase, with relevant phase in bold).

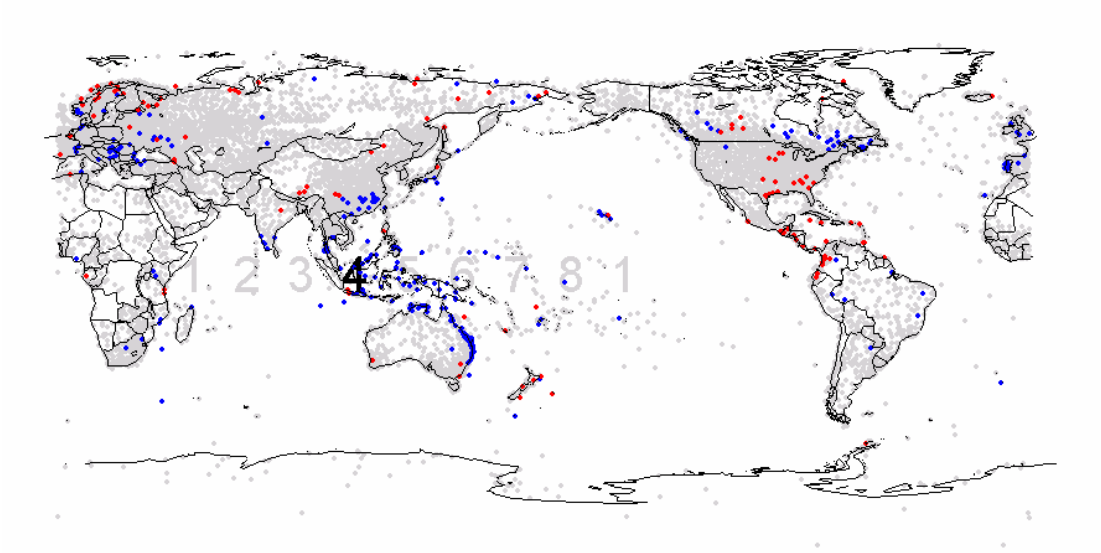

Figure 4.4.c Significant sites (p=.05) for K-S distribution of the WMO rainfall dataset for MJO Phase 4 (Blue enhanced rainfall, Red suppressed rainfall, Grey site not significant).

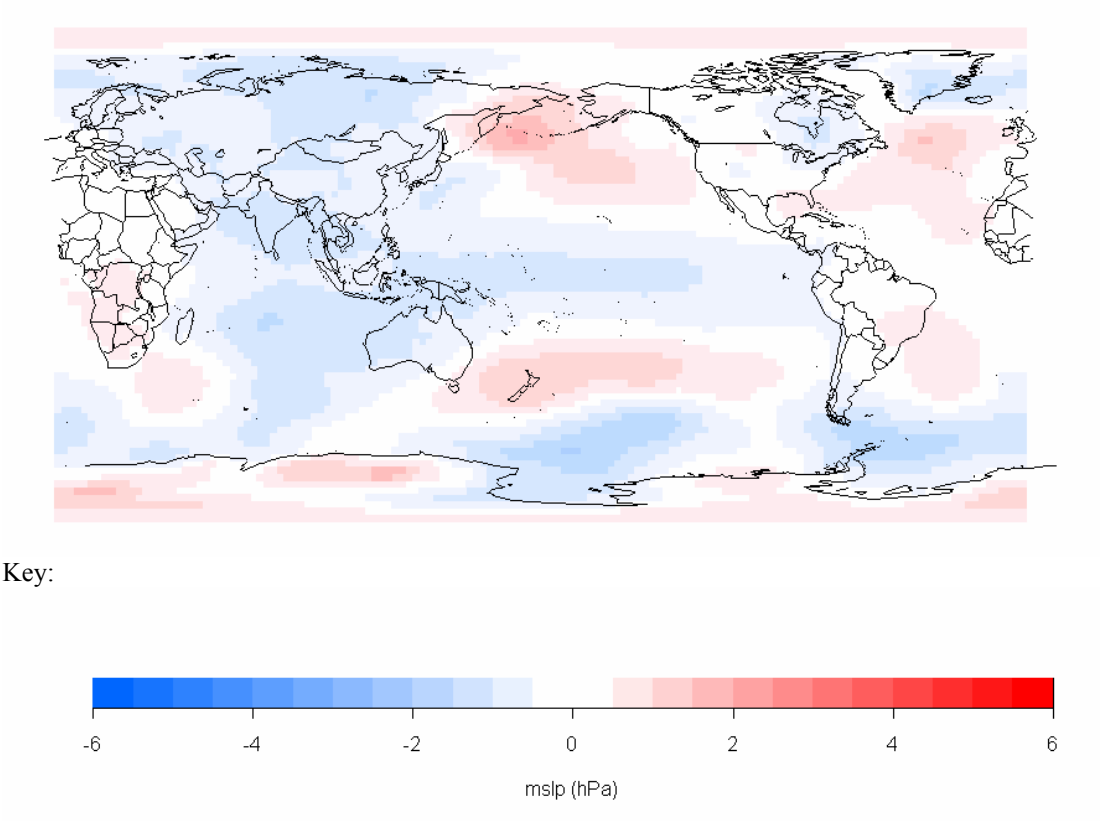

Figure 4.4.d Phase 4 MSLP anomalies. (Blue low pressure MSLP anomaly, Red high pressure MSLP anomaly).

4.4.1.5 PHASE 5:

The enhanced rainfall conditions noted for Phase 4 have penetrated south as the MJO travelled east. For the hq and BoM (Figure 4.5.a. and b) data sets enhanced rainfall conditions were identified for southern Western Australia, South Australia, as well as New South Wales, Victoria and Tasmania. The BoM (Figure 4.5.b) set shows that the northern tropics, near the MJO's active centre of convection, does experience the expected discernable increased rainfall effect, but southeast Australian response os more coherent.

The WMO rainfall data demonstrates the direct influence of the MJO on northern Australia's rainfall during Phase 5. Much of Asia is also experiencing enhanced rainfall conditions (Figure 4.5.c). North and south of the location of the MJO are two areas of L MSLP anomalies (Figure 4.5.d), which dominate the results. To the north of and slightly behind (west of), and to the south of and slightly in front of (east of) the MJO, lie two areas of L MSLP anomaly that accounted for the enhanced rainfall conditions noted for Phase 5.

The L pressure anomaly off the east coast of Australia has intensified, with a distinct centre, extending well of east the continent. The large L anomaly continued to travel east with an L tongue along the mid-Pacific Ocean. This tongue diverges into two streams when it reaches South America. The clockwise circulation with the L pressure anomaly (Figure 4.5.d) over the Tasman Sea would bring moist onshore winds onto northern and eastern Australia. An almost direct reflection of this is seen in the rainfall pattern (Figures 4.5.c and d) with broad spread precipitation enhancement throughout the Northern Territory, Victoria and New South Wales.

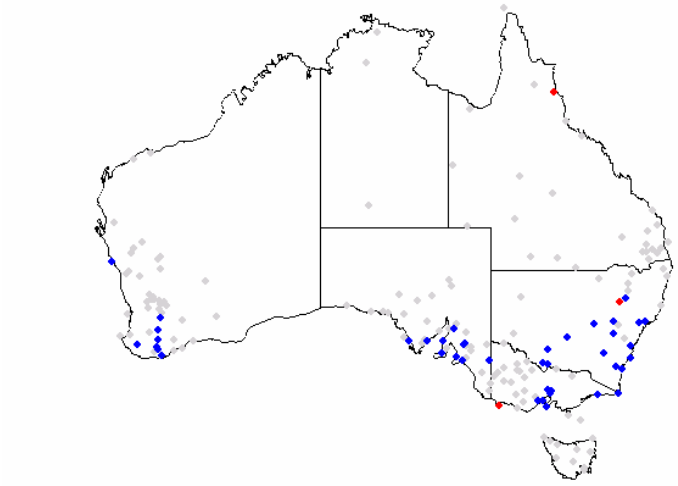

Figure 4.5.a Significant sites (p=.05) for K-S distribution of the WMO rainfall dataset for MJO Phase 5 (Blue enhanced rainfall, Red suppressed rainfall, Grey site not significant)

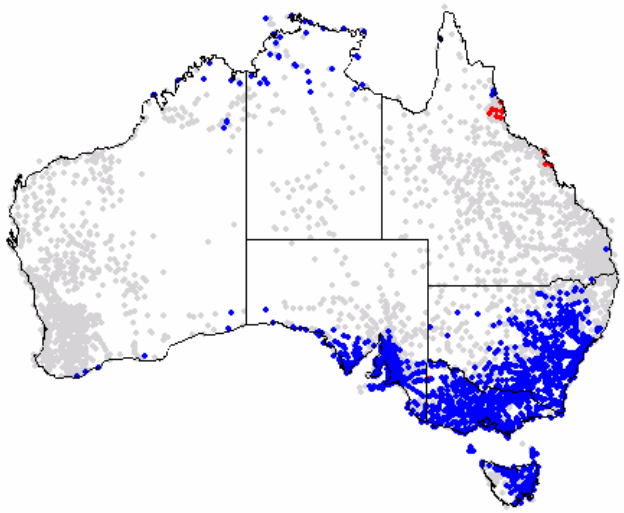

Figure 4.5.b Significant sites (p=.05) for K-S distribution of the WMO rainfall dataset for MJO Phase 5 (Blue enhanced rainfall, Red suppressed rainfall, Grey site not significant)

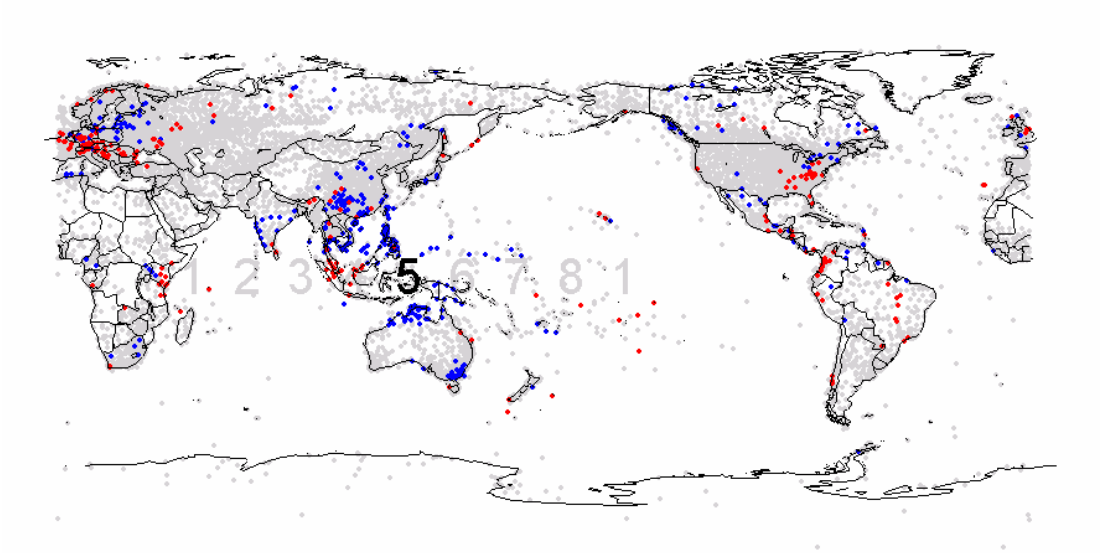

Figure 4.5.c Significant sites (p=.05) for K-S distribution of the WMO rainfall dataset for MJO Phase 5 (Blue enhanced rainfall, Red suppressed rainfall, Grey site not significant. Numbers represent the relative approximate location of active MJO convection for each phase, with relevant phase in bold)

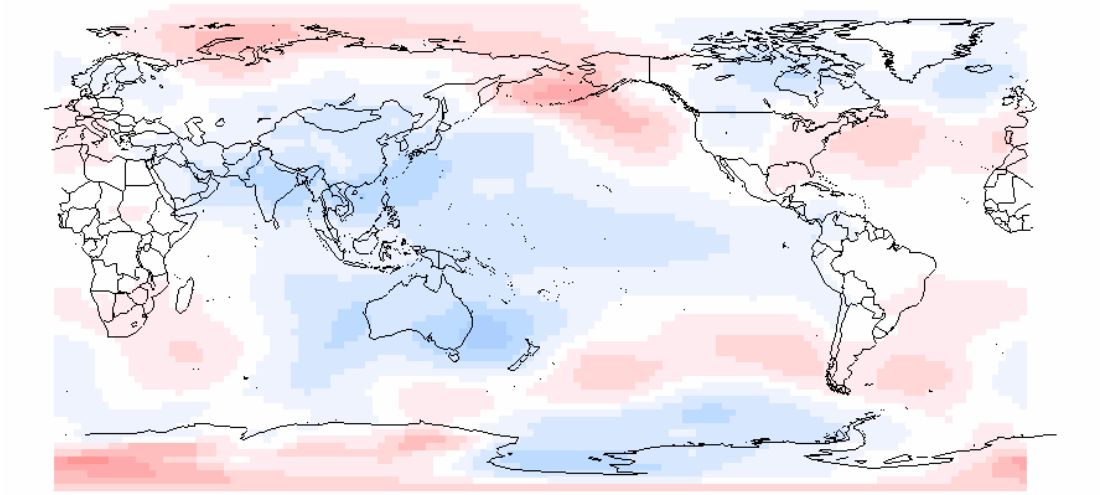

Key:

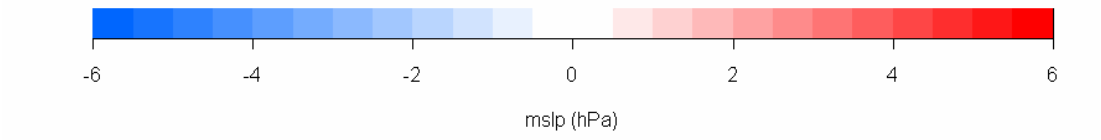

Figure 4.5.d Phase 5 MSLP anomalies. (Blue low pressure, negative MSLP anomaly. Red high pressure, positive MSLP anomaly).

4.4.1.6 PHASE 6

The phase 6 hq (Figure 4.6.a) data set showed enhanced rainfall conditions south east of Australia, while the BoM (Figure 4.6.b) sets revealed a more extensive pattern of significant enhanced rainfall over southeastern and northern Australia (north of approximately 20 degrees latitude S).

The WMO (Figure 4.6.c) data set revealed areas of rainfall suppression trailing the MJO in the tropics, with enhanced rainfall conditions over Australia, northern New Zealand, Thailand, Vietnam and the Philippines. Central China, eastern Indonesia, Malaysia and Japan experienced some rainfall suppression during Phase 6.

Australia's north and southeast experienced enhanced rainfall from the onshore flow associated with the location of the L pressure MSLP anomaly (Figure 4.6.d). The active phase of the MJO moved over the western Pacific Ocean (Micronesia, Nauru, Solomon Islands region) during RMM Phase 6, and the L MSLP pressure anomaly (figure4.6.d) has deepened and broadened, with the maxima still located over the Tasman Sea.

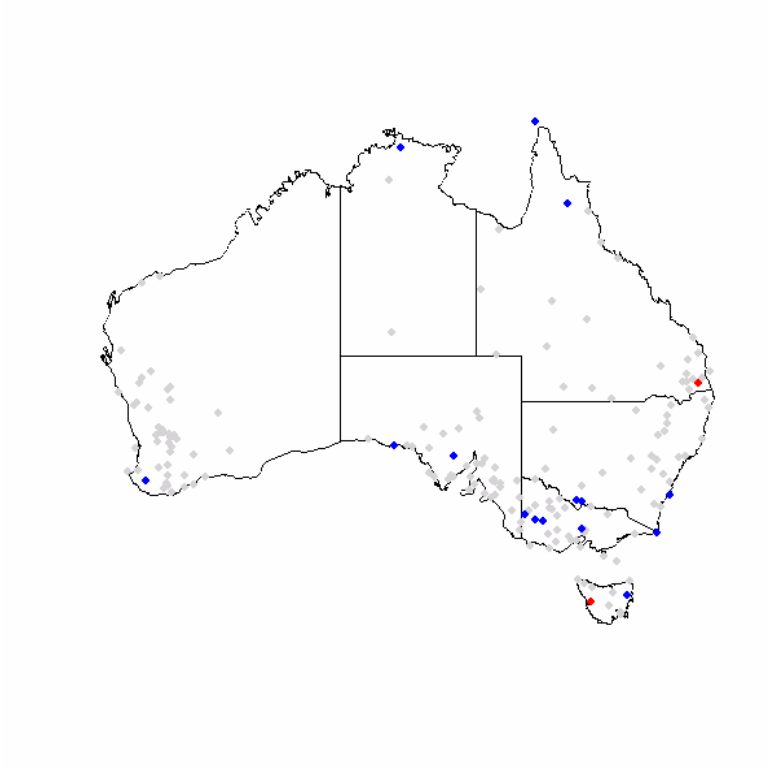

Figure 4.6.a Significant sites (p=.05) for K-S distribution of the hq rainfall dataset for MJO Phase 6 (Blue enhanced rainfall, Red suppressed rainfall, Grey site not significant)

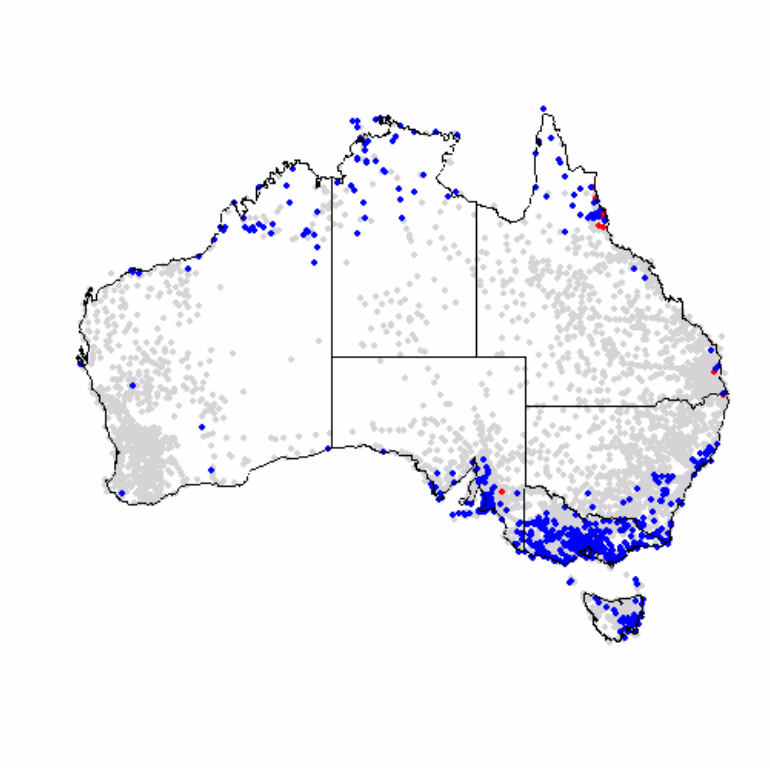

Figure 4.6.b Significant sites (p=.05) for K-S distribution of the BoM rainfall dataset for MJO Phase 6 (Blue enhanced rainfall, Red suppressed rainfall, Grey site not significant)

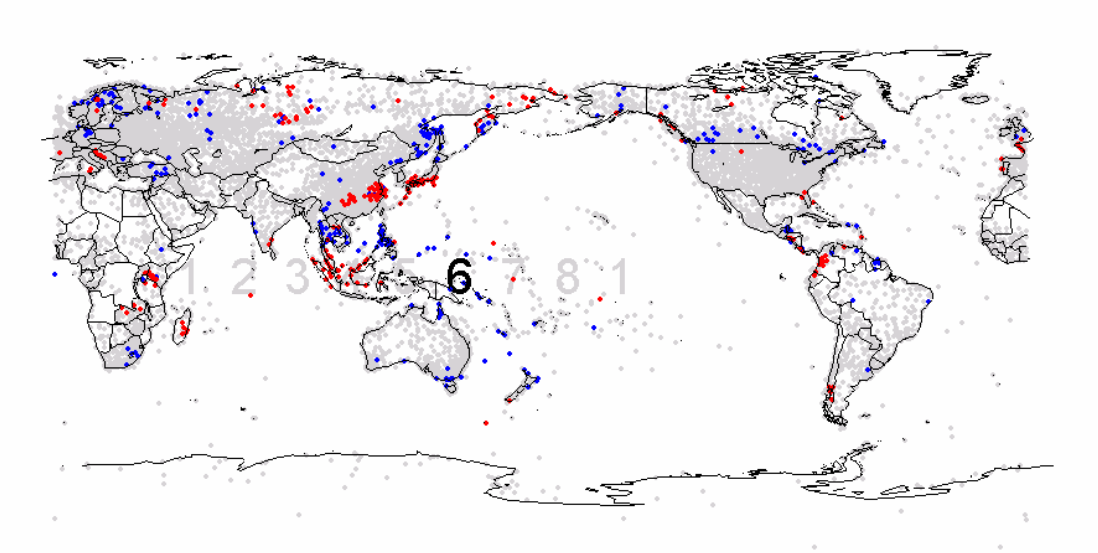

Figure 4.6.c Significant sites (p=.05) for K-S distribution of the WMO rainfall dataset for MJO Phase 6 (Blue enhanced rainfall, Red suppressed rainfall, Grey site not significant)

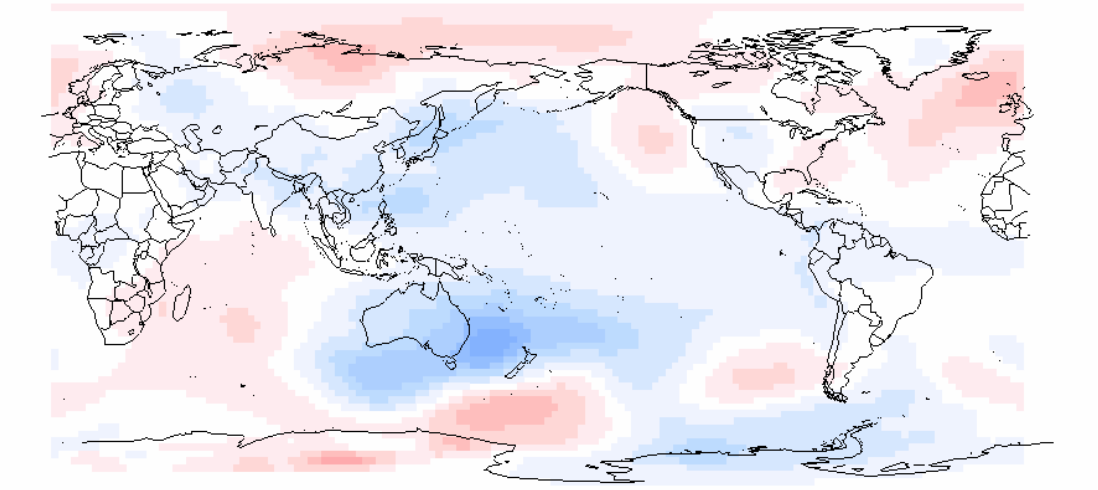

Key:

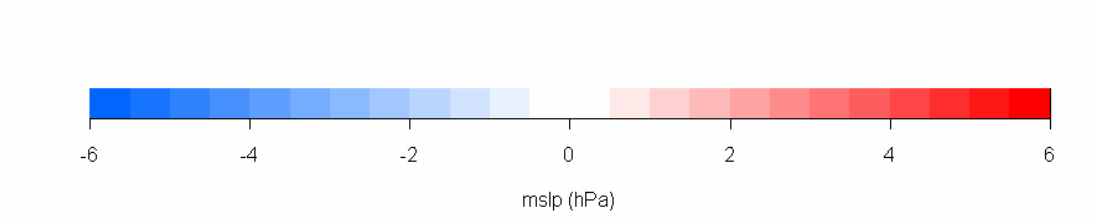

Figure 4.6.d Phase 6 MSLP anomalies. (Blue low pressure MSLP anomaly, Red high pressure MSLP anomaly).

4.4.1.7 PHASE 7

Enhanced rainfall conditions across Australia's north, and suppressed rainfall conditions in the south suggested by the hq (Figure 4.7.a) set, became more apparent using the BoM (Figure 4.7.b) set. The region of rainfall suppression for Australia encompassed much of Victoria, Tasmania and southern Western Australia in RMM Phase 7. Much of northern Australia's grazing country, and possibly isolated areas of the east coast, experienced enhanced rainfall conditions during RMM Phase 7.

The large scale rainfall suppression seen over India, northern and central Asia and most of southeast Asia is reflected by the H MSLP anomaly that covers Eurasia (Figure 4.7.c). A narrow tongue of enhanced rainfall conditions was identified over southern Indonesia (West Timor) and East Timor, and extended across northern Australia and throughout the southern central Pacific Nations (Fiji, Tuvalu, Kiribati, and French Polynesia).

The MSLP (Figure 4.7.d) anomalies calculated for Phase 7 revealed two broadscale L anomalies over the northern and southern Pacific Oceans. These two lobes of L MSLP anomaly first become apparent in Phases 4 and 5, trailing the tongue of L that extends along the tropics in Phases 3, 4, and 5. By Phase 6 these have resolved into two clear L MSLP anomalies travelling east around the mid-latitudes. In Phase 7 these L MSLP anomalies clearly dominate the synoptic weather about the Pacific Rim. At the same time a vast H MSLP anomaly dominates the entire Eurasian continent and extends into northern Africa.

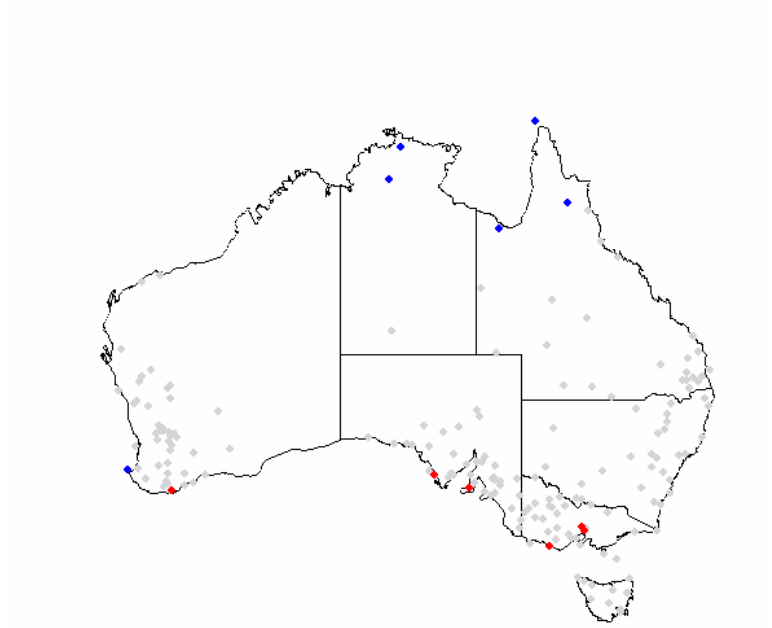

Figure 4.7.a Significant sites (p=.05) for K-S distribution of the hq rainfall dataset for MJO Phase 7 (Blue enhanced rainfall, Red suppressed rainfall, Grey site not significant).

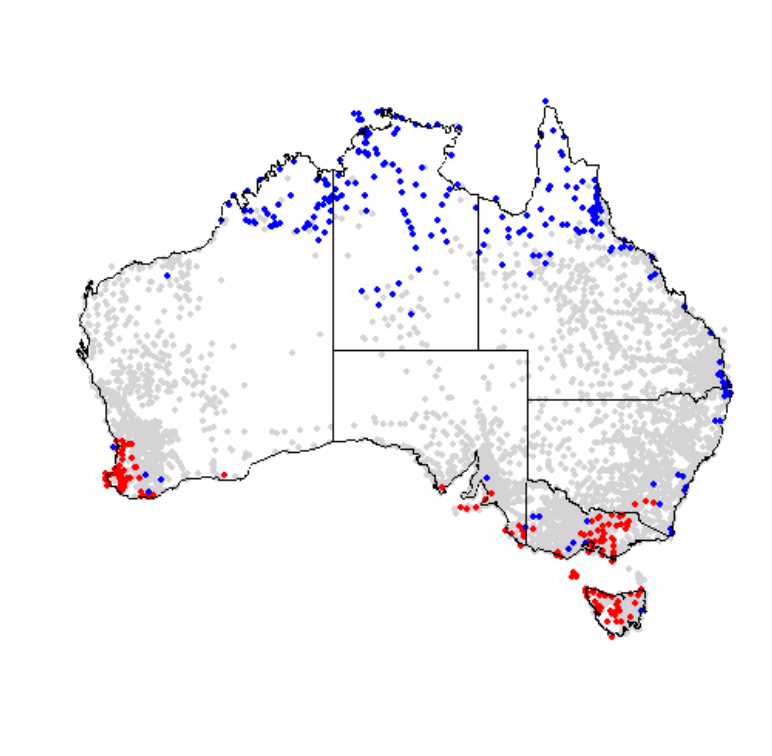

Figure 4.7.b Significant sites (p=.05) for K-S distribution of the BoM rainfall dataset for MJO Phase 7 (Blue enhanced rainfall, Red suppressed rainfall, Grey site not significant)

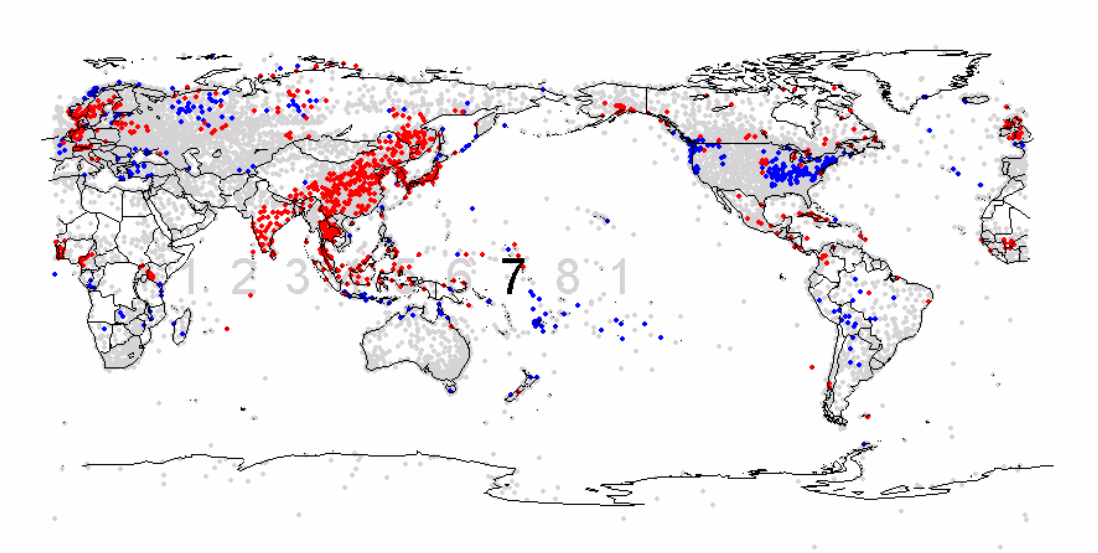

Figure 4.7.c Significant sites (p=.05) for K-S distribution of the WMO rainfall dataset for MJO Phase 7 (Blue enhanced rainfall, Red suppressed rainfall, Grey site not significant. Numbers represent the relative approximate location of active MJO convection for each phase, with relevant phase in bold)

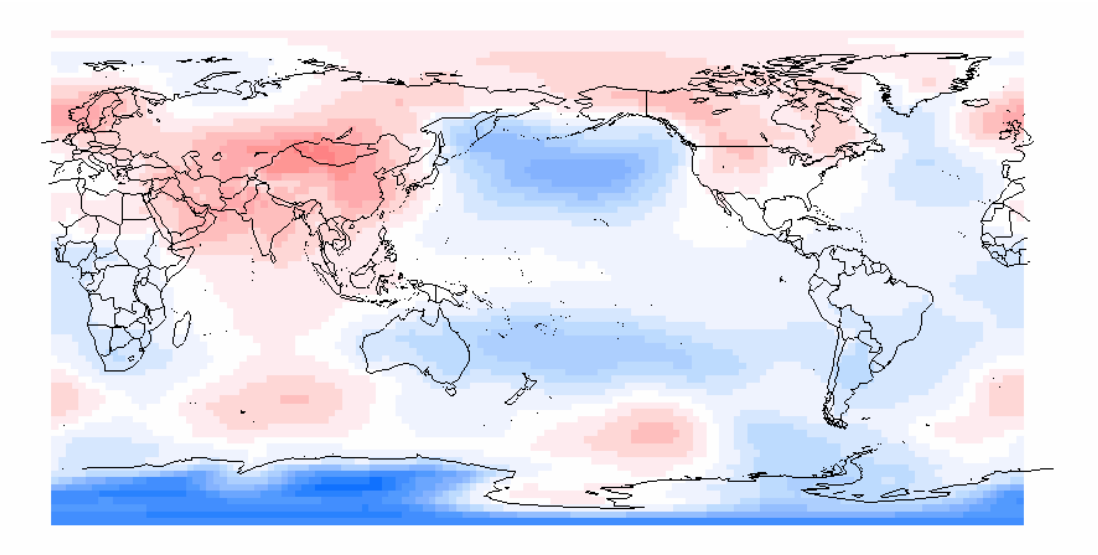

Key:

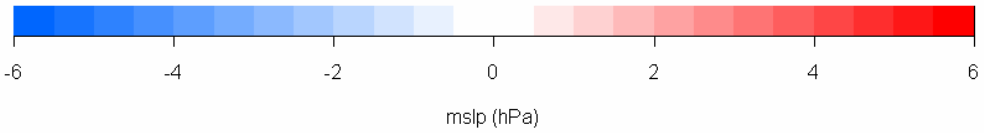

Figure 4.7.d Phase 7MSLP anomalies. (Blue low pressure MSLP anomaly, Red high pressure MSLP anomaly).

4.4.1.8 PHASE 8

While no trends were readily apparent for the Phase 8 hq (Figure 4.8.a) data set, rainfall suppressed conditions were apparent for at least the east coast of Australia in the BoM (Figure 4.8.b) data set. It could be expected that the westerly wind bursts trailing the MJO would now impact on the synoptic conditions for much of Australia. The wind anomalies may help explain the observed RMM Phase 8 rainfall suppressed conditions.

The H MSLP (Figure 4.8.d) encompassing Eurasia in Phase 7 has shifted east across Asia and encroached upon the west and north of Australia. As a result much of Asia experiences suppressed rainfall conditions (Figure 4.8.c). The tail of the L anomaly over Australia's east coast would be associated with dry southerly winds for northern Australia.

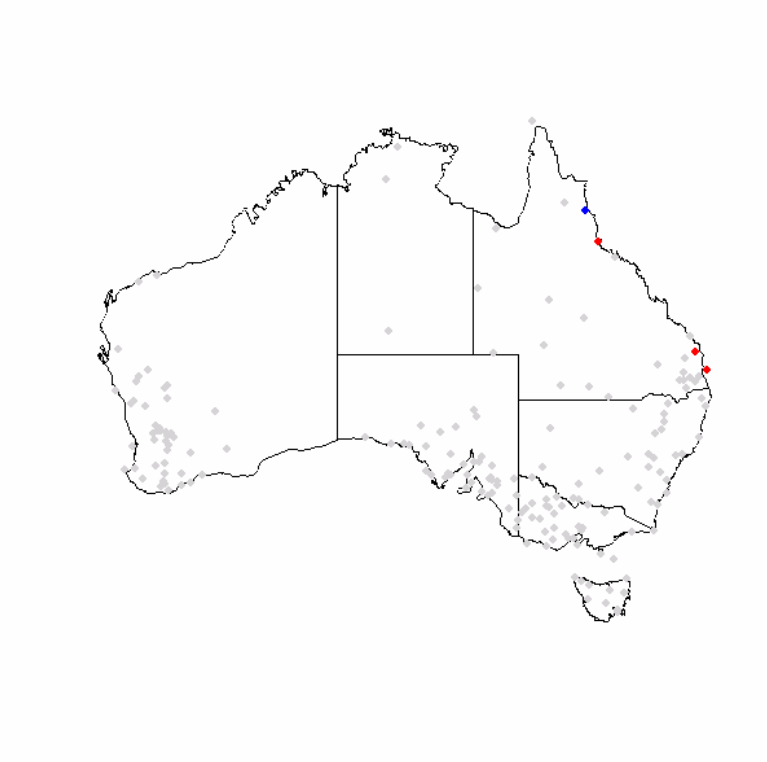

Figure 4.8.a Significant sites (p=.05) for K-S distribution of the hq rainfall dataset for RMM Phase 8 (Blue enhanced rainfall, Red suppressed rainfall, Grey site not significant)

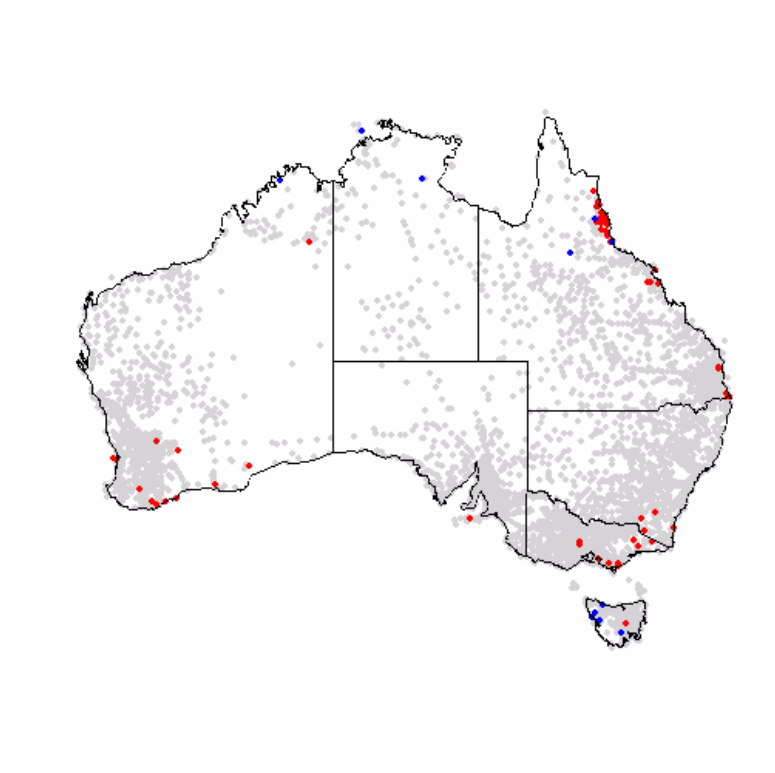

Figure 4.8.b Significant sites (p=.05) for K-S distribution of the BoM rainfall dataset for RMM Phase 8 (Blue enhanced rainfall, Red suppressed rainfall, Grey site not significant.)

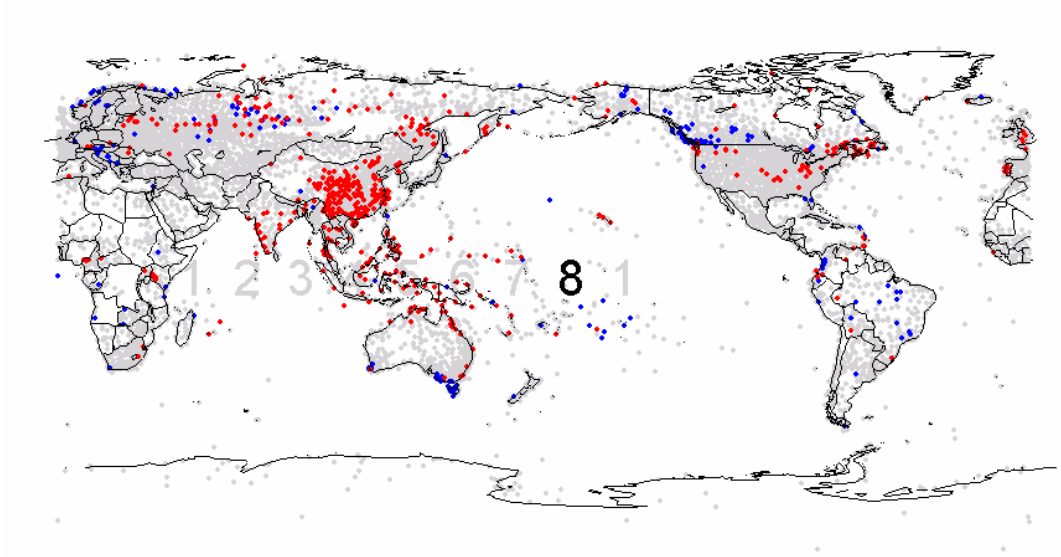

Figure 4.8.c Significant sites (p=.05) for K-S distribution of the WMO rainfall dataset for RMM Phase 8 (Blue enhanced rainfall, Red suppressed rainfall, Grey site not significant. Numbers represent the relative approximate location of active MJO convection for each phase, with relevant phase in bold)

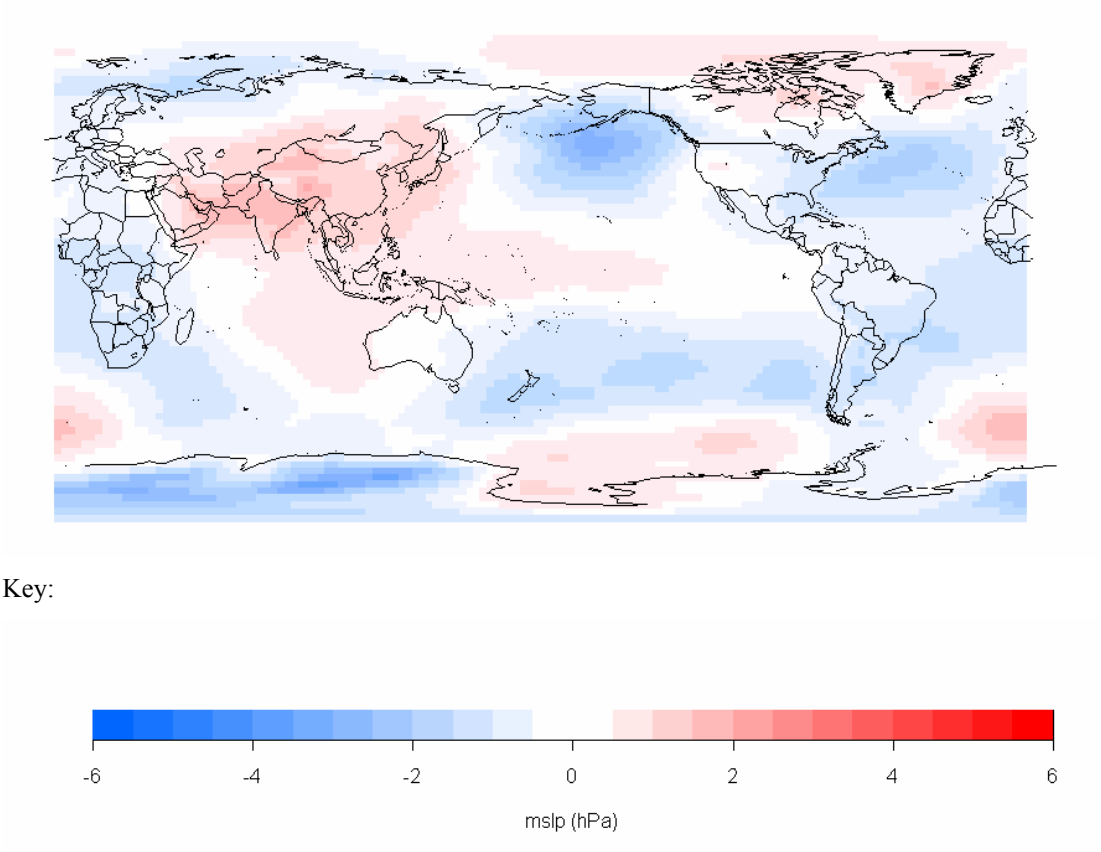

Key:

Figure 4.8.d Phase 7MSLP anomalies. (Blue low pressure MSLP anomaly, Red high pressure MSLP anomaly).

4.4.2 Rainfall lagging MJO

To lag the rainfall behind the MJO over the entire comparison period and at every station required the KW test to analyse the entire result (Figure 4.9). The plot of this KW testing showed a strong decline in the count of significant sites from about day 10. At about 25-30 days lag a marked recurrence of significance site totals returned. The number of significant correlations then continued to fall, until there are very few at 60 days, a time frame spanning most MJO cycles of 22 to 70 days (Madden and Julian, 1994). It is of note that each of the peaks is around 10 days apart, the time defined as the (longest) length of a RMM phase. This is with the notable exception of the trough between the second peak and third peak at time 10 –15 days, with a rapidly declining count of significant sites.

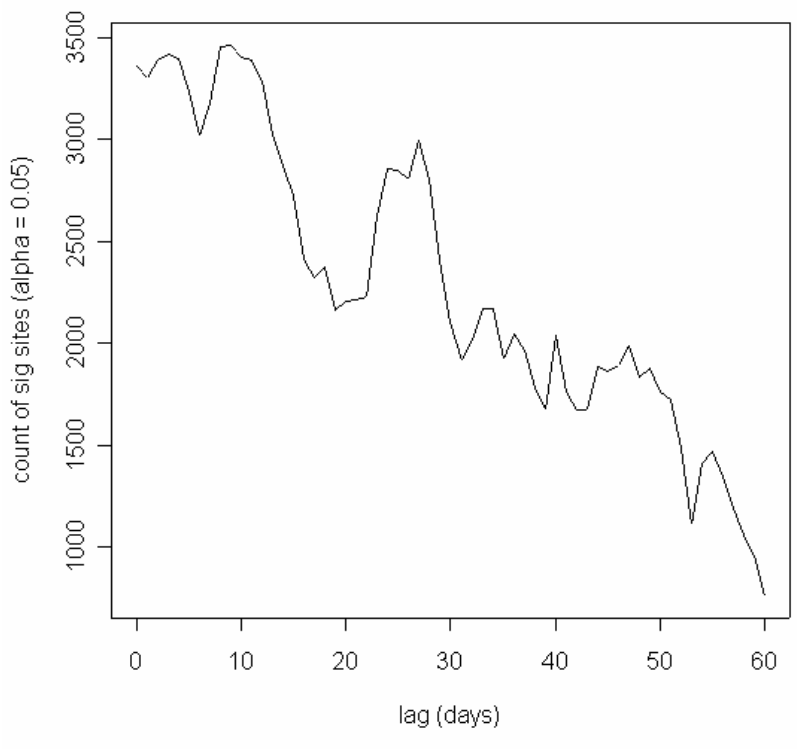

Figure 4.9 K-W test of rainfall lagged (0-60 days) behind MJO by a count of significant sites. There is marked decrease in the number of significant sites after 10 days. After day 10 there are a number of spectral peaks corresponding with MJO time frames of less than sixty days, with a broad spectral peak at about 45 days, the median MJO cycle temporal length.

4.4.3 Strong MJO Signals

When both the RMM 1 and 2 have an absolute value of less than 1 the amplitude of the MJO can be described as weak (Figure 3.2). When this occurs both RMM1 and RMM2 approach the centre of the phase space. Empirical forecasting of anomalies associated with the MJO using RMM1 and RMM2 as predictors is not possible when the EOF values are this low (Wheeler and Hendon, 2004). When the RMM phase system is too weak to allow MJO forecasting it might not be appropriate to forecast the MJO associated rainfall influences using the RMM system.

K-W tests were performed for each station to determine if the distribution of precipitation for each phase is different in location (median differs) to the distribution of any other phase (tests phase by phase instead of all phases as a K-S distribution does). Performing the K-W tests it was determined that using all signals 3521 out of 4234 were significant. For strong signals, 3688 out of 4234 were significant. The K-S distributions were re-constructed deleting weak RMM days from the analogue datasets.

These K-S distributions were assembled using only the strong MJO signals when the absolute values of both RMM1 and RMM2 were greater than 1, and the corresponding days of BoM rainfall data (Figure 4.10.a and b). The K-S distribution constructed may be compared with those using all RMM Index data, to ascertain if the amplitude of the signal had a discernible affect on the output.

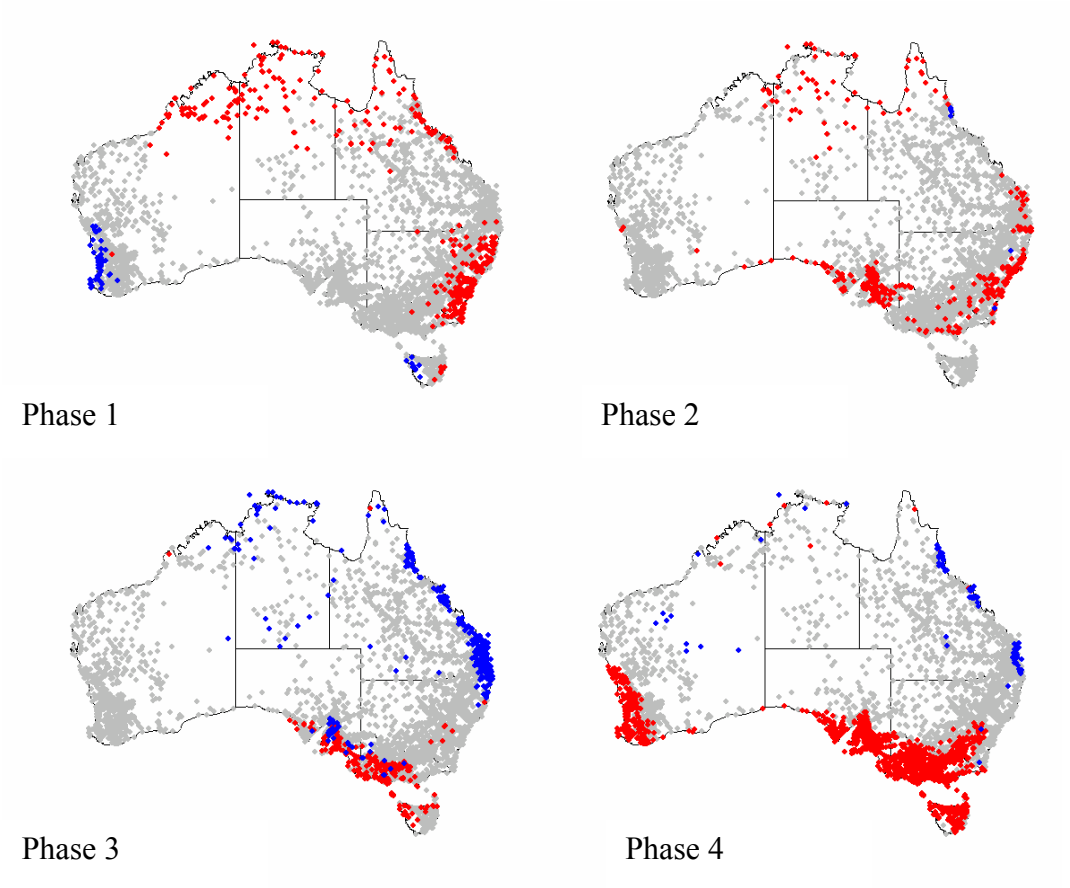

Figure 4.10.a RMM Strong Signals (RMM1 >|1|, RMM2 >|1|) Phases 1- 4 (Clockwise from top left) (Blue enhanced rainfall, Red suppressed rainfall, Grey site not significant). Compare to Figure 4.10.a.b below

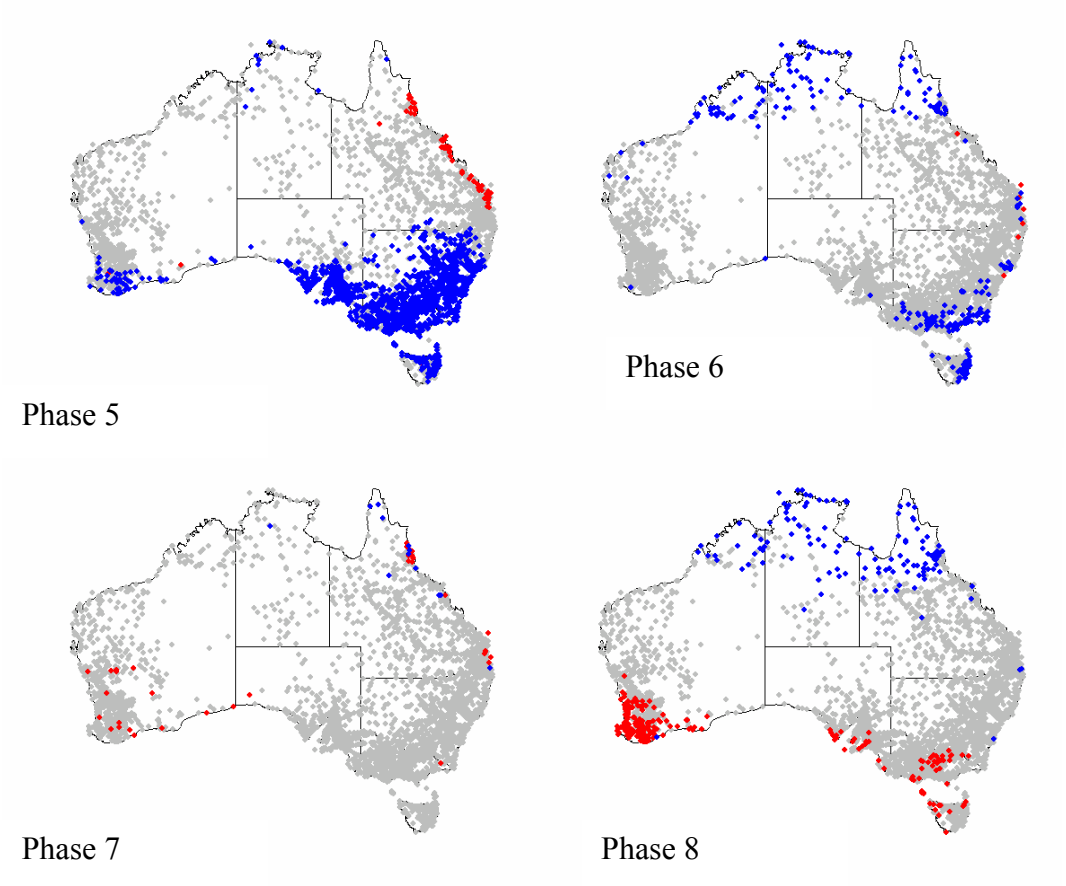

Figure 4.10.b RMM Strong Signals (RMM1 >|1|, RMM2 >|1|) Phases 5-8 (Blue enhanced rainfall, Red suppressed rainfall, Grey site not significant).

4.4.4 Phase locking:

Locking the phases (as described in Section 4.3.4 above) provided a more general view of the MJO-rainfall response in Australia. Given that the MJO is in any phase for 6 plus or minus 4 days (Wheeler and Hendon, 2004) can be better forecast enhanced and/ or suppressed rainfall conditions, because we have increased our lead time by increasing the temporal coverage of our phases by combining them. Useful guidance for industry, especially agriculture required a forecast with some skill, and a lead time permitting intervention strategies.

When Phases 1 and 2 were treated as one phase (Figure 4.11.a), it was noted that there was a clear increase in the spatial extent of the suppression of rainfall.

Together, these phases correlate significantly with suppressed rainfall conditions over the northeastern three quarters of the continent. A widespread suppression response, not apparent when Phases 1 and 2 were separately treated, affected much of Australia.

Phase 4 is important to the east coast and southern Queensland because of the enhanced rainfall conditions experienced there. The Phase 3 and 4 superset (Figure 4.11.b) showed little alteration to these enhanced conditions, however the suppressed conditions for South Australia, Victoria and Tasmania are more intense and extensive, particularly for the Eyre Peninsula region.

Enhanced rainfall conditions for southeastern Australia occurred during Phases 5 and 6 (Figure 4.11.c), and this response is maintained when we lock the phases together. There is minor southward contraction of the enhanced response in the New England Tablelands. Combining Phases 7 and 8 (Figure 4.11.d) provides a response much like that for Phase 7, with some northward contraction of the enhanced rainfall response.

Locking the phases assists by providing a more general overview of the rainfall response for Australia, and given that the MJO is in any phase 6 plus or minus 4 days forecast skill improves, as the lead time was increased. This increase in lead time may only encompass a number of days, but this provides scope for rural managers to respond.

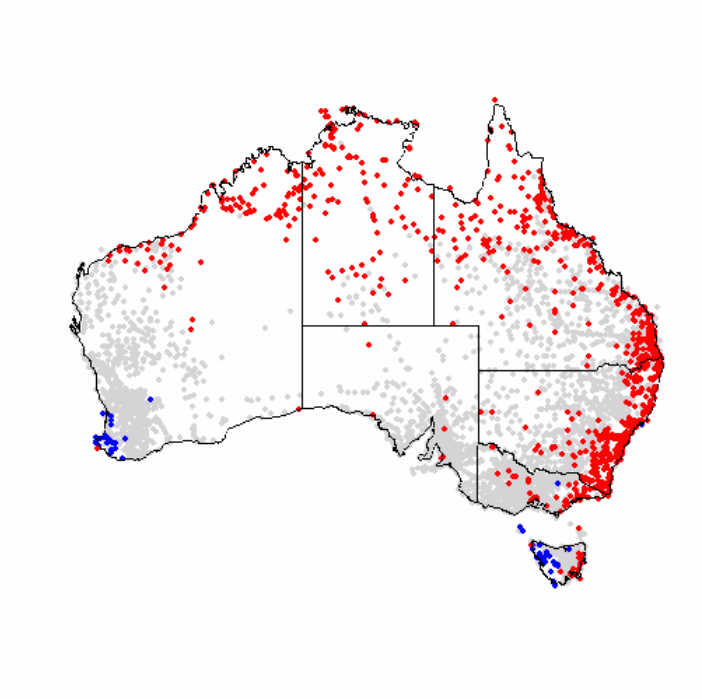

Figure 4.11.a Significant sites (p=.05) for K-S distribution of the BoM rainfall dataset for MJO Phases 1 and 2 (Blue enhanced rainfall, Red suppressed rainfall, Grey site not significant).

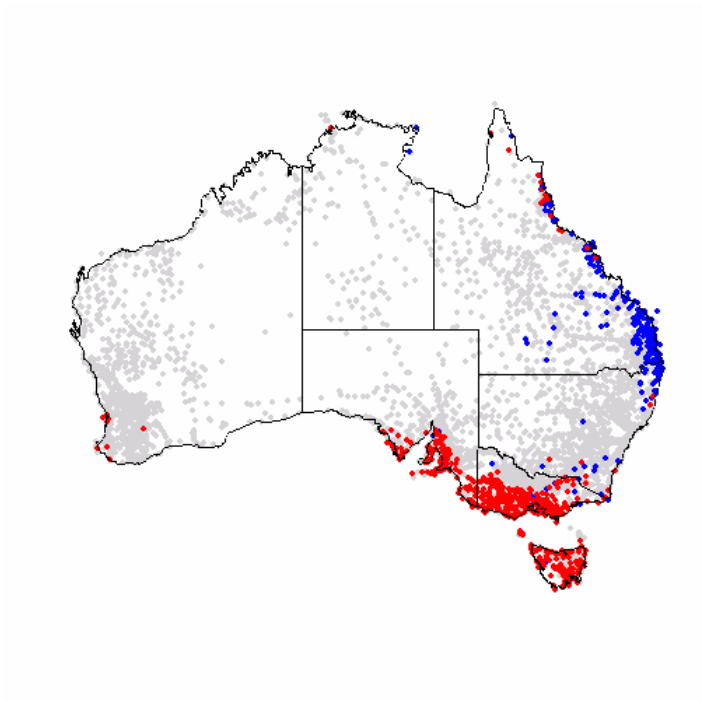

Figure 4.11.b Significant sites (p=.05) for K-S distribution of the BoM rainfall dataset for MJO Phases 3 and 4 (Blue enhanced rainfall, Red suppressed rainfall, Grey site not significant).

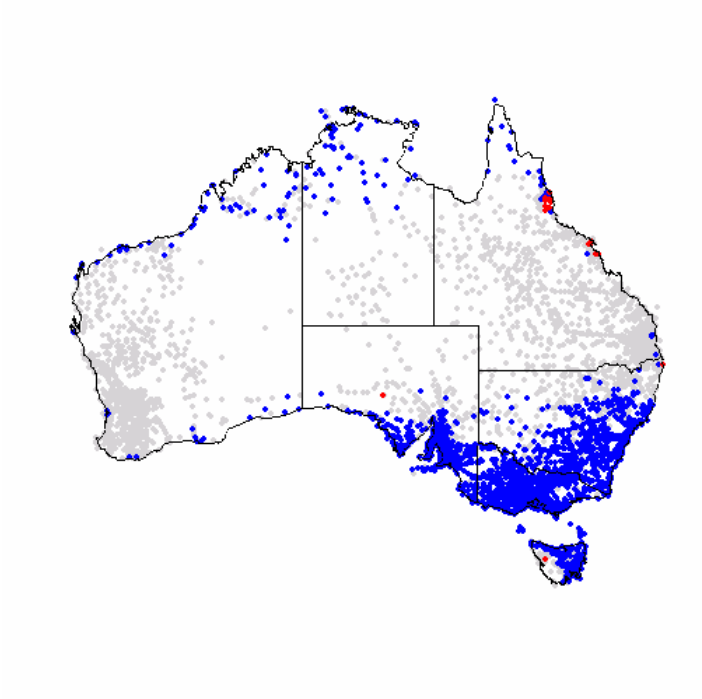

Figure 4.11.c Significant sites (p=.05) for K-S distribution of the BoM rainfall dataset for MJO Phases 5 and 6 (Blue enhanced rainfall, Red suppressed rainfall, Grey site not significant).

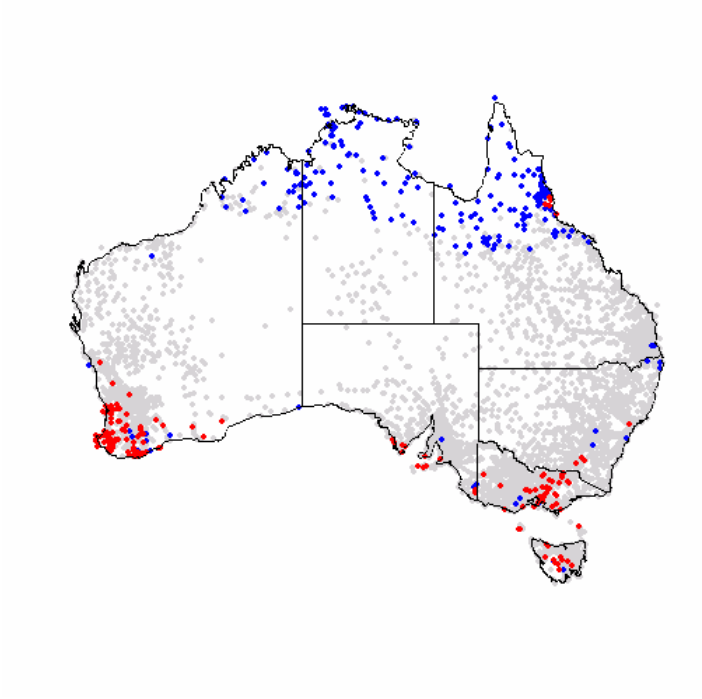

Figure 4.11.d Significant sites (p=.05) for K-S distribution of the BoM rainfall dataset for RMM Phases 7 and 8 (Blue enhanced rainfall, Red suppressed rainfall, Grey site not significant).

4.5 Discussion

4.5.1 MJO rainfall and MSLP

As the MJO propagated east from over the Indian Ocean, there were corresponding broadscale changes in the precipitation pattern outside the tropics. Enhanced and suppressed precipitation areas across Australia and the world responded to the tropical passage of the MJO. Similarly to the findings of Bond and Vecchi (2003) convection along the eastern United States and Canadian coasts is affected when the MJO centre of active convection is located near the mid-Pacific Ocean (Phases 6, 7 and 8). The MSLP anomalies also concur with the findings of Chen and Murakami (1988) that regional weather systems beyond the tropics respond to the passage of the MJO.

A number of rainfall data sets were assessed in an attempt to get a high degree of spatial coverage, while having a high quality data set as a reference. Results from the Australian daily rainfall data sets were consistent. The world rainfall data set results were consistent with the Australian data sets where they overlap, but the WMO spatial coverage within the overlap is poorer, and as a result only the broader rainfall trends are apparent. The concurrence of the results from different data sets suggested that even results from the poorer quality data sets could be relied upon. As data quality was reduced, the interpretation became less specific, and more regionalised.

Based on the RMM phase distinct regions of enhanced and suppressed rainfall can be established. Regions of enhanced rainfall tally with low pressure anomalies, or are coastal regions that would experience enhanced onshore flow because of the local MSLP anomaly. Where areas of suppressed rainfall were identified, corresponding

regions of anomalous high pressure or off shore flow complied with the rainfall results. The large scale flow resulting from the MSLP values can explain, to some extent, the broad scale precipitation suppression and enhancement patterns.

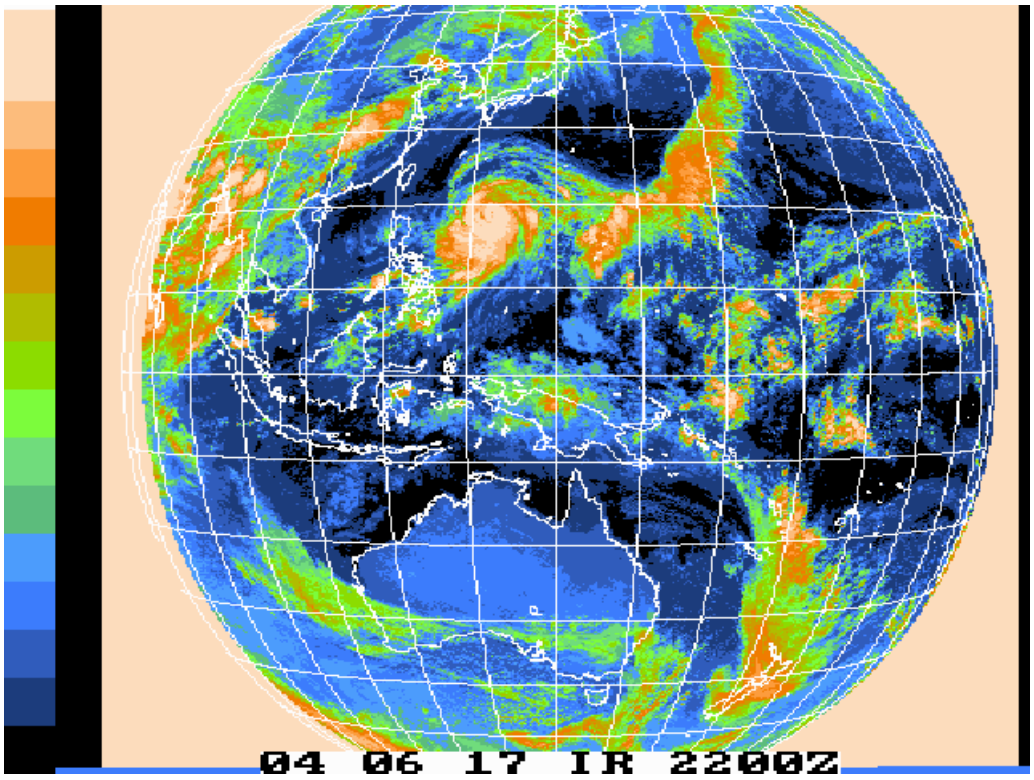

Figure 4.12 Satellite image of the Western Pacific Region, 18/06/04. Cloud over southern Australia and clear skies over the north correspond with results for RMM Phase 5. Enhanced rainfall predicted for the South China Sea is also detectable. The active centre of the MJO is located over the Maritime Continent. (Image courtesy of GMS-5 backup with GOES-9 operated by the joint effort of JMA and US NOAA NESDIS over the western Pacific.)

For example, on 18 June 2004 (RMM Phase 6) (Figure 4.12) there was cloud visible over southern Australia, congruous with the enhanced rainfall pattern generated with the BoM data set for Phase 6(4.6.b). The WMO results for Phase 5 indicate enhanced rainfall throughout central Asia, and cloud and a large low can be observed on satellite pictures of the region (Figure 4.12). The broadscale MSLP patterns for Phase 5 (4.6.d) are represented to some extent, with synoptic lows over the Tasman Sea and northeast of the South China Sea (Figure 4.12 and 4.13). The regions of rainfall forecast for Victoria and Tasmania (Figure 4.13) correspond with those areas of enhanced rainfall identified for RMM Phase 5 (Figure 4.6.b)

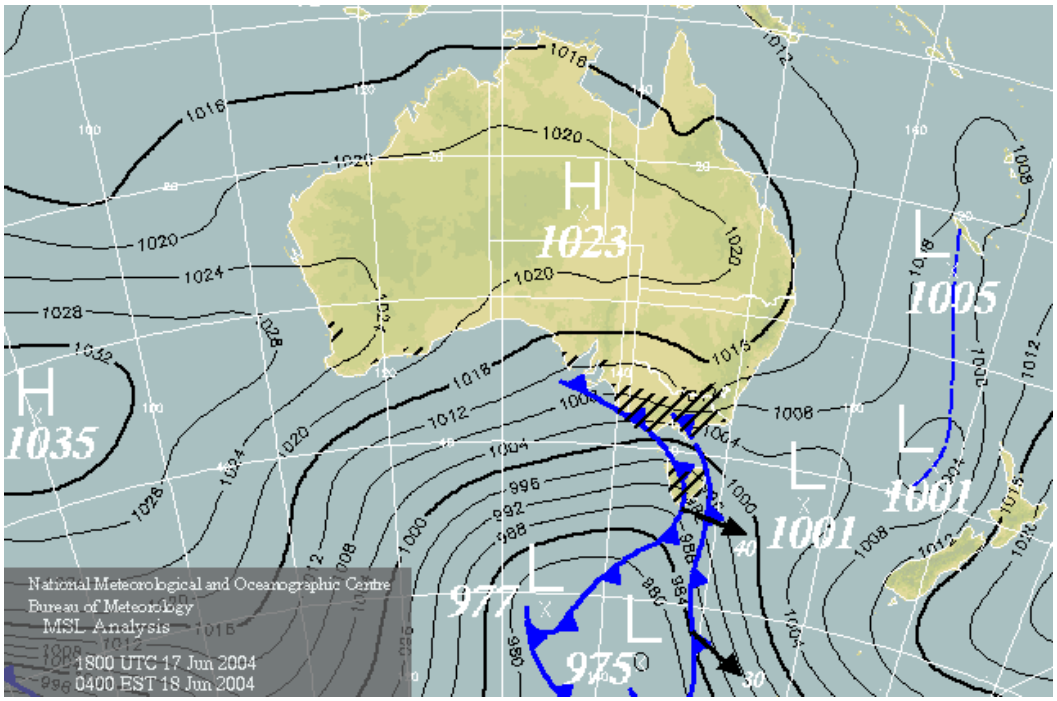

Key:

Figure 4.13 Australian Region Mean Sea Level Analysis, 18/06/04. The rainfall forecast for southern Australia agrees with the forecast for Phase 6. The low pressure systems located over the Tasman Sea tally with the forecast Phase 6regions of anomalous L. (Figures 4.6.b and 4.6.d respectively). (Image courtesy Commonwealth of Australia Bureau of Meteorology).

Significantly enhanced rainfall regions were clearly allied with areas of anomalously low pressure, or coastal regions that would experience on-shore (wind) flow as a result of the regional MSLP anomaly. Regions where rainfall was described as suppressed were associated with zones of anomalously high pressure or offshore winds associated with MSLP anomalies. The rainfall and MSLP data sets were statistically independent, and illustrated a physical relationship between the MJO and rainfall, because of their independent correlations with RMM phase.

While the exact nature of the teleconnections between the MJO and rainfall remain to be defined, the RMM Index can be utilised to provide information about the response. While the response for each phase has been discussed, any lag between the response, and the causal phase have not been investigated. A region by region examination of phase and possible lag is required. Advances in modelling the MJO should assist in resolving the nature of the teleconnection established by this research. Kidson et al (2002) suggested that forcing of extra-tropical Rossby waves was responsible for the mid- and high-latitude changes to atmospheric circulation they observed.

Although the magnitude of the MSLP anomalies does not appear to be considerable, they are statistically significant, and their spatial scale is very extensive. In addition, a synoptic chart generally ranges between the extremes of 970 and 1030 hectaPascal, and anomalies of up to 6 hectaPascal like those determined, have the potential to exert a fairly strong influence on the weather. The location and nature (positive or negative) of the MSLP anomalies corroborates the reported rainfall response to the MJO.

4.5.2 Lag

Diffuse spectral peaks can be identified by plotting the K-W test (Figure 4.9). From about 10 days lag, there is a marked decrease in the number of significant sites. The spectral peaks post day 10 (10-60 days) might be indicative of MJO cycle lengths as they occur from about 22 days lag, the shortest time frame expected for an MJO. That is, the observed spectral peaks occurring after 10 days may be a measure of MJO cycles in the data set that are shorter than a 60 day oscillation period. The median MJO cycle is 45 days (Madden and Julian, 1994), and a broad spectral peak can be identified at this lag time.

These spectral peaks might also be indicatory of the MJO 'shadow wave'- a secondary oscillation travelling about halfway between MJO oscillations and identified on some analyses. This shadow wave is expected approximately 14days after the passage of the MJO oscillation, or at around half a median MJO temporal scale (22.5 days), and there is a distinct spectral peak at about 22 to 28 days.

4.5.3 Strong signals

Although the K-W testing showed an improvement in the number of results when using strong signals (RMM Index absolute value of greater than 1) in comparison to the full RMM Index data set, little extra information is generated. The maps constructed do not better delineate the influence of the MJO. The aim was to produce a simple predictive index. Excluding weak signals does not particularly assist and/ or limit the comparison (strong phase to strong other phase instead of Phase 1 to anything else that can happen). Only predicting rainfall when the RMM signal is

strong reduces spatial extent of the tool developed here, and does not add any information. It may then be appropriate to forecast rainfall occurrence using all RMM Index values, as the system developed is accurate independent of the MJO signal strength. The main impact of low amplitude on the forecasting tool developed here is that the RMM Index may not be predicting phase, and subjective phase determinations must be made.

4.5.4 Locking the phases

Treating the 8 phases as 4 supersets did not improve the information provided by the simple predictive tool developed. However, this treatment of the phases (combining them) might assist in future analyses of the role of seasons in the predictive tool (see chapter 5 below). While this element of the analysis did not produce marked results, even a ‘dead-end’ may provide information for later analysis and research.

Chapter 5 MJO and Seasonal Rainfall for Australia

5.1 Introduction

Much of the behaviour of the MJO is seasonally dependant, including amplitude, frequency and path of travel (Hendon, Zhang and Glick, 1999; Slingo et al, 1996; Maloney and Kiehl, 2002: Wang and Rui, 1989). Kidson et al (2002) found distinct seasonal variations in the MJO and in the MJO's ability to influence associated convective anomalies at higher latitudes. As the seasonally influenced MJO impacts upon rainfall, a seasonal component to that MJO rainfall impact could be detectable. The forecasts may gain greater skill if the data were separated according to season, and seasonal adjustments to the forecast outputs were made. Each season would provide different forecast maps for the RMM phases. Accordingly, the K-S distributions were reconstructed based on four seasons, and as a wet and dry season.

The tropics, extra topics and higher latitudes experience very different timing for the bulk of their annual rainfall. For example, Australia's north and south experience different seasonal rainfall responses. Australia's north (from approximately 25degrees S to the northern extremities) tends to lack four distinct seasons, instead having hot, wet summers, and cool, dry winters (Sturman and Tapper, 1996). The south (from approximately 28 degrees S to the southern extremities) tends to experience the traditional, manifest four seasons, with most of the annual precipitation received during the winter months (Figure 5.1). The scope of this work did not permit seasonal analysis of the global data sets.

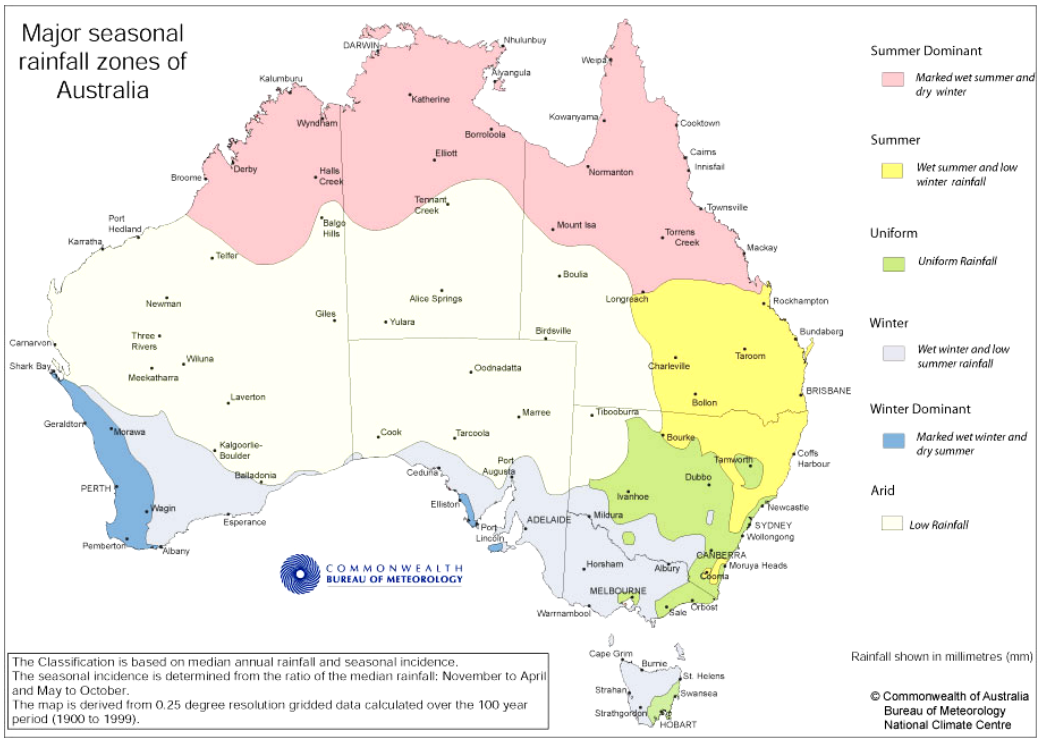

Figure 5.1 Major seasonal rainfall Zones of Australia. Northern Australia experiences most rainfall during the summer months, the south predominantly receives rainfall during winter. (From Commonwealth of Australia Bureau of Meteorology (ii))

Wheeler (2002) produced seasonal composites with two of the RMM fields, OLR and 850hPa wind anomalies, and generated weekly rainfall anomalies. The seasons overlapped and were of four months duration: Spring (September, October, November, December); summer (December, January, February, March); autumn (March, April, May, June); and winter (June, July, August, September) (Figure 5.2 .a, b, c and d respectively) (Sturman and Tapper 1996). It is apparent from Wheeler's (2002) seasonal composite rainfall anomaly maps that the MJO has a greater impact on both positive and negative weekly rainfall anomalies. During summer and autumn, the MJO appears to be enhancing rainfall in Phases 4, 5, 6 and 7. There are distinct negative rainfall anomalies during summer for Phases 1, 2 and 3.

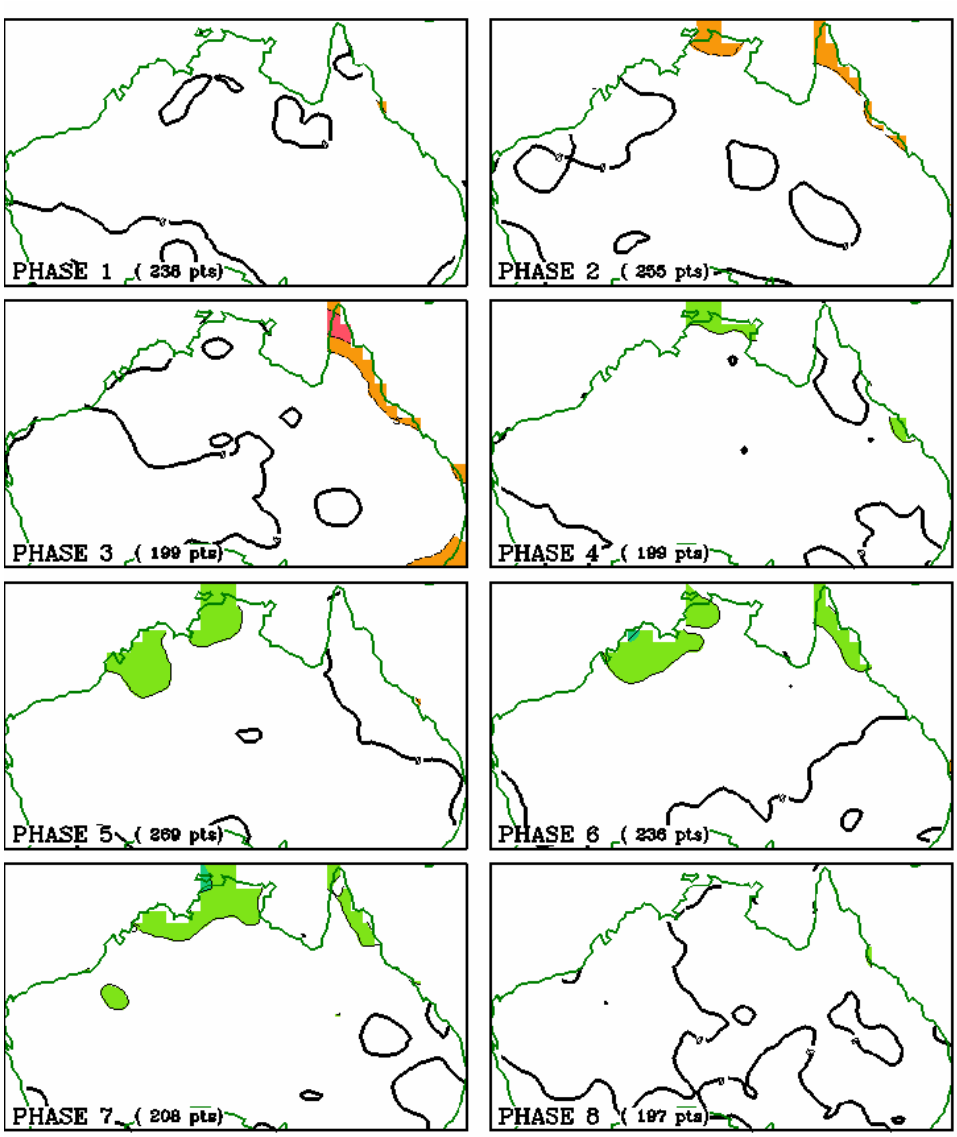

Figure 5.2.a Spring weekly rainfall anomalies (mm) for each phase (Positive anomalies blue/green tones, negative anomalies red/brown tones)(From Wheeler 2002)

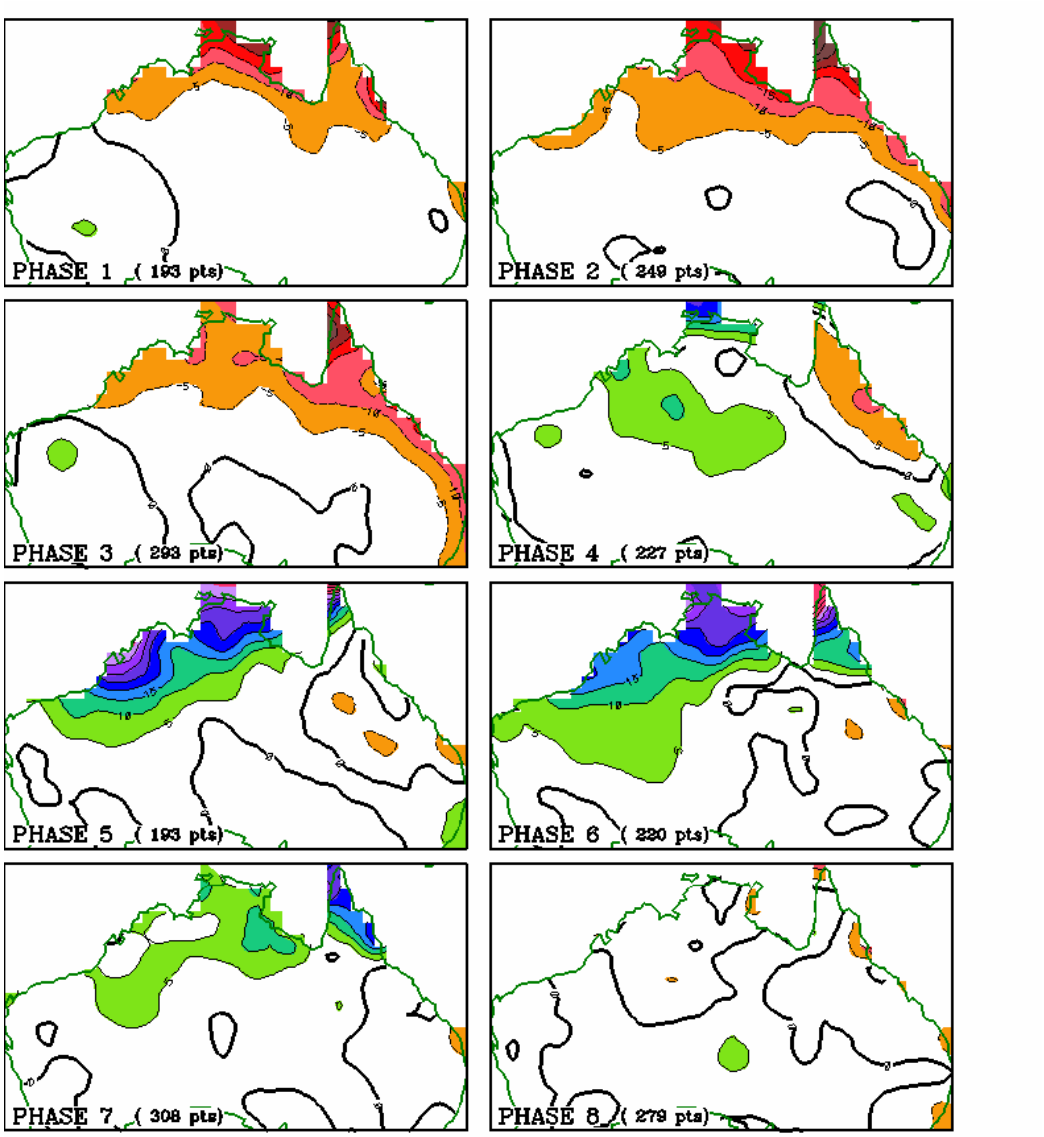

Figure 5.2.b Summer weekly rainfall anomalies (mm) for each phase (Positive anomalies blue/green tones, negative anomalies red/brown tones) (From Wheeler, 2002).

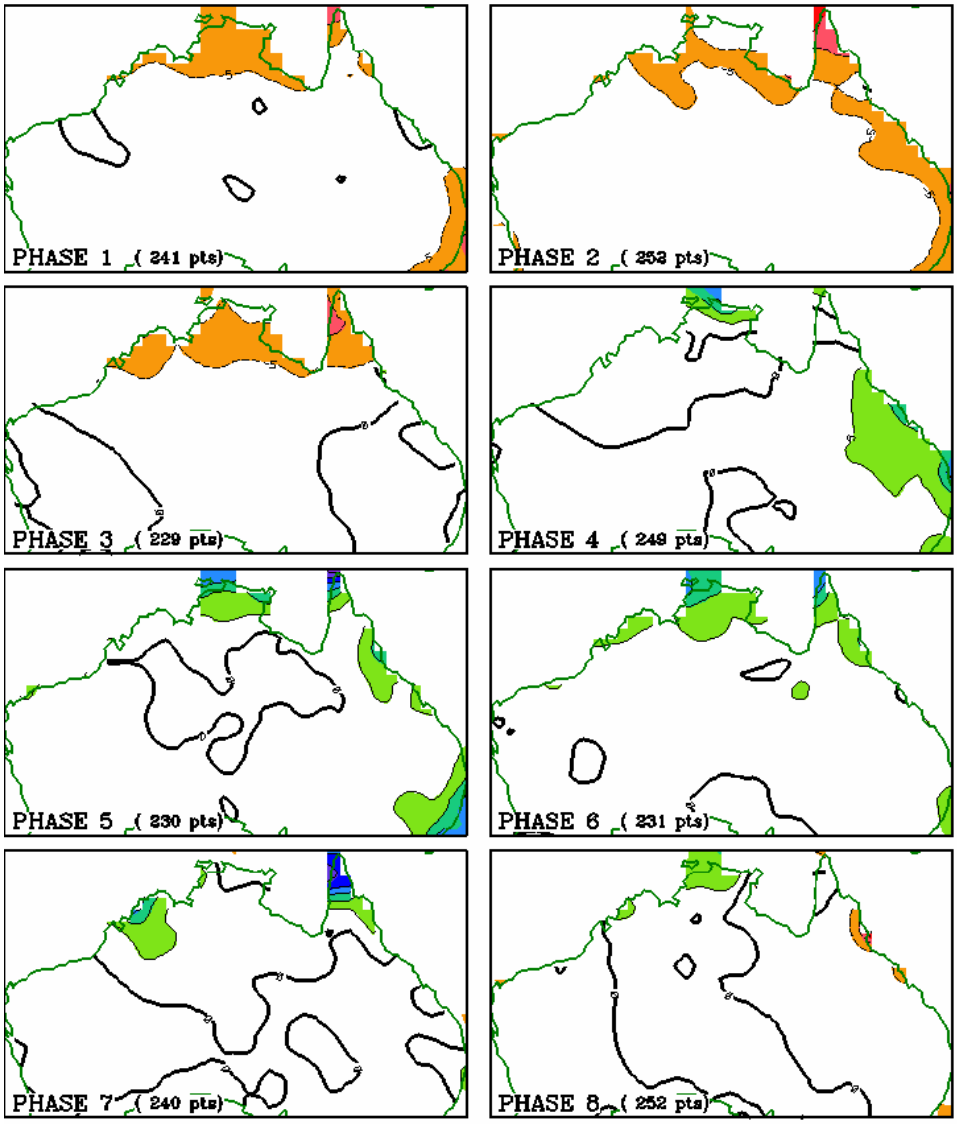

Figure 5.2.c Autumn weekly rainfall anomalies (mm) for each phase (Positive anomalies blue/green tones, negative anomalies red/brown tones). From Wheeler, 2002)

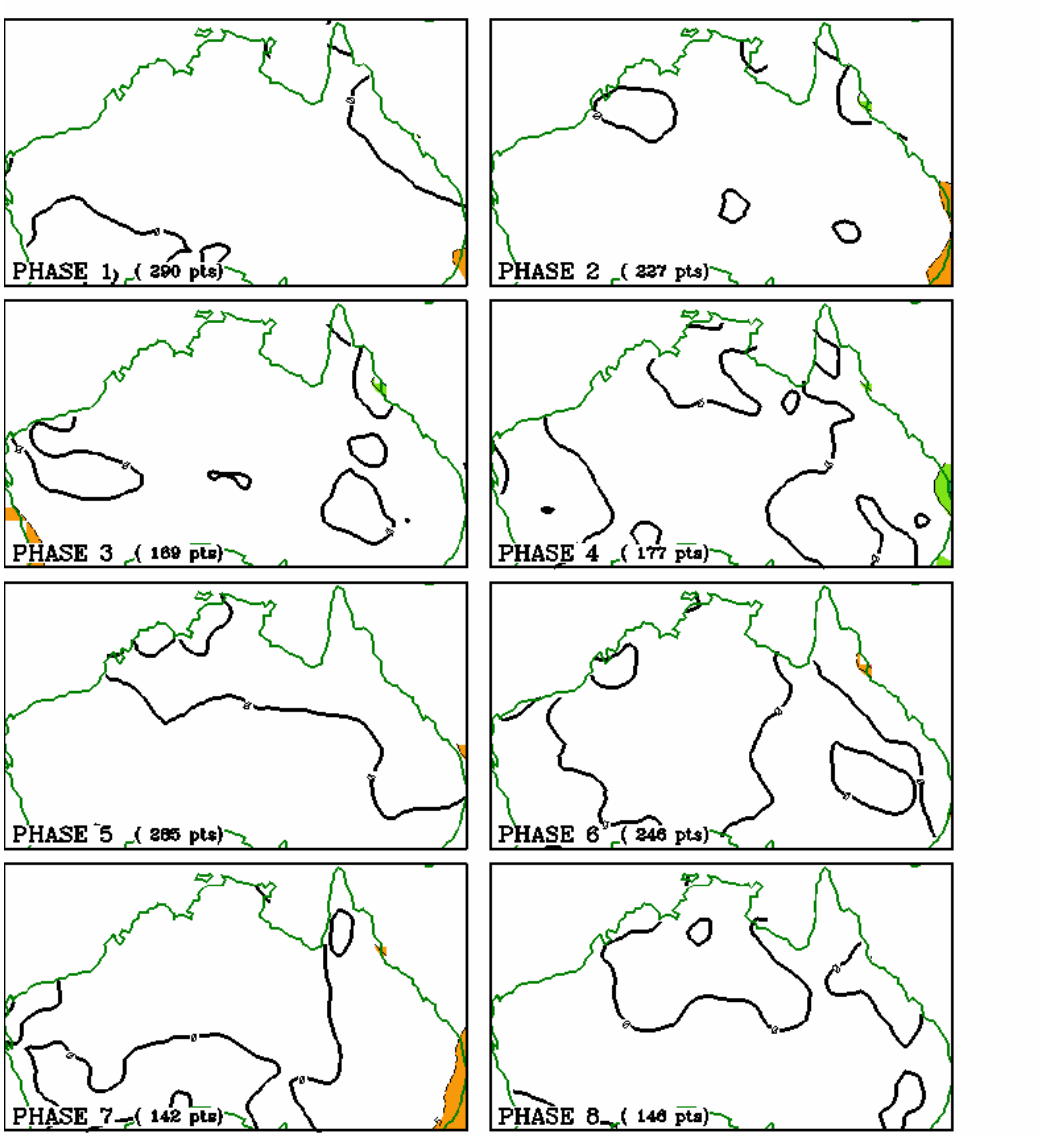

Figure 5.2.d Winter weekly rainfall anomalies (mm) for each phase (Positive anomalies blue/green tones, negative anomalies red/brown tones).(From Wheeler, 2002).

5.2 Data

The data used to calculate the seasonal influence of the MJO were as per Chapter 4 BoM and RMM.

5.3 Methodology

5.3.1 Four Seasons

The data were separated into season: spring; summer; autumn; and winter. The seasons were defined as follows: spring (September, October, November); summer (December, January, February); autumn (March, April, May); and winter (June, July, August) (Commonwealth of Australia Bureau of Meteorology ii, 2004) (Figure 5.2). For each phase (1-8) a K-S test was performed, comparing the rainfall distribution each season for each phase compared with the rainfall distribution for each season for all other phases. For each station there were 8 phase results, divided into the 4 seasonal components. The results were extremely sparse spatially, so in an attempt to highlight the few significant stations in the results, non-significant result stations were not produced on the output maps (5.3.a, b, c and d) for this section.

5.3.2 Wet Season/ Dry Season

The data were separated into two seasons: wet; and dry. The dry season was defined as May to October inclusive, and the wet season as November to April inclusive (Commonwealth of Australia Bureau of Meteorology ii, 2004) (Figure 5.2). For each phase (1-8) a K-S test was performed, comparing rainfall each season for each phase compared with rainfall for each season for all other phases. For each station there were 8 phase results, divided into the two components. In broad terms the wet season was spring and summer combined, the dry season autumn and winter.

While related to the MJO, the heavy monsoonal rains that northern Australia experiences during the summer, are not the MJO, however the timing and strength of the monsoons are affected by the MJO. Monsoonal rains might mask individual MJO events, so that the MJO's impact during summer is 'hidden' in the daily rainfall totals. Conversely, during northern Australia's dry season (Southern Hemisphere winter), when MJO events have a good chance to obviously influence the rainfall, the MJO does not encroach so physically close to the region.

5.4 Results

5.4.1 Four Seasons

5.4.1.1 Spring

Spring (Figure 5.3.a) saw a markedly reduced MJO influence and associated impact on Australian rainfall. While no influence was discerned for Phases 1, 2, 4, 7 and 8, the MJO still produced some significant relationships with rainfall. In the course of Phase 3 there was a strong suppressed rainfall response in the south east, and this response was more spatially extensive and intensive than the all season response to Phase 3. During spring the output demonstrated suppressed rainfall conditions for the southeast. It was determined that the enhanced rainfall responses observed during all seasons in Phases 5 and 6 in the south east, also occurred in spring. The passage of an MJO in spring was most likely to affect rainfall in Australia's southeast corner, during Phases 3, 5 and 6.

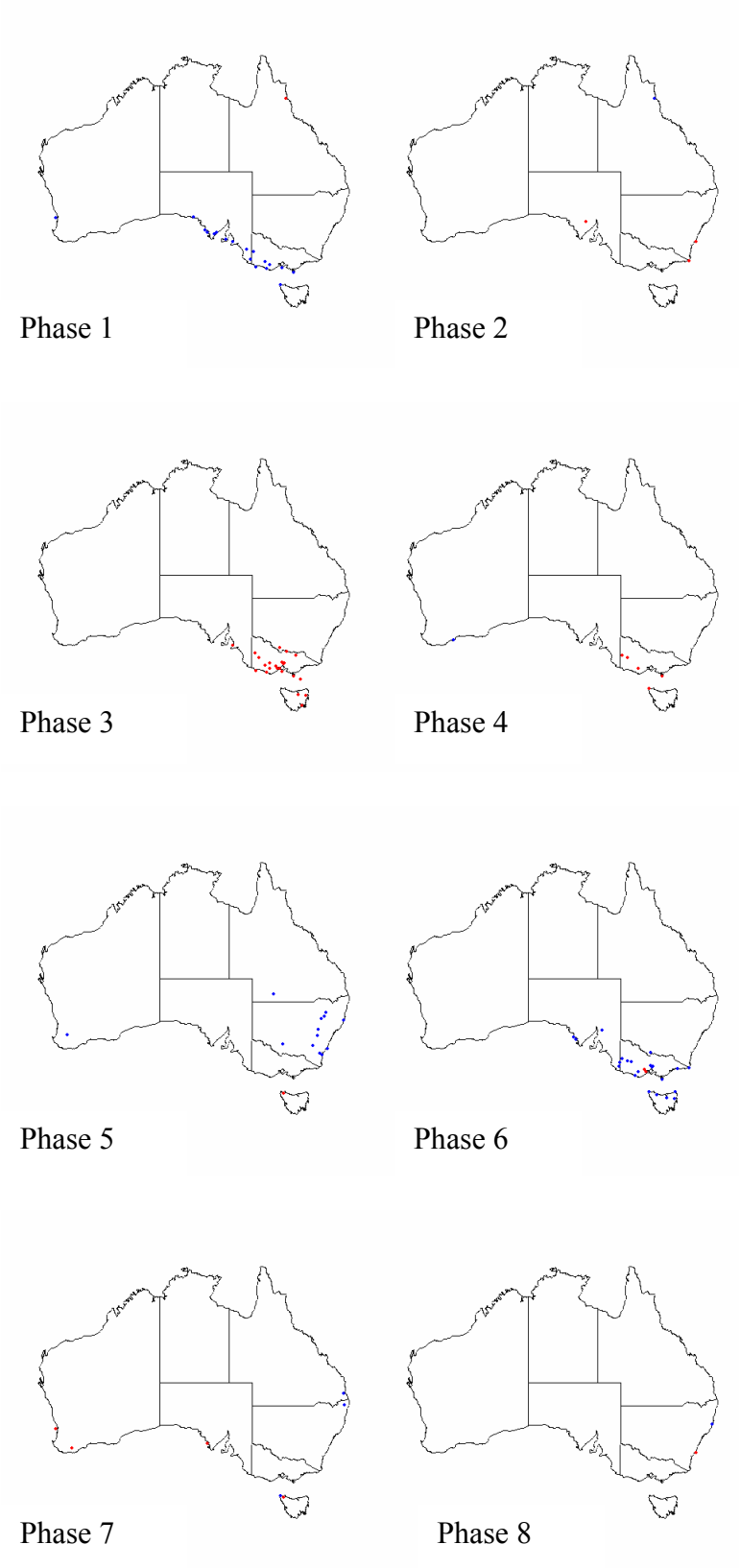

Figure 5.3.a Spring K-S distributions of RMM Phases 1-8 and BoM rainfall data (Blue enhanced rainfall, Red suppressed rainfall).

5.4.1.2 Summer

During the Southern Hemisphere summer (Figure 5.3.b) months the MJO peaks in strength, and travels closest to Australia (Wang and Rui, 1989;Wheeler, personal communication, 2004.), and the strongest response to the MJO might be expected. However, there is little remarkable rainfall response to the MJO during summer that cannot be observed in the analogue treatments. Spatially reduced suppression responses during Phases 1, 2 and 3 can be observed, with little or no suppression adjacent the east coast (Phases1 and 2) or South Australia (Phases 3) in the summer. The only season an enhanced rainfall response is observed in northwestern Australia is summer.

The enhanced rainfall response across Australia's western tropics is a summer phenomenon. While the general response to all Phase 7 is suppression of rainfall across Victoria 7, summer Phase 7 results in enhanced rainfall conditions. During summer Phase 8 results in regions of suppressed rainfall in the northwest, and this response is not observed for the analogue years. During summer the MJO reduces regions of suppression during Phases 1, 2 and 3, enhances rainfall throughout the tropics (possibly enhancing monsoonal effects), and increases regions of suppression during Phase 8.

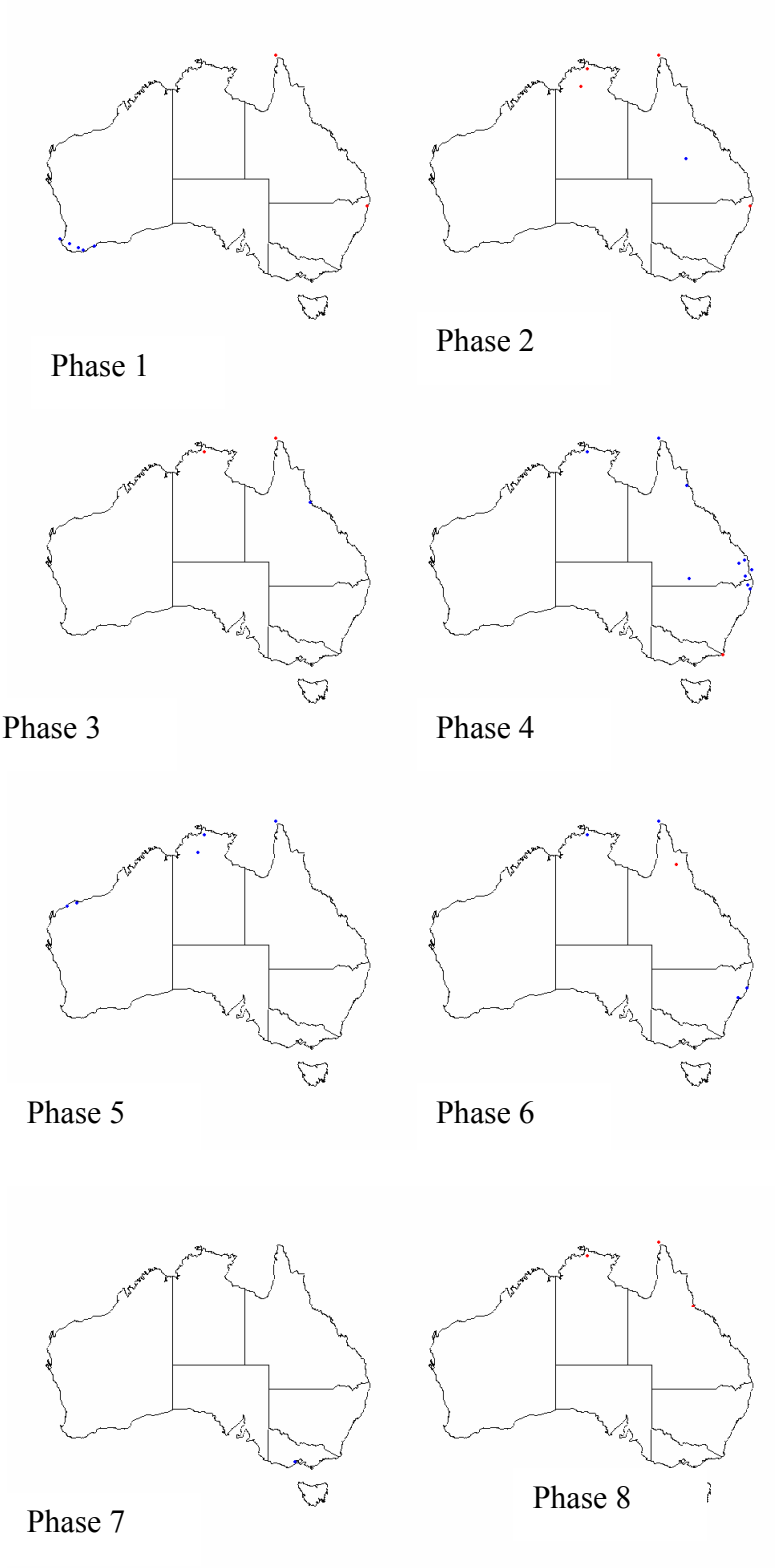

Figure 5.3.b Summer K-S distributions of RMM Phases 1-8 and BoM rainfall data (Blue enhanced rainfall, Red suppressed rainfall).

5.4.1.3 Autumn

Autumn (Figure 5.3.c) was associated with spatial reduction of the suppressed condition Phases 1 and 2 outputs for northern Australia. During Phase 3, there was some indication of reduced suppression, and indeed enhanced convection in the southeast. Autumn Phase 4 accounted for much of the rainfall along the east coast with enhanced rainfall conditions apparent across the southeast, in contrast to the suppression observed in that region during analogue years. During autumn the enhanced effects did not appear to penetrate as far south in Phases 5 and 6, in contrast to the response observed in Phases 3 and 4, when the effects appeared to infiltrate further south. Suppression of rainfall along Australia's east coast seems stronger during Phase 8 in autumn.

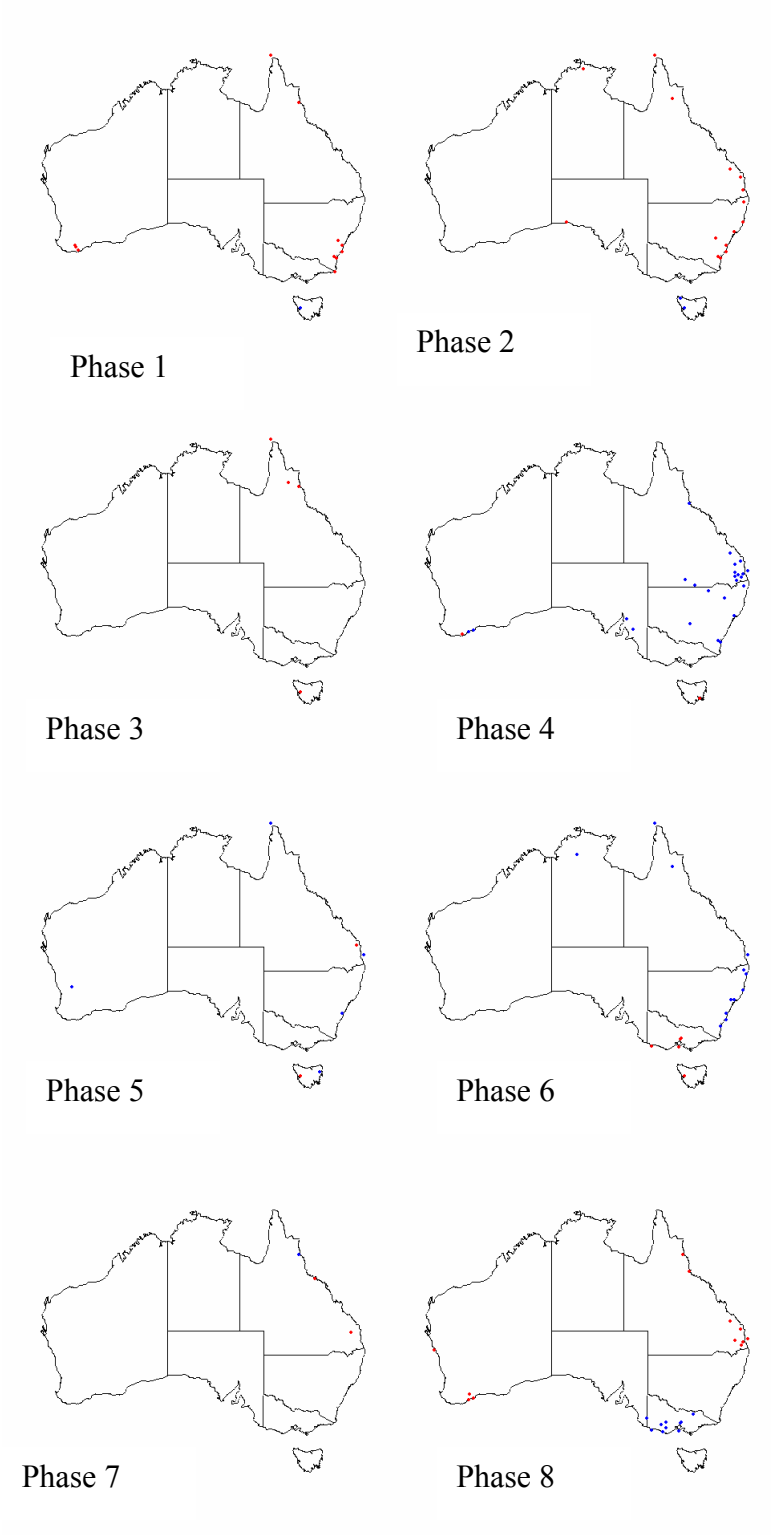

Figure 5.3.c Autumn K-S distributions of RMM Phases 1-8 (top to bottom left to right) and BoM rainfall data (Blue enhanced rainfall, Red suppressed rainfall, Grey site not significant).

5.4.1.4 Winter

Winter (Figure 5.3.d) heralds some distinct changes to the impact of the MJO. In Phases 1 and 4 strong suppression across the south is apparent, with Phases 4 and 5 still generating some enhanced rainfall conditions in similar regions to the analogue years. The enhanced conditions in the north noted in the analogue years Phase 7 are not apparent in Phase 7 winter, presumably because the MJO is travelling north of its southern summer path. Thus, the South China Sea is experiencing the more direct MJO impact, rather than northern Australia.

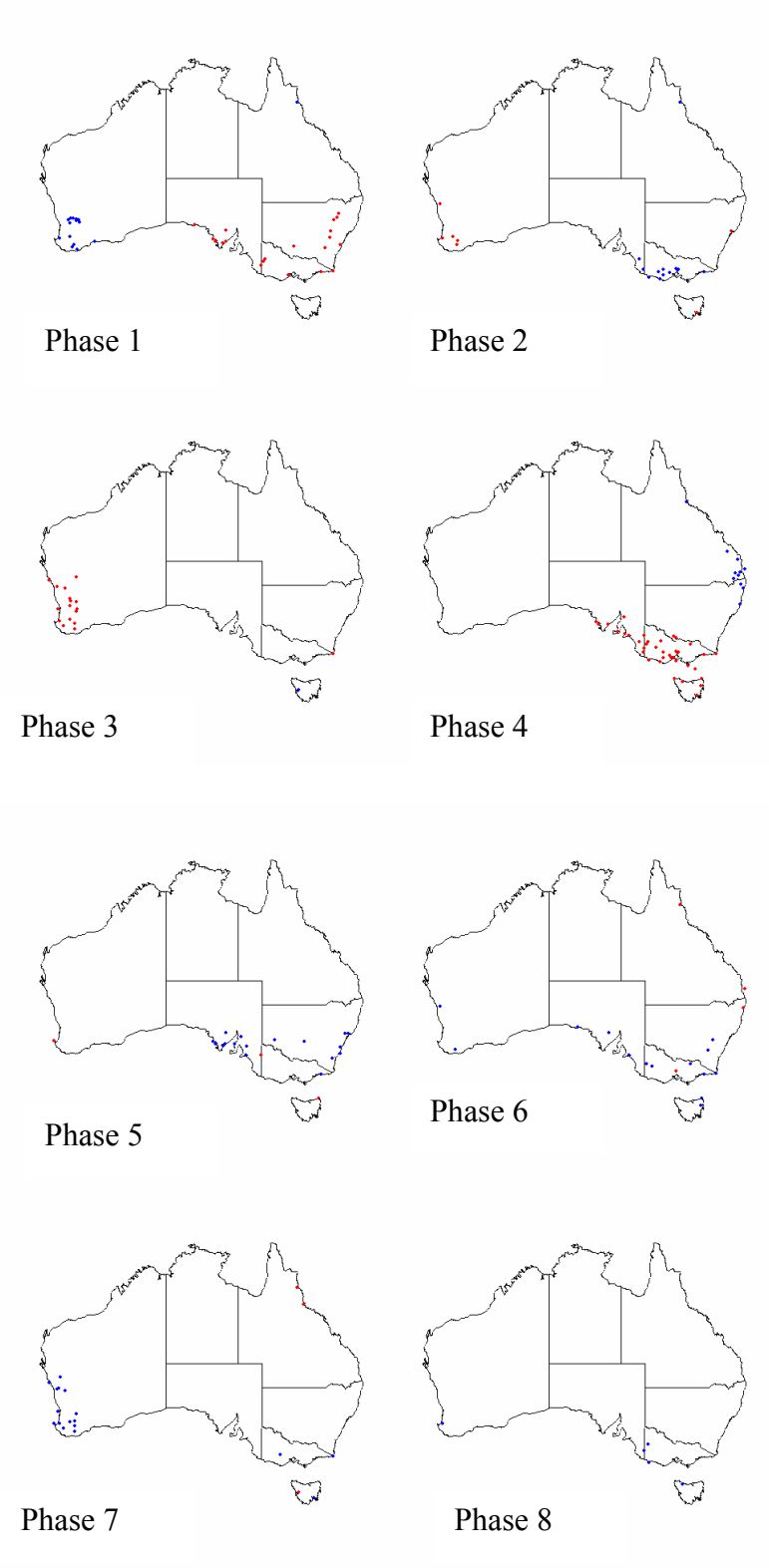

Figure 5.3.d Winter K-S distributions of RMM Phases 1-8 and BoM rainfall data (Blue enhanced rainfall, Red suppressed rainfall).

5.4.2 Wet Season/Dry Season

The wet and dry season rainfall distributions were also contrasted using a K-S distribution based on the RMM phases. The dry season was defined as May to October, and the wet season as November to April. The dry season is roughly analogous with the winter period, and the wet season with the summer months. This definition conforms with that represented by the major seasonal rainfall zones of Australia (Figure 5.2).

While in Phase 1 (Figure 5.4.b) a clear suppression signal can be observed in southeast Australia during the dry season. This region of rainfall suppression is more extensive than the suppression seen for the all seasons result (Figure 4.1.b). The dry season appears to account for much of the rainfall suppression seen in southeast Australia, as there is little rainfall suppression during the wet season (Figure 5.4.a). During the wet season the suppression observed over the northern Australia for all seasons is present. The rainfall enhancement in Tasmania appears to be a dry season response, while that observed in western Australia was identified during the wet season.

The rainfall suppression observed during Phase 2 all seasons (Figure 4.2.b) is a wet season response, so the MJO is not only linked with convection, but also wet season breaks. The small area of rainfall enhancement observed in north Queensland is a dry season event. During Phase 3 (Figure 5.4.a and b) there is a limited wet/dry season response, compared with the all season (Figure 4.3.b) result. Perhaps the only inference to be drawn is that the rainfall suppression seen in southern Victoria (Figure 5.4.b) is predominantly a dry season occurrence.

The wet/dry season results (Figure 5.4.a and b) for Phase 4 suggest the rainfall enhancement identified along Australia's east coast is present in both the wet and dry season, but is more likely to push inland during the wet season. During the Phase 4 dry season the suppression of rainfall over Victoria (Figure 5.4.b) could be expected. The enhancement of rainfall observed during all season Phase 5 (Figure 4.5.b) is predominantly a dry season trend. During Phase 6 the enhancement patterns are a dry season response in the south, and a wet season event in the north.

Through Phase 7 (Figure 5.4 a and b) the enhanced rainfall conditions in northern Australia appear to be primarily a wet season effect, while the dry season seems to be responsible for much of the suppression observed during all seasons (Figure 4.7.b). The all seasons output for Phase 8 (Figure 4.8.b) did not generate clear results, however the wet season results (Figure 5.4.a) appear to suggest tropical region rainfall suppression after the passage of the MJO.

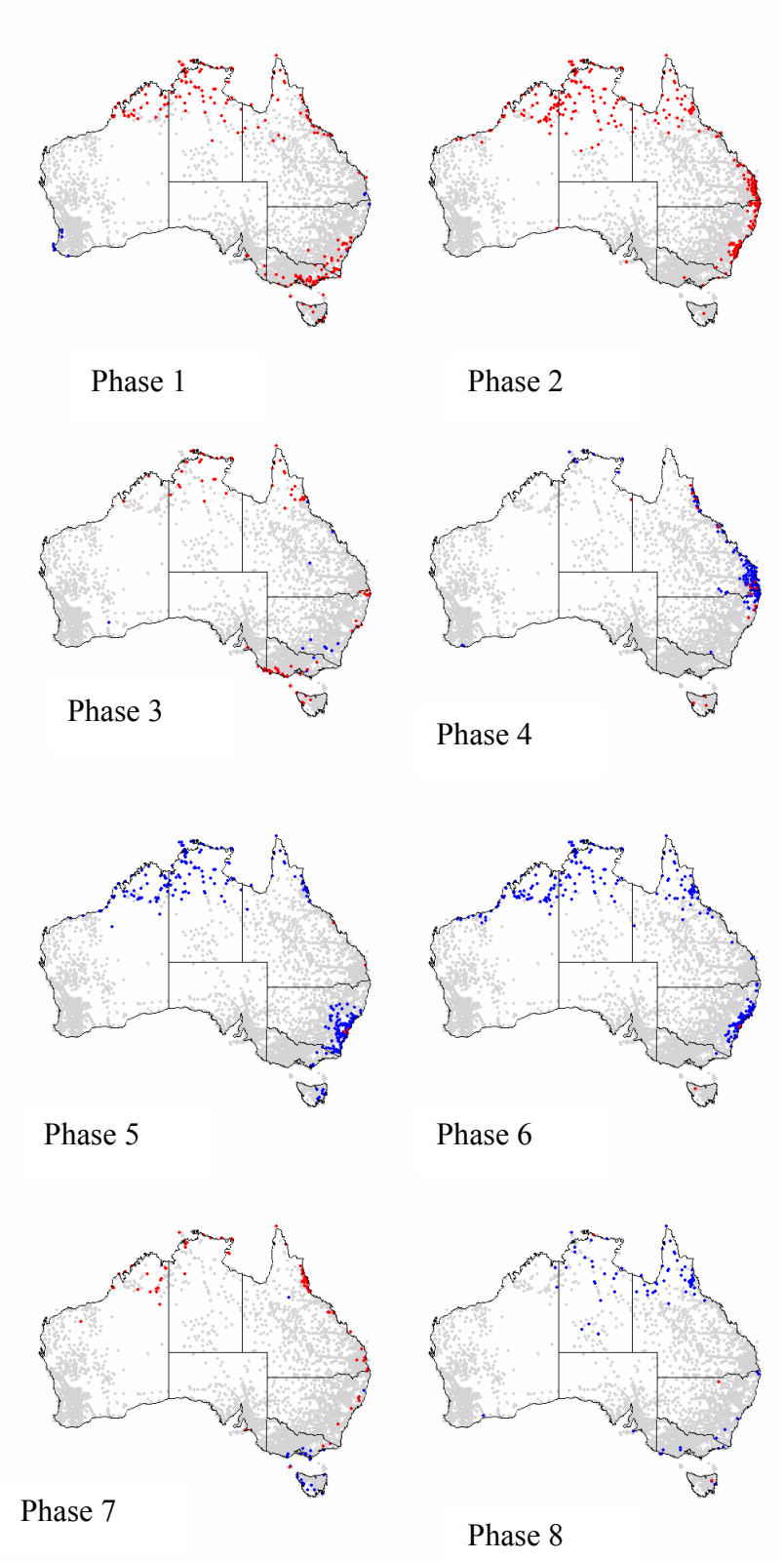

Figure 5.4.a Wet Season K-S distributions of RMM Phases 1-8 (top to bottom, left to right) and BoM rainfall data (Blue enhanced rainfall, Red suppressed rainfall, Grey site not significant).

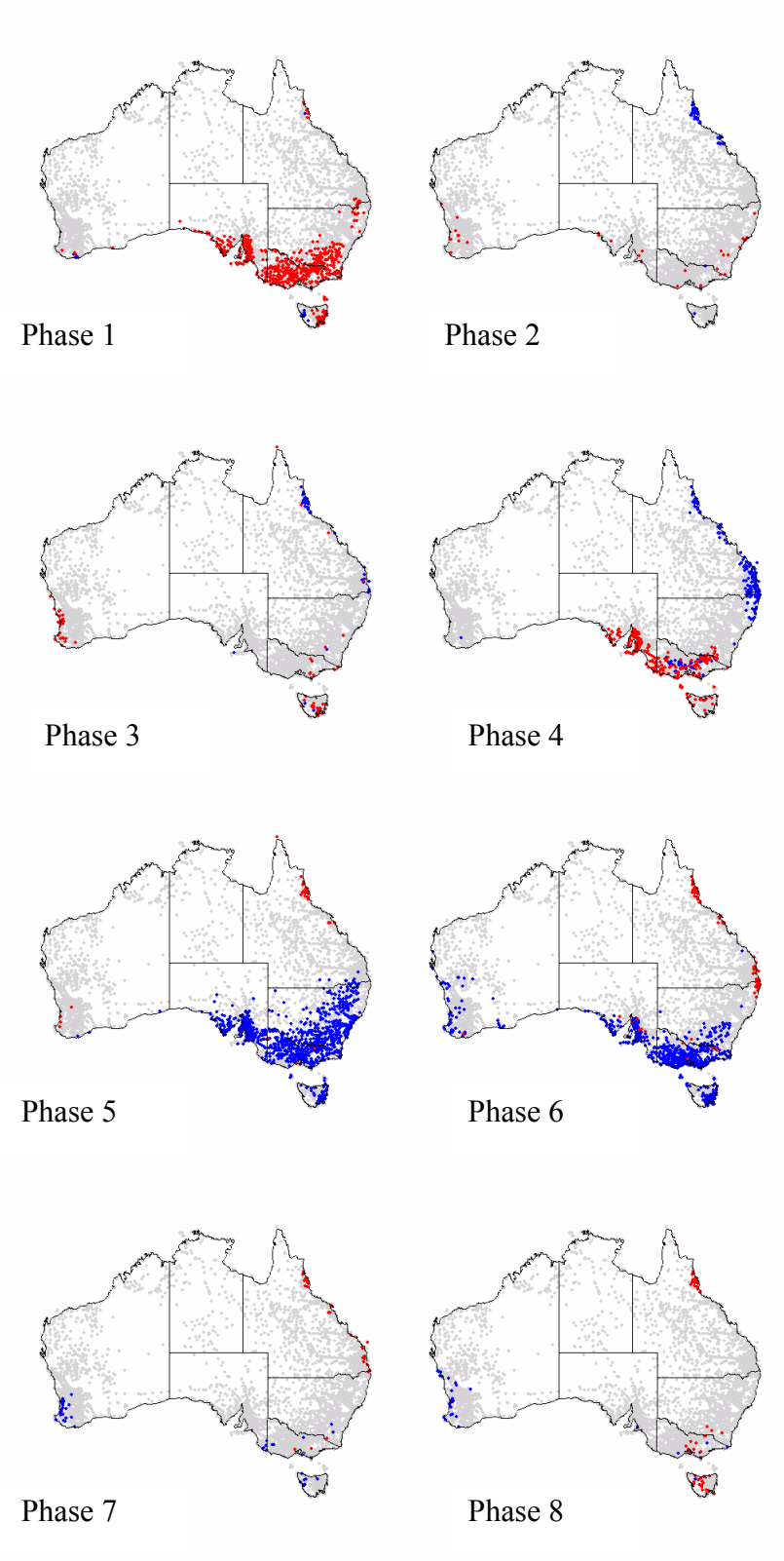

Figure 5.4.b Dry Season K-S distributions of RMM Phases 1-8 (top to bottom, left to right) and BoM rainfall data (Blue enhanced rainfall, Red suppressed rainfall, Grey site not significant).

5.5 Discussion

Interestingly no seasonal component to the impact of the MJO on Australia's rainfall could be discerned by this work. Perhaps the groupings did not contain enough data to discern daily rainfall anomalies. Weekly anomalies (Wheeler, 2002) did reveal a seasonal response of Australian rainfall to the MJO so possibly the size of the cohesive data units (each phase divided by season) simply did not contain enough data and therefore could not illustrate the response observed in Wheeler's (2002) results. Further study combing phase locking and seasonal analysis might provide information about the seasonal variance of the impact of the MJO, by providing a larger data set to divide into seasons.

The wet and dry seasons did reveal some of the differences between the impact of the MJO for northern and southern Australia not revealed by analysis of the analogue data sets. Although the northern parts of Australia are the areas that experience wet and dry seasons as distinct from four seasons, a considerable impact across the south can be noted. This may be because the autumn and winter, and summer and spring, treated together, reveal trends not apparent from the reduced size data sets available for four season calculations.

Dividing the year into two broader seasons provides a better response. This response might be more analogous with the MJO, as it is a tropical phenomenon. The responses observed in the wet and dry season analysis suggest the division into four seasons does produce groups too small to produce the significant results seen for wet/dry and all seasons.

The north and the south east corner of Australia respond to the passage of a wet season (spring and summer) MJO. Phases 1 and 2 experience rainfall suppression, with some suggestion of suppression during Phase 7. The influence of the passage of the MJO during the dry season (autumn and winter) is a possible enhancement of southern Australia's winter precipitation during Phases 5 and 6. The east coast receives dry season rainfall during Phase 3, but there is suppression of precipitation for the south in Phases 1 and 3.

Chapter 6 Conclusions

An evaluation of RMM phase system's forecasting/predictive ability indicated that it could be applied to produce forecast output delineating areas with enhanced or suppressed relationship with rainfall dependant upon the RMM Index phase. The RMM Index has been successfully applied in statistical analyses, and those analyses established that the tropical passage of the MJO is capable of influencing rainfall well beyond the tropics.

In this dissertation rainfall data from across both Australia and the globe has been used to provide the basis for a simple predictive tool, in map form. These maps provide information about the location for the potential of enhanced or suppressed rainfall regimes that might be expected as the MJO travels east along the tropics from its origin over the Indian Ocean. The results, in map form, clearly demonstrate that, via teleconnections, the MJO is capable of positively and negatively impacting upon the temporal and spatial variability of rainfall well into the mid-latitudes.

The mapping system developed here comprises an accessible, adaptable, and easily comprehensible forecasting tool for use by the rural sector. The ability to discern coloured regions is the only requirement for using the tool. Simple practical applications for this research within the agricultural sector are extensive. Many management decisions are made at the intraseasonal time scale and knowledge of the timing of potentially wet or dry conditions is an important decision making factor. The rudimentary tool developed is a new facet of the existing climate variability buffer techniques.

Current best practice synoptic weather forecasting looses much of its accuracy beyond five days, and is not routinely available beyond 10 days. At present, there is a temporal scale gap between synoptic weather and seasonal climate forecasting that the results (of this study) begin to address. There are few scientifically based alternative strategies available for prediction of rainfall at these intraseasonal time scales. The ability of the RMM Index phase to be predicted allows this predictive tool to provide a 14 day forecast of possible rainfall suppressed or enhanced conditions. The tool is limited by the ability of the RMM Index to maintain amplitude and accurately identify the MJO. No analysis of the lag between the response and the casual phase has been made, and these refinements could be completed at a regional level.

Little or no seasonal component to the impact of the MJO on Australia's rainfall was determined, in contrast with Wheeler's (2002) seasonal composites. Perhaps the seasonal groupings did not contain enough data to discern the daily rainfall anomalies in this context. Dividing the year into two broader seasons provided a more discernable response. The MJO impacts on southern Australia's rainfall during the dry season (autumn and winter) by enhancing their winter precipitation, while the north and the southeast corner of the continent respond to the passage of a wet season (spring and summer) MJO.

Using MSLP to provide an overview of what (synoptic scale) anomalies the MJO might initiate over its cycle provides a real insight into the possible nature of MJO/rainfall teleconnections. This basic analysis offers a basis for further research

delineating the MJO by identifying anomalies in recognised synoptically scaled features.

There are acknowledged limitations to the accuracy of these results. Some of these are based in inherent problems in the data collection in the past. Others are based in the statistical analyses used. While I assert that impact of type I and II errors and autocorrelation are minimal and do not affect the overall accuracy, these errors will have occurred in the results. K-S tests were not designed to evaluate such large data sets, nor data sets that contain as many zeroes (no rain days). Recently defined statistical methods, such as the Tweedie Distribution, may provide a more accurate statistical analysis.

These results represent a real contribution to the body of MJO knowledge. In this dissertation the MJO has been definitively linked to both the enhancement and suppression of rainfall on a global scale, not just adjacent the tropics. Prior attempts to define MJO related rainfall modulations were hampered by the quality of the MJO estimate. Potentially, other synoptic factors such as temperature, frost risk and wind vectors could all be forecast, using a method similar to the rainfall forecasting tool developed here. The spatial and temporal impact of the MJO on rainfall might be further refined using other statistical techniques.

References

Barlow, M., Wheeler, M., Lyon, B., Cullen, H. (in review): Modulation of Daily Precipitation Over Southwest Asia by the Madden-Julian Oscillation. Monthly Weather Review.

Bond, N. and Vecchi, G. (2003): The influence of the Madden-Julian Oscillation on Precipitation in Oregon and Washington. Weather and Forecasting, 18, 600-613.

Chao, W. and Chen, B. (2001): The Role of Surface Friction in Tropical Intraseasonal Oscillation. Monthly Weather Review, 129, 896-904.

Chappel, L.C. and Bate, P. W. (2000): The South Pacific and southeast Indian Ocean tropical cyclone season 1997-98. Australian Meteorological Magazine, 49, 121-138.

Chen, S.S., Zhang, C and Houze R.A. Jr. (1998): The Diurnal cycle of atmospheric convection and surface boundary layer conditions over the warm pool in TOGA COARE-98 Conference Proceedings, World Meteorological Organization, Boulder, Colorado, USA.

Chen, T-C. and Murakami, M. (1988): The 30-50 Day Variation of Convective Activity over the Western Pacific Ocean with Emphasis on the Northwestern Region. Monthly Weather Review, 116,4, 892-906

Chen, T-C., Yen, M-C. and Murakami, M. (1988): The Water Vapour Transport Associated with the 30-50 Day Oscillation over the Asian Monsoon Regions during 1979 Summer. Monthly Weather Review, 116,10, 1983-2002.

Chen, X., Wang, H., Xue, F. and Zeng, Q. (2001): Intraseasonal oscillation: the global coincidence and its relationship with ENSO cycle. Advances in Atmospheric Sciences, 18, 445-453.

Colon, E., Lindesay, J. and Suarez, M. J. (2002): The Impact of Surface Flux and Circulation Driven Feedbacks on Simulated Madden-Julian Oscillations. Journal of Climate, 15, 624-641.

Commonwealth of Australia Bureau of Meteorology (Date not provided), Date Accessed June11, 2004. Rainfall Variability September to November. http://www.bom.gov.au/climate/map/variability/VARSEP.GIF

Commonwealth of Australia Bureau of Meteorology (Last updated May 2003): Australian Daily Rainfall Sites. Product Reference Number IDCJDC03.200305. http://www.bom.gov.au/climate/how/newproducts/IDCdr.shtml.

i Commonwealth of Australia Bureau of Meteorology (2004), Date Accessed June11, 2004. Climate Glossary. http://www.bom.gov.au/climate/glossary/seasons.shtml)

ii Commonwealth of Australia Bureau of Meteorology (2004), Date Accessed June11, 2004. Major Seasonal Rainfall Zones of Australia. http://www.bom.gov.au/climate/environ/other/seas_group.shtml

Drodowsky, W. (1996): Variability of the Australian summer monsoon at Darwin 1957-1992. Journal of Climate, 9, 85-96.

Elleman, R. (Last updated 1997): http://www.ces.ucsb.edu/esrg/ess_sum97/Students_ESS.1997/Rob-Elle... /paper_rob.htm

Feng, M., Lukas, R., Hacker, P., Weller, R. A. and Anderson, S. P. (2000): Upper-ocean heat and salt balances in the western equatorial Pacific in response to the intraseasonal oscillation during TOGA COARE. Journal of Climate, 13, 2409-2427.

Fink, A. and Speth, P. (1997): Some potential forcing mechanisms of the year-to-year variability of the tropical convection and its intraseasonal (25-70-day) variability. International Journal of Climatology, 17, 1513-1534.

Flatau, M., Flatau, P., Phoebus, P. and Niller, P. P. (1997): The feedback between equatorial convection and local radiative and evaporation processes. Journal of the Atmospheric Sciences, 54, 19, 2373-2386.

Flatau, M., Flatau, P., Rudnick, D. and Niller, P. P. (1998): Intraseasonal oscillations and Asian monsoon onset in TOGA COARE-98 Conference Proceedings, World Meteorological Organization, Boulder, Colorado, USA.

Fogiel, M. (1996): The Statistics Problem Solver. Research and Education Association, New Jersey, 876-883, 914-924.

Geerts, B. and Wheeler, M. (Last updated 1998): The Madden-Julian Oscillation. http://weather.uwyo.edu/~geerts/cwx/notes/chap12/mjo.html.

Gill, A. E. (1980): Some simple solutions for heat-induced tropical circulation. Quarterly Journal of the Royal Meteorological Society, 106, 447-463.

Goswani, B. N. and Rameshan, K. (2000): Convective coupling and interannual and intraseasonal coupled variability in the tropics. Journal of the Atmospheric Sciences, 57, 2445-2462.

Goswani, B. N. and Mohan, R. S. A. (2001): Intraseasonal Oscillations and Interannual Variability of the Indian Summer Monsoon. Journal of Climate, 14, 1180-1198.

Goswani, B. N., Ajayamohan, R.S., Xavier, Prince K. and Sengupta, D. (2003): Clustering of Synoptic Activity by Indian Summer Monsoon Intraseasonal Oscillations. Geophysical Research Letters, 30, 8, 1431.

Goswani, B. N. and Xavier, Prince K. (2003): Potential predictability and extended range prediction of Indian summer monsoon breaks. Geophysical Research Letters, 10,18, 1966.

Grabewski, W.W. (2003): MJO-like Coherent Structures: Sensitivity Simulations Using the Cloud-Resolving Convection Parameterization (CRCP). Journal of the Atmospheric Sciences, 60, 6, 847-864.

Gualdi, S., Navarra, A. and Tinarelli, G. (1999): The interannual variability of the Madden Julian Oscillation in an ensemble of GCM simulations. Climate Dynamics, 15, 643-658.

Hall, J.D., Matthews, A.J. and Karoly, D.J. (2001): The Modulation of Tropical Cyclone Activity in the Australian Region by the Madden-Julian Oscillation. Monthly Weather Review, 129, 12,2970-2982.

Hartmann and Maloney (2001): The Madden-Julian Oscillation, Barotropic Dynamics, and North Pacific Tropical Cyclone Formation. Part II: Stochastic Barotropic Modelling. Journal of the Atmospheric Sciences, 58,17,2445-2558.

Hendon, H. H. and Liebmann, B. (1994): Organization of convection within the Madden-Julian oscillation. Journal of Geophysical Research, 99, 8073-8083.

Hendon, H. H. and Salby, M. L. (1994): The life cycle of the Madden-Julian oscillation. Journal of the Atmospheric Sciences, 51, 2225-2237.

Hendon, H. H. and Glick, J. (1997): Intraseasonal air-sea interaction in the tropical Indian and Pacific Oceans. Journal of Climate, 10, 647-661.

Hendon, H. H., Liebmann, B. and Glick, J. (1998): Oceanic Kelvin Waves and the Madden-Julian oscillation. Journal of the Atmospheric Sciences, 55, 88-101.

Hendon, H. H., Zhang, C. and Glick, J. (1999): Interannual variation of the Madden-Julian oscillation during austral summer. Journal of Climate, 12, 2538-2550.

Hendon, H. H., Liebmann, B., Newman, M., Glick, J. and Schemm, J.K. (2000): Medium-range forecast errors associated with active episodes of the Madden-Julian oscillation. Monthly Weather Review, 128, 69-86.

Hendon, H. H. (2000): Impact of air-sea coupling on the Madden-Julian oscillation in a general circulation model. Journal of the Atmospheric Sciences, 57, 3939-3952.

Horsley,P. and Buckley, D. (2004): Climate Risk for Graziers. Farming Ahead, 144, January 2004.

Hsu, H-H. (2002): Madden-Julian Oscillation in the Western Pacific Warm Pool. Submitted Taiwan AO July 2003.

Johnson, R. H., Rickenbach, T.M., Rutledge S.A, Cielielski, P. E. and Schubert, W. (1999): Trimodal characteristics of tropical convection. Journal of Climate, 12, 2379-2418.

Jones, C. and Gautier, C. (1998): Coupled Modes of air-sea interaction and the Madden and Julian Oscillation in TOGA COARE-98 Conference Proceedings, World Meteorological Organization, Boulder, Colorado, USA.

Jones, C., Waliser, D. E., Schemm, J-K. and Lau, K. M. (2000): Prediction skill of the Madden and Julian Oscillation in dynamical extended range forecasts. Climate Dynamics, 16, 273-289.

Kayano, M. T. and Kousky, V. E. (1999). Intraseasonal (30-60 day) variability in the global tropics: principal modes and their evolution. Tellus, 51A, 373-386.

Kemball-Cook, S. R. and Weare, B. C. (2001): The onset of the Madden-Julian Oscillation. Journal of Climate, 14, 780-793.

Kessler, W. S. and Kleeman, R. (2000): Rectification of the Madden-Julian oscillation into the ENSO cycle. Journal of Climate, 13, 3560-3575.

Kessler, W. S. (2001): EOF representations of the Madden-Julian Oscillation and its connection with ENSO. Journal of Climate, 14, 3055-3061.

Kistler, R., Kalnay, E., Collins, W., Saha, S., White, G., Woollen, J., Chelliah, M., Ebisuzaki, W., Kanamitsu, M., Kousky, V., van den Dool, H., Jenne, R., Fiorino, M.(2000): The NCEP–NCAR 50–Year Reanalysis: Monthly Means CD–ROM and Documentation. Bulletin of the American Meteorological Society, 82, 2, 247–268.

Kidson, J., Revell, M., Bhaskaran, B., Mullan, B., Renwick, J. (2002): Convection Patterns in the Tropical Pacific and Their Influence on the Atmospheric Circulation at Higher Latitudes. Journal of Climate, 15, 137-159.

Knutson, T. R. and Weickmann, K. M. (1987). 30-60 day atmospheric oscillations: Composite life cycles of convection and circulation anomalies. Monthly Weather Review, 115, 1407-1436.

Lau, K. M. and Peng, L. (1987): Origin of low-frequency (intraseasonal) oscillations in the tropical atmosphere, Pt.1, Basic theory. Journal of the Atmospheric Sciences, 44, 950-972.

Lavery B., Kariko, A. and Nicholls, N. (1992): A historical rainfall data set for Australia, Australian Meteorological Magazine, 40, 33-39, 1992.

Lawrence, P. M. and Webster, P. J. (2001): Interannual Variations of the Intraseasonal Oscillation in the South Asian Summer Monsoon Region. Journal of Climate, 14, 2910-2922.

Lee, M. I., Kang, I. S., Kim, J. K. and Mapes, B. E. (2001): Influence of cloud-radiation interaction on simulating tropical intraseasonal oscillation with a

atmospheric general circulation model. Journal of Geophysical Research, 106, 14219-14233.

Liebmann, B., Hendon, H. and Glick J. (1994): The relationship between tropical cyclones of the Western Pacific and Indian Oceans and the Madden-Julian Oscillation. Journal of the Meteorological Society of Japan, 72, 401-411.

Lin, J., Neelin, J. and Zeng, N. (2000): Maintenance of tropical intraseasonal variability in an intermediate-complexity atmospheric model. Journal of the Atmospheric Sciences, 57, 2793-2823.

Lin, J., Mapes, B., Zhang, M and Newman M. (2003): Stratiform precipitation, vertical heating profiles and the Madden-Julian Oscillation. Journal of the Atmospheric Sciences, 61, 296-309.

Linacre, E. and Geerts, B. (Last updated: 1998): Date accessed March 5 2002.Wet Spells during the Australian monsoon. http://weather.uwyo.edu/~geerts/cwx/notes/chap13/monsoon_wet.html

Lo, F. and Hendon, H. H. (2000): Empirical extended-range prediction of the Madden-Julian oscillation. Monthly Weather Review, 128, 2528-2543.

Madden, R. A. and Julian, P. R. (1971): Description of a 40-50 day oscillation in the zonal wind in the tropical Pacific. Journal of the Atmospheric Sciences, 43, 702-708.

Madden, R. A. and Julian, P. R. (1972): Description of Global-Scale Circulation Cells in the Tropics with a 40-50 Day Period. Journal of the Atmospheric Sciences, 29, 1109-1123.

Madden, R. A. and Julian, P. R. (1994): Observations of the 40-50-Day Tropical Oscillation – A Review. Monthly Weather Review, 122, 814-837.

Maloney, E. D and Hartmann, D. L. (1998): Frictional moisture convergence in a composite life cycle of the Madden-Julian oscillation. Journal of Climate, 11, 2387-2403.

Maloney, E. D. and Hartmann, D. L. (2000): Modulation of hurricane activity in the Gulf of Mexico by the Madden-Julian oscillation. Science, 287, 2002-2004.

Maloney, E. D and Hartmann, D. L. (2001): The Madden-Julian Oscillation, Barotropic Dynamics, and North Pacific Tropical Cyclone Formation. Part I: Observations. Journal of the Atmospheric Sciences, 58,17,2445-2558.

Maloney, E. D. (2002): An Intraseasonal Oscillation Composite Life Cycle in the NCAR CCM3.6 with Modified Convection. Journal of Climate, 15, 964-982.

Maloney, E. D. and Kiehl, J. T. (2002): MJO –Related SST Variations over the Tropical Eastern Pacific during Northern Hemisphere Summer. Journal of Climate, 15, 675-689.

Mantua, N. (Last updated 2000): http://tao.atmos.washington.edu/pdo/

Matthews, A. J., (No last update date provided): Accessed March 5, 15, May 1. 2002. Madden-Julian oscillation htpp://envam.env.ac.uk/~e058/mjo.html

Matthews, A.J (1993): The intraseasonal oscillation. PhD Thesis, University of Reading.

Matthews, A.J Hoskins B.J. Slingo J.M. Blackburn M. (1996): Development of convection along the SPCZ with a MJO. Quarterly Journal of the Royal Meteorological Society, 122, 669-688.

Matthews, A.J and Kiladis G.N. (1997): Modulation of wave activity and deep convection in the Pacific ITCZ by the MJO. Proceedings 22nd conference on Hurricanes and Tropical Meteorology, Fort Collins Colorado, USA pp225-226

Matthews, A.J and Kiladis G.N. (1999): The tropical-extratropical interaction between high-frequency transients and the MJO. Monthly Weather Review, 127, 661-677.

Matthews, A. J., Slingo, J. M., Hoskins, B. J. and Inness, P. M. (1999): Fast and slow Kelvin waves in the Madden-Julian Oscillation of a GCM, Quarterly Journal of the Royal Meteorological Society, 125, 1473-1498.

Milliff, R. and Morzel, J. (2003): Surface Convergence and the Madden Julian Oscillation: Preliminary results from Probability Distributions for Surface Windfields. Proceedings, IUGG, Japan.

Miyahara, S. (1987): Simple model of the tropical intraseasonal oscillation. Journal of the Meteorological Society of Japan, 65, 341-351.

Mo, K. C. (2001): Adaptive Filtering and Prediction of Intraseasonal Oscillations. Monthly Weather Review, 129, 802-817.

Mote, P., Clark, H., Dunkerton, T., Harwood, R., Pumphrey, H. (2000): Intraseasonal variations of water vapour in the tropical upper troposphere and tropopause region. Journal of Geophysical Research, 105, 13, 17457-1770.

Murakami, T. (1980)i: Temporal Variations of Satellite-Observed Outgoing Longwave Radiation over the Winter Monsoon Region. Part I: Long-Period (15-30 Day) Oscillations. Monthly Weather Review, 108, 4, 408-426.

Murakami, T. (1980) ii: Temporal Variations of Satellite-Observed Outgoing Longwave Radiation over the Winter Monsoon Region. Part II: Short-Period (4-6 Day) Oscillations. Monthly Weather Review, 108, 4, 427-444.

Murakami, T., Chen L-X., and Xie, A. (1986): Relationship among Seasonal Cycles, Low-Frequency Oscillations, and Transient Disturbances as Revealed from Observed Outgoing Longwave Radiation Data. Monthly Weather Review, 114, 8, 1456-1465.

Myers, D., and Waliser, D. (2003): Three Dimensional Water Vapour and Cloud Variations Associated with the Maddden-Julian Oscillation during Northern Hemisphere Winter. Journal of Climate, 16, 929-950.

Nakazawa, T. (1988): Topical super clusters within Intraseasonal Variations over the Western Pacific. Journal of the Meteorological Society of Japan, 66, 823-839.

Nakazawa, T. (1998): MJO A key component in the atmosphere for triggering ENSO in TOGA COARE-98 Conference Proceedings, World Meteorological Organization, Boulder, Colorado, USA.

Nicholls, N. (1987): El-Niño Southern Oscillation and rainfall variability. Journal of Climatology, 1, 418-421.

Nogués-Paegle, J. and Mo, K. (1997): Alternating Wet and Dry Conditions over South America during Summer. Monthly Weather Review, 125, 2, 279-291.

Raymond, D. J. (2001): A New Model of the Madden-Julian oscillation. Journal of the Atmospheric Sciences, 58, 2807-2819.

Schrage, J. M., Vincent DG, and Fink A.H. (1999): Modulation of intraseasonal (25-70 day) processes by the superimposed ENSO cycle across the Pacific Basin. Meteorology and Atmospheric Physics, 70, 15-27.

Seo, K-H., and Kim, K-Y (2003): Propagation and initiation mechanisms of the Madden-Julian Oscillation. Journal of Geophysical Research, 108, 13, 4384.

Shinoda, T and Hendon, H. (2002): Rectified Wind Forcing and Latent Heat Flux Produced by the Madden-Julian Oscillation. Journal of Climate, 15, 3000-3508.

Slingo, J. M., Sperber, K. R., Boyle, Ceron, J. P., Dix, M., Dugas, B., Ebisuzaki, W., Fyfe, J., Gregory, D., Gueremy, J. F., Hack, J., Harzallah, A., Inness, P. M., Kitoh, A., Lau, K. M., McAvaney, B., Madden, R. A., Matthews, A. J., Palmer, Park, C. K., Randall, D. and Renno, N. (1996): Intraseasonal oscillations in 15 atmospheric general circulation models: results from an AMIP diagnostic test. Climate Dynamics, 12, 325-358.

Slingo, J. M., Rowell, D. P., Sperber, K. R. and Nortley, F. (1999): On the predictability of the interannual behaciour of the Madden-Julian oscillationand its relationship with El Nino. Quarterly Journal of the Royal Meteorological Society, 125, 582-609.

Sperber, K. R., Slingo, J. M., Inness, P. M. and Lau, K. M. (1997): On the mainteance and initiation of the intraseasonal oscillation in the NCEP/NCAR reanalysis and in the GLA and UKMO AMIP simulations. Climate Dynamics, 13, 769-795.

Sperber, K., Gualdi, S., Li, W. and Slingo, J. (2001): Madden-Julian Variability in Coupled Models. Conference Proceedings: National Oceanic and Atmospheric Administration 26th Annual Climate Diagnostics and Prediction Workshop.

Stone, R.C. and McKeon, G.M. (1993):Prospects for using weather prediction to reduce pasture establishment and risk. Tropical Grasslands, 27, 406-413.

Stringer, R. (1992): Effects of the 40 to 50 day oscillation on Darwin rainfall. MSc Thesis, National Meteorological Library.

Sturman, A. and Tapper, N. (1996): The weather and climate of Australia and New Zealand. Oxford University Press, Melbourne, Australia, pp166-221.

Suppiah, R. (1991) Intraseasonal variability in the Australian Summer Monsoon during ENSO and anti-ENSO Episodes. In: Conference on Agricultural Meteorology 1991, pp28-30.

Swinbank, R. (1986): Simulation of intraseasonal oscillation in GCM experiments. World Climate Research Programme 1986 Report, 9,7.

United Kingdom Universities Global Atmospheric Modelling Project. (Date Not Provided), Date Accessed March 5 2002. The Madden-Julian Oscillation: a coupled atmosphere-ocean phenomenon? http://www.ugamp.rdg.ac.uk/hot/um/mjo.html

Vitart, F. (2003): The Madden-Julian Oscillation in the ECWMF monthly Forecasting system. Proceedings, Informal Seminar April 2003, European Centre For Medium-Range Weather Forecasts.

von Storch, H. and Xu, J. (1990): Principal Oscillation Pattern analysis of the 30- to 60-day oscillation in the tropical troposphere. Climate Dynamics, 4, 175-190.

von Storch, H. and Zwiers, F.W., (1999): Statistical Analysis in Climate Research . Cambridge University Press.

Waliser, D. E., Lau, K. M. and Kim, J.-H. (1998): The influence of coupled sea surface temperatures on the Madden-Julian oscillation: a model perturbation experiment in TOGA COARE-98 Conference Proceedings, World Meteorological Organization, Boulder, Colorado, USA.

Waliser, D.E., Murtuguude, R., and Lucas, L.L. (2003): Indo-Pacific Ocean response to atmospheric intraseasonal variability:1. Asutral summer and the Madden-Julian Oscillation. Journal of Geophysical Research, 109, C5.

Waliser, D. E., Lau, K. M., Stern, W. Jones, C. (2004): Potential Predictability of the Madden-Julian Oscillation. Journal of the American Meteorological Society, 84, 1, 33-50.

Wang, B. and Rui, H. (1989) Activity of transient tropical intraseasonal convective anomalies: 1975 – 1985. In: Proceedings-Fourth International Meeting on Statistical Climatology, 1989, Rotoua, New Zealand.

Wang, H., Chen, X., Xue, F. and Zeng, Q. (2001): The intraseasonal oscillation and its interannual variability: a simulation study. Acta Meteorologica Sinica, 15, 49-58.

Watterson, I. G. (2002): The sensitivity of subannual and intraseasonal tropical variability to model ocean mixed layer depth. Journal of Geophysical Research, 10, D2.

Weickmann, K. M. (1991): El Nino/ Southern Oscillation and the Madden-Julian (30-60 day) oscillations during 1981-1982. Journal of Geophysical Research, 96, 3187-3195.

Wheeler, M. and Kiladis, G. (1999): Convectively Coupled Equatorial Waves: analysis of Clouds and Temperature in the Wavenumber-Frequency Domain. Journal of the Atmospheric Sciences, 56, 374-399.

Wheeler, M. and Weickmann, K. M. (2001): Real-Time monitoring and Prediction of Modes of Coherent Synoptic to Intraseasonal Tropical Variability. Monthly Weather Review, 129, 2677-2694.

Wheeler (2002): Seasonal composites from the index. Weekly Rainfall Anomalies (mm)
http://www.bom.gov.au/bmrc/clfor/cfstaff/matw/maproom/RMM/composites/index.htm

Wheeler, M. and Hendon, H. H. (2004): An All-Season Real-time Multivariate MJO Index: Development of the index for monitoring and prediction in Australia. Monthly Weather Review,132, 1917-1932

Woolnough, S. J., Slingo, J. M. and Hoskins, B. J. (2000): The relationship between convection and sea surface temperature of intraseasonal timescales. Journal of Climate, 13, 2086-2104.

Wu, R. and Wang, B. (2000): Interannual variability of summer monsoon onset over the western North Pacific and the underlying processes. Journal of Climate, 13, 2483-2502.

Yamagata, T., and Y. Hayashi (1984): A simple diagnostic model for the 30-50 day oscillation in the tropics. Journal of the Meteorological Society of Japan, 62, 70-717.

Yanai, M. and Chen, B. (1998) The Madden-Julian oscillation observed during TOGA-COARE Intensive observing period. Part I: Global view in TOGA-COARE-98 Conference Proceedings, World Meteorological Organization, Boulder, Colorado, USA.

Yanai, M., Chen, B. and Tung, W. (2000): The Madden-Julian oscillation observed during TOGA-COARE IOP: global view. Journal of the Atmospheric Sciences, 57, 2374-2396.

Yasunari, T. (1979): Cloudiness fluctuations associated with the Northern Hemisphere summer Monsoon. Journal of the Meteorological Society of Japan, 57, 227-242.

Zhang, C. and Hendon, H. H. (1997): Propagating and standing components of the intraseasonal oscillation in tropical convection. Journal of the Atmospheric Sciences, 54, 741-752.

Zhang, G. J. (1998): The effects of westerly wind bursts and calm conditions on the air-sea fluxes during TOGA COARE in TOGA COARE-98 Conference Proceedings, World Meteorological Organization, Boulder, Colorado, USA.

Zhang, C. (2001): Intraseasonal perturbations in sea surface temperatures of the equatorial Pacific and their association with the Madden-Julian oscillation. Journal of Climate, 14, 1309-1322.

Zhang, C. and Gottschalck, J. (2002): SST Anomalies of ENSO and the Madden Julian Oscillation in the Equatorial Pacific. Journal of Climate, 15, 2965-2997.

Ziemke, J.R., and Chandra, S. (2003): A Madden-Julian Oscillation in Tropospheric Ozone. Geophysical Research Letters, 30,23, 2182.

Zou, J. and Cho, H. (2000): A nonlinear Schroedinger equation model of the intraseasonal oscillation. Journal of the Atmospheric Sciences, 57, 2435-2444.

APPENDICES

Appendix 1 The hq dataset daily rainfall raw data sample

hq dataset rainfall stations for daily data, 180 stations.

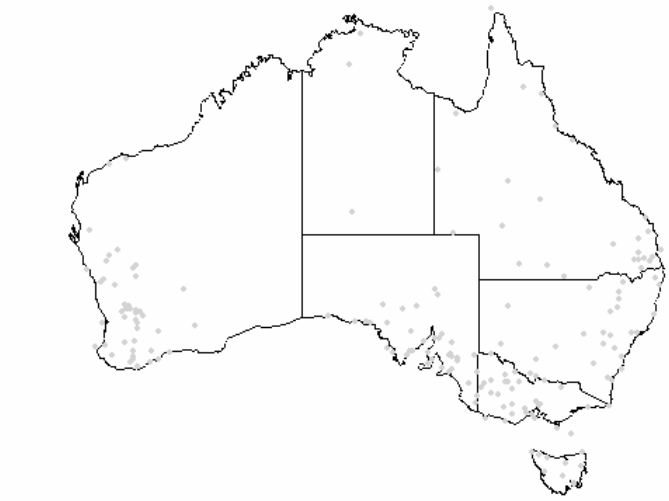

hq data set sample data

year	day	radn	maxt	mint	rain	pan	vpd	code
1889	22	23	20.5	14	0	5.4	15	777277
1889	23	22	20.5	14	0	5.2	15	777277
1889	24	22	20.5	14	0.5	5.2	15	777277
1889	25	23	20.5	14.5	1	5	15	777277
1889	26	23	20.5	14.5	0	5.2	15	777277
1889	27	23	20.5	14.5	7.2	5.2	15	777277
1889	28	23	21	14.5	2.1	5.2	15	777277
1889	29	22	20.5	14	0.6	5.4	15	777277
1889	30	22	20.5	14	0	5.4	16	777277
1889	31	22	20.5	14.5	0	5.2	15	777277
1889	32	22	20.5	14.5	0	5.2	16	777277
1889	33	22	21	14.5	0.1	5	15	777277
1889	34	21	21	14.5	3.6	4.8	15	777277
1889	35	21	21	14.5	2.2	4.8	15	777277
1889	36	21	21	14.5	1.9	4.8	16	777277
1889	37	21	21	15	2.5	4.8	16	777277
1889	38	20	20.5	15	2.3	4.8	16	777277
1889	39	20	20.5	14.5	1.2	4.8	16	777277
1889	40	21	20.5	14.5	0.1	4.8	15	777277
1889	41	21	21	14.5	0.1	4.8	15	777277

Appendix 2 The BoM dataset rainfall stations and daily rainfall raw data sample

BoM dataset sample stations and data.

1001|FORREST RIVER MISSION | -15.20| 127.83|WA |Rainman|Rain | 0| 0| 0| 2084| 3592| 2923| 3290| 3652| 2802| 0| 0| 0| 0

1005|WYNDHAM PORT | -15.46| 128.10|WA |Climate|Rain | 246| 1770| 3621| 3652| 3653| 3652| 3653| 3624| 2830| 2161| 3548| 1567| 0

1005|WYNDHAM PORT | -15.46| 128.10|WA |Climate|TMax | 0| 0| 0| 0| 0| 0| 0| 1093| 2774| 0| 0| 0| 0

1005|WYNDHAM PORT | -15.46| 128.10|WA |Climate|TMin | 0| 0| 0| 0| 0| 0| 0| 1084| 2761| 0| 0| 0| 0

1009|KURI BAY | -15.49| 124.52|WA |Climate|Rain | 0| 0| 0| 0| 0| 0| 0| 0| 3044| 3647| 2298| 3288| 1498

1009|KURI BAY | -15.49| 124.52|WA |Climate|TMax | 0| 0| 0| 0| 0| 0| 0| 0| 1826| 3620| 2268| 2935| 1471

1009|KURI BAY | -15.49| 124.52|WA |Climate|TMin | 0| 0| 0| 0| 0| 0| 0| 0| 1826| 3628| 2208| 2878| 1449

1012|MITCHELL PLATEAU | -14.79| 125.83|WA |Climate|Evap | 0| 0| 0| 0| 0| 0| 0| 0| 0| 0| 1633| 0| 0

1012|MITCHELL PLATEAU | -14.79| 125.83|WA |Climate|Rain | 0| 0| 0| 0| 0| 0| 0| 0| 731| 3583| 2466| 0| 0

1012|MITCHELL PLATEAU | -14.79| 125.83|WA |Climate|TMax | 0| 0| 0| 0| 0| 0| 0| 0| 0| 3003| 2360| 0| 0

1012|MITCHELL PLATEAU | -14.79| 125.83|WA |Climate|TMin | 0| 0| 0| 0| 0| 0| 0| 0| 0| 2849| 2288| 0| 0
1013|WYNDHAM | -15.49| 128.12|WA |Climate|Rain | 0| 0| 0| 0| 0| 0| 0| 0| 640| 3652| 3652| 3652| 1497
1013|WYNDHAM | -15.49| 128.12|WA |Climate|TMax | 0| 0| 0| 0| 0| 0| 0| 0| 607| 3600| 3504| 3598| 1409
1013|WYNDHAM | -15.49| 128.12|WA |Climate|TMin | 0| 0| 0| 0| 0| 0| 0| 0| 592| 3634| 3524| 3621| 1377
1021|KALUMBURU MISSION | -14.30| 126.64|WA |Climate|Rain | 0| 0| 0| 0| 0| 0| 1705| 3169| 3441| 3652| 3622| 3649| 1496
1021|KALUMBURU MISSION | -14.30| 126.64|WA |Climate|TMax | 0| 0| 0| 0| 0| 0| 2682| 3650| 3651| 3651| 3463| 3592| 1455
1021|KALUMBURU MISSION | -14.30| 126.64|WA |Climate|TMin | 0| 0| 0| 0| 0| 0| 2686| 3648| 3638| 3627| 3444| 3481| 1407
1025|DOONGAN | -15.38| 126.31|WA |Climate|Rain | 0| 0| 0| 0| 0| 0| 0| 0| 0| 0| 731| 3646| 1408
1025|DOONGAN | -15.38| 126.31|WA |Climate|TMax | 0| 0| 0| 0| 0| 0| 0| 0| 0| 0| 444| 3337| 1028
1025|DOONGAN | -15.38| 126.31|WA |Climate|TMin | 0| 0| 0| 0| 0| 0| 0| 0| 0| 0| 494| 3180| 1015
2000|ALICE DOWNS | -17.76| 127.94|WA |Rainman|Rain | 0| 0| 1340| 3168| 3378| 3621| 2710| 1952| 3653| 3650| 3646| 1892| 382
2001|ARGYLE DOWNS | -16.51| 128.92|WA |Rainman|Rain | 0| 1194| 2015| 3559| 3653| 3652| 3653| 3441| 3653| 3643| 3653| 2676| 73
2002|BOHEMIA DOWNS | -18.88| 126.23|WA |Rainman|Rain | 0| 0| 1187| 3256| 2770| 3075| 2865| 1855| 0| 0| 0| 0| 0
2005|CARLTON HILL | -15.49| 128.53|WA |Rainman|Rain | 0| 185| 2095| 3529| 3228| 3622| 3502| 2527| 3653| 1706| 2541| 3320| 973
2007|DUNHAM RIVER STATION | -16.32| 128.25|WA |Rainman|Rain | 0| 0| 0| 0| 1948| 2801| 3351| 3652| 3378| 365| 0| 0| 0
2009|GIBB RIVER | -16.42| 126.44|WA |Rainman|Rain | 0| 0| 0| 0| 2922| 3621| 3653| 3652| 3653| 3639| 3014| 2220| 895
2010|GORDON DOWNS | -18.75| 128.58|WA |Rainman|Rain | 0| 0| 0| 61| 3591| 3500| 3592| 3652| 3561| 3198| 1063| 1496| 0
2011|OLD HALLS CREEK | -18.25| 127.78|WA |Climarc|Rain | 0| 1430| 3652| 3652| 3653| 3652| 3653| 3591| 798| 119| 294| 1389| 0
2011|OLD HALLS CREEK | -18.25| 127.78|WA |Climarc|TMax | 0| 723| 3521| 3651| 3649| 3651| 3636| 880| 353| 0| 0| 0| 0
2011|OLD HALLS CREEK | -18.25| 127.78|WA |Climarc|TMin | 0| 0| 0| 0| 0| 0| 0| 0| 295| 0| 0| 0| 0
2012|HALLS CREEK AIRPORT | -18.23| 127.66|WA |Climate|Evap | 0| 0| 0| 0| 0| 0| 0| 0| 414| 3645| 3592| 3594| 1465
2012|HALLS CREEK AIRPORT | -18.23| 127.66|WA |Climate|Rain | 0| 0| 0| 0| 0| 0| 2192| 3652| 3653| 3652| 3653| 3652| 1496
2012|HALLS CREEK AIRPORT | -18.23| 127.66|WA |Climate|TMax | 0| 0| 0| 0| 0| 0| 1108| 3627| 3543| 3651| 3634| 3648| 1497
2012|HALLS CREEK AIRPORT | -18.23| 127.66|WA |Climate|TMin | 0| 0| 0| 0| 0| 0| 1107| 3608| 3521| 3647| 3633| 3648| 149

Appendix 3 The WMO dataset daily rainfall raw data sample

WMO sample data set

#GSOD data for WMO station 877740
#name='MAQUINCHAO'
#latitude=-41.417 (dd North)
#longitude=-69.217 (dd West)
#elevation=888 (m)
#ymd mint(oC) maxt(oC) prcp(mm)
19791206 8.0 20.0 0.0
19791209 5.0 25.0 0.0
19791210 14.0 22.0 0.0
19791212 6.0 18.0 0.0
19791213 4.0 17.0 0.0
19791214 3.0 19.0 0.0
19791215 13.0 26.0 0.0
19791216 18.0 31.0 0.0
19791217 17.0 30.0 0.0
19791218 10.0 26.0 0.0
19791219 11.0 25.0 0.0
19791221 8.0 29.0 0.0
19791222 20.0 31.0 0.0
19791223 16.0 32.0 0.0
19791224 10.0 24.0 0.0
19791225 6.0 27.0 0.0
19791226 12.0 31.0 0.0
19791228 10.0 27.0 0.0
19791230 10.0 25.0 0.0
19800101 13.0 30.0 0.0
19800102 10.0 26.0 0.0
19800109 20.0 27.0 0.0
19800111 13.0 34.0 0.0
19800112 16.0 26.0 0.0
19800113 12.0 30.0 0.0
19800114 16.0 30.0 0.0
19800116 20.0 28.0 0.0
19800117 11.0 29.0 0.0
19800118 12.0 28.0 0.0
19800119 12.0 30.0 0.0
19800120 13.0 34.0 0.0
19800121 17.0 33.0 0.0
19800122 13.0 25.0 0.0
19800123 6.0 19.0 0.0
19800124 3.0 22.0 0.0
19800125 14.0 24.0 0.0
19800127 11.0 28.0 0.0
19800130 10.0 27.0 0.0
19800131 9.0 27.0 0.0

Appendix 4 The MJO dataset daily rainfall raw data sample

RMM values sample data
year, month, day, RMM1, RMM2, phase, amplitude. Missing Value= 1.E36 or 999
1974 6 1 1.63447 1.20304 5 2.02948
1974 6 2 1.60289 1.01512 5 1.89729
1974 6 3 1.51625 1.08551 5 1.86476
1974 6 4 1.50981 1.03573 5 1.83092
1974 6 5 1.55906 1.30518 5 2.03326
1974 6 6 1.20626 1.62889 6 2.0269
1974 6 7 0.611101 1.72248 6 1.82767
1974 6 8 0.326395 1.77818 6 1.80789
1974 6 9 9.38282E-02 1.35694 6 1.36018
1974 6 10 -8.61263E-02 0.775476 7 0.780244
1974 6 11 0.111394 0.389534 6 0.405148
1974 6 12 0.120489 1.38852E-02 5 0.121286
1974 6 13 1.92806E-02 -0.21767 3 0.218519
1974 6 14 -0.10436 -0.38105 2 0.395082
1974 6 15 -0.18294 -0.64535 2 0.670775
1974 6 16 -0.23596 -0.47107 2 0.526865
1974 6 17 -0.49869 -0.48752 1 0.697402
1974 6 18 -0.5698 -0.36398 1 0.676134
1974 6 19 -0.69503 -0.35557 1 0.780705
1974 6 20 -0.72915 -0.47646 1 0.871015
1974 6 21 -1.09443 -0.83275 1 1.37523
1974 6 22 -1.09851 -0.83867 1 1.38206
1974 6 23 -1.06244 -0.50405 1 1.17594
1974 6 24 -0.88507 -0.32444 1 0.942658
1974 6 25 -0.76582 -0.33355 1 0.835304
1974 6 26 -0.83447 -0.41418 1 0.931607
1974 6 27 -0.8013 -0.35989 1 0.878413
1974 6 28 -0.56442 -0.29799 1 0.63825
1974 6 29 -9.70497E-02 -0.40189 2 0.413442
1974 6 30 9.14870E-03 -0.24385 3 0.244017
1974 7 1 0.26055 8.71013E-02 5 0.274724
1974 7 2 0.267024 0.23012 5 0.352501
1974 7 3 0.355582 0.387155 6 0.525669
1974 7 4 0.844383 0.426138 5 0.945821
1974 7 5 1.12066 0.400394 5 1.19004
1974 7 6 1.07635 0.595407 5 1.23006
1974 7 7 0.812902 0.870444 6 1.191
1974 7 8 0.431732 1.08825 6 1.17076
1974 7 9 8.10154E-02 1.17053 6 1.17333
1974 7 10 -0.12074 1.12966 7 1.13609
1974 7 11 -0.27892 0.998571 7 1.03679
1974 7 12 -0.13957 0.702709 7 0.716435

Appendix 5 The MSLP dataset daily rainfall raw data sample

MSLP from 01/01/01/970, daily analogue set time series lat 30, long 45 of 2.5 x2.5 km grid.

1 101103
2 101200
3 101263
4 101285
5 101385
6 101710
7 101940
8 101805
9 101703
10 101480
11 101443
12 101583
13 101540
14 101463
15 101633
16 101628
17 101600
18 101355
19 101230
20 101273
21 101278
22 101265
23 101183
24 101098
25 100993
26 100935
27 100950
28 100970
29 100995
30 100850
31 101170
32 101445
33 101420
34 101383
35 101848
36 102093
37 102100
38 102230
39 102040
40 101763
41 101435
42 101273
43 101340